Generating Immunological Signatures of Diseases by Multiplex Analysis of Single Cells

by

Qing Han

M.S., Biology
Tsinghua University, Beijing, P.R. China (2007)

B.E., Chemical Engineering
Tsinghua University, Beijing, P.R. China (2004)

SUBMITTED TO THE DEPARTMENT OF CHEMICAL ENGINEERING IN PARTIAL FULFILLMENT OF THE REQUIREMENTS FOR THE DEGREE OF

DOCTOR OF PHILOSOPHY IN CHEMICAL ENGINEERING

AT THE

MASSACHUSETTS INSTITUTE OF TECHNOLOGY

June 2012

Signature of Author: ______________________

Qing Han
Department of Chemical Engineering
May 14, 2012

Certified by: ______________________

J. Christopher Love
Latham Family Career Development Professor
Thesis Supervisor

Accepted by: ______________________

Patrick S. Doyle
Professor of Chemical Engineering
Chairman of the Committee for Graduate Students

Generating Immunological Signatures of Diseases by Multiplex Analysis of Single Cells

by

Qing Han

Submitted to the Department of Chemical Engineering on May 14, 2011 in Partial Fulfillment of the Requirements for the Degree of Doctor of Philosophy in Chemical Engineering

Abstract

The large diversity of cells that comprise the human immune system requires methods that can resolve the contributions of individual cells to an immunological response. The release of cytokines is one of several important functions carried out by immune cells. Analytical methods that yield multiple measures of the breadth and quality of cytokine secretion from heterogeneous populations are highly desired in basic and clinical immunology. Microengraving is a process that uses a dense, elastomeric array of nanowells to generate microarrays of proteins secreted from large numbers of individual live cells. In this thesis, we improved the sensitivity and multiplicity of microengraving and adapted it to detect cytokine secretions from primary immune cells. We demonstrated that microengraving could provide quantitative measurements of both the frequencies and the distribution in rates of secretion for up to four cytokines simultaneously. The experimental limits of detection ranged from 0.5 to 4 molecules/s for most cytokines in our experiments. These multidimensional measures resolve functional responses by cells exposed to stimuli with greater sensitivity than single-parameter assays. Primary T cells with specific profiles of secretion can also be recovered after microengraving for subsequent expansion in vitro.

The release of multiple cytokines by T cells has been associated with beneficial immune responses. To date, however, time-integrated end-point measurements have not resolved the temporal dynamics of these functions. Here, we used serial microengraving to measure Th1-skewed cytokine responses (IFNγ, IL-2, TNFα) from individual cells after activation ex vivo. The results show that multifunctional cytokine responses are initiated asynchronously but the ensuing dynamic trajectories of these responses evolve programmatically in a sequential manner. Furthermore, these dynamic trajectories are strongly associated with the various states of cell differentiation, suggesting that transient programmatic activities of many individual T cells contribute to sustained, population-level responses. The trajectories of responses by single cells may also provide unique, time-dependent signatures for immune monitoring that are less compromised by the timing and duration of integrated measures. Together, these results demonstrate the utility of quantitative, multidimensional profiles of single cells for analyzing the diversity and dynamics of immune responses in vitro, thus generating immune signatures for diseases.

Thesis Supervisor: J. Christopher Love
Title: Latham Family Career Development Professor

Acknowledgements

I would like to thank my advisor, Prof. J. Christopher Love, for his guidance and advice in this thesis work. I feel very lucky to work with Prof. Love and have such great opportunity to conduct cutting-edge researches in the field of biotechnology. Prof. Love always has great insights into the direction of research and novel ideas, which inspire my passion on technology development and its biomedical application. During these years, he taught me how to creatively formulate research topics, how to logically design experiments, and how to efficiently solve problems. I appreciate the time and efforts he has spent on my project, and his great patience on training me in writing scientific paper and presenting my work.

I also would like to thank Prof. Dane Wittrup, Prof. Darrell Irvine, and Prof. David Hafler for serving in my thesis committee and for their valuable advice and suggestions that help to improve the quality of this work. Thanks to Dr. Elizabeth Bradshaw and Dr. Sally Kent at Brigham And Women's Hospital, whom I collaborated with in the early stage of my research, for their help in sample preparation, experiments, and discussion. Thanks to Dr. Neda Bagheri and Prof. Douglas Lauffenburger in the Department of Biological Engineering for their great contribution to the work on single-cell dynamics (Chapter 6), especially for Neda's efforts on the computational analysis and inspiring discussion. Thanks to Dr. Douglas Kwon at Massachusetts General Hospital for his kind help in ICS and Luminex measurements.

I am so glad to work together with all wonderful colleagues in the Love Lab. Thanks to all current and past members whom I have worked with: Dr. Qing Song, Yuan Gong, Adebola Ogunniyi, Dr. Kerry Love, Dr. Navin Varadarajan, Yvonne Yamanaka, Vasiliki Panagiotou, Dr. Jonghoon Choi, Timothy Politano, Dr. Ayca Yalcin Ozkumur, Dr. Todd Gierahn, Viktor Adalsteinsson, Denis Loginov, Dr. Rita Lucia Contento, Dr. Alexis Torres, Dr. Sangram Bagh, Dr. Bin Jia, Brittany Thomas, Abby Hill, Lionel Lam, Kimberly Ohn, Dr. Joe Couto, Rachel Barry, and Narmin Tahirova for their help and suggestions in experiments, their contribution that makes the lab run smoothly and efficiently, and creating such friendly atmosphere in the lab. I also would like to thank my UROP Flora Cheng for her great help in performing experiments and data analysis. Thanks to other collaborators: Gregory Szeto, Kelly Benedict, and Meichen Liao for discussion and introducing me new ideas from other scientific fields.

Thanks to all my friends in the Chinese student community for sharing good time in my life in the U.S. I want to express my appreciation especially to Jie Chen, Yin Fan, Jingjing Xu, Ying Diao, Yang Chen, Yuxi Zhang, Xiaochuan Yang, and Fei Chen. Thanks for bringing me so much fun, inviting me to join your activities, sharing your valuable experiences in both study and life, and making my days at MIT so enjoyable.

Finally, my special thanks are to my family. Thanks to my parents for their priceless education and support in my life. Thanks to my husband, Mingguang Xu, for his love and effort to make our life wonderful, and also for his consideration and encouragement in my research.

Table of contents

List of Figures

List of Tables

Abbreviations

APC — antigen-presenting cell

BSA — bovine serum albumin

ELISA — enzyme-linked immunosorbent assay

ELISpot — enzyme-linked immunospot

ICS — intracellular staining

IFN — interferon

IL — interleukin

LPS — lipopolysaccharide

MFI — mean fluorescence intensity

MHC — major histocompatibility complex

PBMC — peripheral blood mononuclear cell

PCA — principal component analysis

PDMS — polydimethylsiloxane

PHA — phytohemagglutinin

PMA — phorbol 12-myristate 13-acetate

PWM — pokeweed mitogen

SOM — self organizing map

TCR —T-cell recepter

TNF — tumor necrosis factor

Chapter 1. Introduction

The activation of T cells is an essential process for coordinating both cellular and humoral immune responses. The release of cytokines is one of several important functions carried out by T cells during either a protective immune response to pathogens or autoimmune responses. The number of responsive cells provides a measure of the magnitude, while the nature and diversity of the functional responses has also been associated with measures of quality. Both the magnitude and quality of cytokine secretion are, therefore, considered important metrics in evaluating the efficacy of an immune response (1). In addition, T cell responses are dynamic upon activation. Resolving when activated T cells initiate the release of cytokines, and how their responses evolve, may provide further insight into how individual cells modulate intercellular signals dynamically to affect population-level responses towards pathological conditions or clinical interventions. Understanding the phenotypes and dynamic functions that indicate effective T cell responses to diseases and clinical interventions has been a central effort to improve immune monitoring. Existing analytical methods can assess the frequencies, magnitude, and number of cytokines produced by individual cells, but few assigns multiple functional and phenotypic characteristics to the same individual cells without affecting their viability or responses. Therefore, most available functional assays of different T-cell subsets lack temporal resolution, and such functional profiles are also hard to further correlate with other cell activities, such as proliferation and cytotoxicity. To solve this technical problem, this thesis aims to develop a high-throughput and multiplexed assay to resolve the dynamic functional responses of individual cells following stimulation while minimizing external perturbations that could unintentionally alter their behaviors.

1.1 Diversity of T cells

1.1.1 T cell differentiation and classification

T cells are an important category of lymphocytes in the immune system and play a significant role in adaptive immune responses to infectious diseases and in the pathogenesis of inflammatory diseases (2). T cells are highly heterogeneous population: an individual T cell expresses a unique receptor (TCR) that recognizes antigens as peptides bound to major histocompatibility complex (MHC) molecules on the surface of antigen-presenting cells (APCs). Two signals are required to activate T cells: binding of TCR to peptide/MHC complexes delivers the first signal to T cells, while a second signal is provided by costimulatory ligands on APCs (3, 4). After antigen-specific stimulation, naïve T cells can undergo clonal expansion, culminating in a higher frequency of antigen-specific cells endowed with effector functions (5).

There are two major classes of T cells: T helper cells (Th cells, $CD4^+$) and cytotoxic T cells (CTLs, $CD8^+$). Naïve $CD4^+$ T cells differentiate into functional subsets, such as Th1 cells and Th2 cells, which produce one or more cytokines and chemokines to induce proliferation, modulate inflammation, mediate cytolysis of other cells, and inhibit viral replication (2). In addition to differences in cytokine repertoire, effector $CD4^+$ T cells exhibit diversity in homing, e.g. migration to lymph node follicles to help B cells versus migration to inflamed tissues. Effector $CD4^+$ T cells also help B-cell responses and enhance $CD8^+$ T-cell development through the activation of APCs. $CD8^+$ T cells mediate their effector functions by the production of cytokines such as IFNγ and TNFα and/or by cytolytic mechanisms (6). These responses are important in preventing or maintaining control against disease in a variety of intracellular infections and perhaps also against certain tumors. Most effector cells are short-lived and rapidly decrease in number towards the end of a response.

Upon clearance of the antigen, two major types of memory T cells remain: central memory cells (T_{CM}) and effector memory cells (T_{EM}), which mediate reactive memory and protective memory, respectively (2, 5, 7). T_{CM} home to T cell-rich areas in secondary lymphoid organs. They have little or no effector function, but readily proliferate and differentiate to effector cells in response to antigenic stimulation. T_{EM} migrate to inflamed peripheral tissues, such as the skin and the gut, and display immediate effector functions, such as killing infected cells and/or secrete inflammatory cytokines that inhibit replication of the pathogen. These memory T cells form the basis for protective immune responses.

T-cell migration is dependent on the expression of a particular set of selectins, chemokine receptors, and integrins, which determine the steps of extravasation and positioning in different tissue microenvironments. Therefore, differentiated subsets of T cells (naïve, memory, and effector cells) can be distinguished by the expression of homing receptors and activation markers, e.g. CD45RA, CCR7, and CD62L (8-10). Naïve T cells have not encountered its cognate antigen within the periphery and express CD45RA and CCR7. Terminally-differentiated effector T cells are $CD45RA^+CCR7^-$ with limited potential for proliferation and expansion after antigenic stimulation.

T_{CM} are $CD45RA^-$ and constitutively express CCR7 and CD62L, which are required for cell extravasation through high endothelial venules and migration to T-cell areas of secondary lymphoid organs. When compared with naïve T cells, T_{CM} have higher sensitivity to antigenic stimulation, are less dependent on costimulation, and upregulate CD40L to a greater extent, thus provide more effective stimulatory feedback to dendritic cells and B cells. Following TCR triggering, T_{CM} produce mainly IL-2, but after proliferation, they efficiently differentiate to effector cells and produce large amounts of cytokines, e.g. IFN-γ or IL-4 (11).

T_{EM} lose constitutive expression of CCR7, are heterogeneous for CD62L expression, and display characteristic sets of chemokine receptors and adhesion molecules that are required for homing to inflamed tissues. When compared with T_{CM}, T_{EM} are characterized by rapid effector function. $CD8^+$ T_{EM} carry large amounts of perforin, and both $CD4^+$ and $CD8^+$ T_{EM} produce IFNγ, IL-4, and IL-5 within hours following antigenic stimulation. Some $CD8^+$ T_{EM} express CD45RA (defined as T_{EMRA}) and carry the largest amount of perforin (11).

The relative proportions of T_{CM} and T_{EM} in blood vary in the $CD4^+$ and $CD8^+$ T cells. T_{CM} is predominant in $CD4^+$ T cells and T_{EM} in $CD8^+$ T cells. Within the tissues, however, T_{CM} and T_{EM} show characteristic patterns of distributions. T_{CM} are enriched in lymph nodes and tonsils, whereas lung, liver, and gut contain greater proportions of T_{EM} (12). When stimulated in vitro, memory T cells show low-activation threshold and vigorous proliferation. Although both

T_{CM} and T_{EM} have a high responsiveness to antigenic stimulation, the expansion potential decreases from T_{CM} to T_{EM} and is very low in $CD8^+$ T_{EMRA} (9).

1.1.2 Functional diversity of Th cells

Th cells exert functions mainly through secreting cytokines and chemokines that activate or recruit target cells. The type and magnitude of cytokine secretions determine the effectiveness of immune responses. Antigen-activated naïve Th cells can develop into various functional subsets, depending on external cues and the transcription factors induced (13). Effector Th cells have been classically considered to contain two subsets: Th1 cells and Th2 cells. Each subset has unique cytokine products, signaling pathways, and lineage-specific transcription factors or master regulators. More types of effector subsets were discovered later, including Th17, Treg, T_{FH}, Th9, Tr1, Th22, etc. (2, 14).

Th1 cells mediate immune response against intracellular pathogens (15). In humans, they play a particular important role in resistance to mycobacterial infections and are also responsible for the induction of some autoimmune diseases. Th1 cells are regulated by transcription factors STAT1, STAT4, and T-bet. Their principle cytokine products are IFNγ, LTα, and IL-2. IFNγ is important in activating macrophages to increase their microbicidal activity (16). IL-2 production is important for $CD4^+$ T cell memory. IL-2 stimulation of $CD8^+$ cells during priming phase is critical for their memory formation (17).

Th2 cells mediate host defense against extracellular parasites (15). They are important in the induction and persistence of asthma and other allergic diseases. Th2 cells are regulated by transcription factor STAT6 and GATA-3, and mainly produce IL-4, IL-5, IL-9, IL-10, and IL-13.

Th17 cells mediate immune responses against extracellular bacteria and fungi (18). They are responsible for, or participate in, the induction of many organ-specific autoimmune diseases. RORγt is important in Th17 differentiation. Th17 cells produce IL-17a, IL-17f, IL-21, and IL-22.

Treg cells play a critical role in maintaining self-tolerance as well as in regulating immune responses (19). Increasing Treg numbers and enhancing their suppressive function may be beneficial for treating autoimmune diseases and for preventing allograft rejection. Treg cells are regulated by transcription factor Foxp3. The molecular basis of suppression in some cases is through their production of TGF-β, IL-10, and IL-35.

Differentiation of naïve T cells to functional specific effectors involves positive feedback of cytokines and cross-inhibition between lineages. For example, IFNγ and IL-4 signaling suppress mutually, TGF-β suppresses both Th1 and Th2 differentiation, and both IL-4 and IFNγ inhibit Th17 differentiation (20). The differentiation of Th cells was originally viewed as an unidirectional process with little plasticity in cytokine responses, however, recent searches reveal that T-cell functions, particularly in iTreg and Th17 cells, are more complex and flexible than what was previously assumed (13).

1.1.3 Multifunctionality and dynamic responses

With the development of multiparameter cytometry, individual T cells were found to have heterogeneous profiles of production of cytokines even within the same functional subsets and may produce multiple cytokines simultaneously. The breadth and magnitude of the production has been associated with productive immune responses to infectious diseases (21-23) or to vaccines (24-26). In the mouse model of *L. major* infection, Th1 cells were able to produce all combinations of three cytokines: IFNγ, IL-2, and TNFα. The generation of multifunctional T cells was found to strongly correlate with protection against subsequent challenges (25). In humans, virus-specific $CD4^+$ T cells are also able to secrete all possible combinations of IFNγ, IL-2, and TNFα. Triple producers were found to express highest level of cytokines per cell and have higher frequency of CD40L expression, which demonstrated a positive association between cytokine coproduction and other functional characteristics of $CD4^+$ T cells (27).

Cytokine responses are also dynamic. The types and concentrations of cytokines in the extracellular milieu, and percentages of cells producing them, are known to shift globally over time (28, 29). Kinetics study on gene expression of naïve $CD4^+$ T cells in response to TCR-mediated activation revealed several cytokine or cytokine-receptor genes (e.g. *IL-2* and *LTα*) that had significant changes in expression level as early as 4 h and then dynamically expressed within

24 h (30). The secretion of both IL-2 and IFNγ by $CD4^+$ T cells in vivo has been shown to begin within hours of stimulation and wane after 16-18 h (31, 32).

Studies on super antigen-stimulated $CD8^+$ T cells showed that production of cytokines segregates into discrete subpopulations and occurs with different kinetics. At the population level, cells first initiated TNFα production that was then tightly followed by IFNγ, and IL-2 production started last. These data indicated sequential acquisition of TNFα, IFNγ, and IL-2 expression in the subpopulation that coexpresses these three cytokines (33). Research on human influenza-specific $CD4^+$ T cells showed that $IL2^+IFN\gamma^-$ single functional cells was committed to $IL2^+IFN\gamma^+$ pattern under subsequent growth regardless of Th1- or Th2-biased media condition, suggesting that the expression of a subset of all potential cytokines by a T cell is transient and reversible (34).

1.2 Single-cell analysis

1.2.1 General review of cell diversity

Besides the apparent diversity of cell types in a population, such as lymphocytes in the immune system, it is also well known that individual cells, even those identical in appearance, differ in numerous characteristics, such as variability in the expression of a particular gene, concentration of a critical metabolite or ion, or pattern of response to a given stimulus (35-38). Living cells possess very low copy numbers of many components, including DNA and important regulatory molecules. Both stochastic events inherent in the biochemical process of gene expression (intrinsic noise) and fluctuations in other cellular components (extrinsic noise) contribute substantially to overall variation (39-41). Cell types, mutations, and fluctuations all contribute to the diversity of cells.

However, most clinical or cell-based assays analyze cells in bulk, for example, using serum, cell culture media, or pooled cell lysates. These assays may overlook the rich information available or attribute the contribution of small subset of cells to the whole population. Bulk analysis cannot provide detailed information that is critical to evaluate the state of biological system, such as whether two or more genes are co-expressed in the same population or in different sub-populations; whether a small increase in expression measured in the ensemble results from a small, homogeneous increase across all cells or a large increase in a subset of cells. Single-cell analysis, therefore, is necessary to resolve the underlying heterogeneity.

So far, some single-cell analyses have demonstrated unique advantages to understand the biological process and the mechanism of disease. Microscopic imaging and chemical separations have elucidated unique biological phenomena in single cells that are not discoverable by bulk sampling procedures (42). One example of these discoveries is the unique patterns of repetitive increase and decrease in Ca^{2+} concentration over time after stimulating single cells (43). This phenomenon is hidden when studying a whole population of cells, due to differences in timing and responses of individual cells. Single-cell measurements are also valuable for studying populations of mixed cells, such as cells in immune system or cells from tissue sample. Single-cell studies of tumor biopsies have shown that the majority of cells within a tumor tissue may be normal and among these abnormal cells, significant heterogeneity exists (44, 45).

1.2.2 Single-cell technologies for immunology

Over the past few decades, series of technologies have been developed for high-throughput studies of the molecular machinery of individual cells.

Enzyme-linked immunospot (ELISpot) and related variants are commonly used to study the release of cytokines from single immune cells (46, 47). In this technology, cells are loaded and grow on a membrane that is functionalized with specific antibodies for target analytes. During culturing, cytokines produced by each cell are captured by the antibodies around the cell. After removing cells, membrane is interrogated by detection antibodies and the secreted product from individual cells can be eventually visualized as colored spots. This method provides both qualitative results of secreted protein and semi-quantitative results of the frequency of responding cells. This assay has limited sensitivity, and typically, only measures one or two analytes per cell (48). Recent modifications that incorporate fluorescence-based analysis of secretions have expanded the number of analytes, but the inefficient capture of analytes still necessitates long time to accumulate sufficient material for detection (49, 50). Furthermore, individual cells cannot be retrieved after the measurements.

Intracellular cytokine staining (ICS) of fixed cells for analysis by flow cytometry has provided a convenient alternative to measure multiple cytokines over short periods of time (4-6 h) (51). In this assay, single cells are stained with fluorescently-labeled antibodies against either surface markers or intracellular proteins. With the development of new detection techniques, up to 19 parameters (17 fluorescent colors and 2 physical parameters) can be detected simultaneously from each cell (51), though routine use is typically limited to 6 to 8 colors. It can analyze several thousands of cells per second. The typical sensitivity is ~0.1%, and requires sufficient staining of the target cells. To further expand the detection capacity, single-cell mass spectrometric (cytometry by time-of-flight or CyTOF) has been developed recently (52). In this approach, heavy metal isotopes are used to label antibodies and then labeled cells are analyzed by high-throughput mass spectrometry. More than 30 parameters can be quantified at the single-cell level with very little crosstalk between channels. This technology enables systematic study on the phenotypic and functional complexity of immune cells (53, 54).

Two modified approaches for flow cytometry—'artificial receptors' and microbeads (55, 56)—allow the capture of secreted cytokines near the extracellular surface of the cell. Analytical models for the mass transport in these two processes indicate, however, that the rate of diffusion of released cytokines into the bulk media limits the sensitivity of these measurements for poor secretors and can introduce cross-contamination among cells (57). Encapsulation of cells at cold temperatures in polymeric matrices may also perturb secretion.

Another set of high-throughput techniques aim to detect rare circulating tumor cells (CTC) from blood, such as CTC-chip (58), microfilter device (59), micropores (60). Some are techniques that improve the efficiency of the detection system, such as rare event imaging system (REIS) (61) and fiber-optic array scanning technology (FAST) (62). The advantage of these methods is the ability to screen and isolate rare cells quickly. However, the cell type that can be captured and downstream analysis of captured cells are limited.

Lab-on-a-chip (LOC) technology is another platform for single-cell detection. Many systems use microfluidics technology to trap and manipulate single cells in nanolitre or picolitre volumes. Arrays of microwells have also been manufactured using a range of materials to facilitate the isolation and interrogation of single cells (63-72). Combining with biochemical assays or imaging techniques, variety of cellular measurements can be adapted on chip with improved sensitivity and throughput: cytometry, transcriptional detection, electrophoretic analysis, cell-environment interactions, and single-cell PCR (42).

1.2.3 Challenges of cytokine detection from single T cells

Heterogeneity among subsets of T cells requires analytical methods that yield multiple measures of the breadth, quality, and dynamics of functions exhibited by individual cells (1). Functions of T cells are usually measured directly ex vivo to reduce the variation and artificial activity introduced by long-term cell culture. This requirement excludes some single-cell technologies that require genetic modification of cells, e.g. construction of stable reporters. Two additional considerations for practical application in clinical studies are that methods should be amenable for characterizing small numbers of cells (10^4-10^6) and sufficient to detect target cells at low frequencies (1 in 10^4 to 10^6). Therefore, desired assay should work in a high-throughput manner to screen all possible individual cells from the sample while maintain a high sensitivity.

Existing analytical methods can assess the frequencies, magnitude, and number of cytokines produced by individual cells. ELISpot use a direct measure of secretion to determine the frequencies of cytokine-producing cells, but quantifying the subtle differences among cells in a population is difficult. The intensities of spots can indicate the rates of secretion (73), but poor sensitivity requires integrating signals over 12-48 h to detect most cytokine-secreting cells (<< 100 molecules/s). ICS has become a common alternative to assess the number and magnitude of cytokines expressed by single cells (74, 75). Mean fluorescence intensities (MFI) provide a relative measure of the quantity of a protein trapped intracellularly, however these values are difficult to compare directly among independent samples. Furthermore, ICS measures only the productive capacity of a cell when prohibited from secretion, and may not accurately reflect the quantity of cytokine that would have been secreted by the cell. More importantly, both technologies are not able to resolve the temporal differences of responses among cells (with time scale of 1-2 h for some cytokines), because they require integrating signal over long periods of time (6-48 h). Although ICS takes snapshot of cytokine production over a shorter period of time than ELIspot, compromise of the timing has to be made between cytokines with rapid producing kinetics (e.g., TNFα) and those with a delay (e.g., some chemokines). Furthermore, both technologies provide only endpoint measures, because neither of them can easily retrieve single live cells after measurement. Therefore, it has not been possible, however, to determine whether cells release multiple cytokines simultaneously or sequentially in time.

1.3 Microengraving technology.

Microengraving is a soft-lithographic method that transfers proteins secreted in a paracrine manner from single cells onto a solid substrate in a manner analogous to intaglio printing (76, 77) (Figure 1.1). An array of nanowells (sub-nanoliter volume) is formed in a biocompatible elastomer, PDMS, by replica molding. Cells are deposited from a suspension onto the array and the cells settle in the wells by gravity. The distribution of cells into the wells is a Poisson process, and ~30% of the wells contain single cells on average. A glass slide supporting one or more affinity-based reagents (e.g., antibodies) is sealed onto the array for a period of time (typically 1-2 h). During incubation, secreted analytes of interest are captured onto the glass. The glass bearing captured proteins is removed and interrogated by applying fluorescent detection antibodies. The array of cells can be placed in a reservoir of media for additional culturing. The spatial address of the wells and the secreted products links the data from each part of the process. Since microengraving is non-destructive, it therefore allows serial measurements from the same cells to expand the breadth of data collected or to monitor temporal-evolving responses (78, 79).

The original process of microengraving was established to screen of hybridoma cells (77). In this implementation, single hybridoma cells are distributed in an array of nanowells, with ~80,000 wells are distributed in 3”×1” area. In this way, thousands of single-cell loaded wells are achieved and the secretion of IgG from individual cells can be tested in parallel. Because of the small volume of each well (0.125 nL), the concentration of secreted IgG can reach detected level (~ng/mL) within short time period (~3-120 min). The overall efficiency of screening is largely improved from traditional methods using 96-well plates. The high sensitivity of this assay also allows the detection of even poor secretors, such as primary cytokine-secreting cells (80).

The same nanowell platform used in microengraving has been further developed to adapt other single-cells measurements, such as detection of specific genes by RT-PCR reaction, measure cytolytic function of $CD8^+$ T cells, single-cell manipulation and cloning (81-83). These different modular operations can either be used alone or integrated together to expand the information gained from single cells (84).

1.4 Objective and structure of the thesis

Heterogeneity of T cells exists at several levels: phenotypes ($CD4^+$ or $CD8^+$), differentiation states (naïve, memory, and effector), functional secretion (types and magnitude of cytokine production), dynamics (timing and duration of responses), proliferation, gene expression, cytotoxic activity, etc. Identifying specific patterns based on these properties could improve the correlation of T-cell function with a protective response to a vaccine or the efficacy of a treatment for a disease. Microengraving is a promising technology that could perform a variety of assays on single cells without reducing cell viability. This thesis focuses on the adaptation of microengraving for cytokine-detection and the development of microengraving into a sensitive, multiplexed, and quantitative analytical tool for generating immunological signatures of diseases.

There are seven chapters in this thesis. Chapter 1 gives an overview of the thesis and provides some related background on the heterogeneity of T cells and current single-cell technologies. Chapter 2 describes all experimental methods, materials, and data analysis that are used in the following chapters.

Chapter 3 emphasizes the technical improvements achieved for microengraving to detect cytokines, including optimization of surface immobilization, expansion of multiplicity in a single assay, validation of antibody pairs, and generation of background images to assist array alignment. At the end of this chapter, we demonstrate the capability of microengraving in multiplexed detection of cytokine from primary T cells and the retrieval of single T cell after detection.

Chapter 4 focuses on the fundamental characterization of analyte capture in the nanowell system, including theoretical characterization of the capturing process and calculation of the rates of secretion from single cells. We first developed a numerical model to quantitatively characterize the capture of analytes during microengraving, and then studied how some of the system parameters affect the capture efficiency. Based on these results, we established a series of criteria to identify positive spots from the images and methods to determine the rate of secretion and detection limit.

Chapter 5 compares microengraving technology with other conventional technologies, including qPCR, ELISpot, ICS, and Luminex, and discusses the unique advantages of microengraving. At the end of this chapter, we showed that the combination of both frequency and rate of secretion improves the resolution of subtle differences of cell responses.

Chapter 6 applies serial microengraving to measure dynamic responses of multifunctional T cells. We examined how the synchronicity and evolution of cytokines released vary among different subsets of primary human CD3$^+$ T cells upon TCR-specific and nonspecific activation. The kinetic measurements showed heterogeneous and dynamic responses by T cells and their multifunctional secretion states were found to be an unstable intermediate state during cell activation. Using computational tools, we calculated the transition probability between functional states and generalized several dominant trajectories of the functional evolution. At the end, we also discussed how these new findings contribute to our current knowledge of T-cell functions.

Chapter 7 concludes the main results of this thesis work, remarks on their significance, and suggests several directions for further work.

1.5 Figures

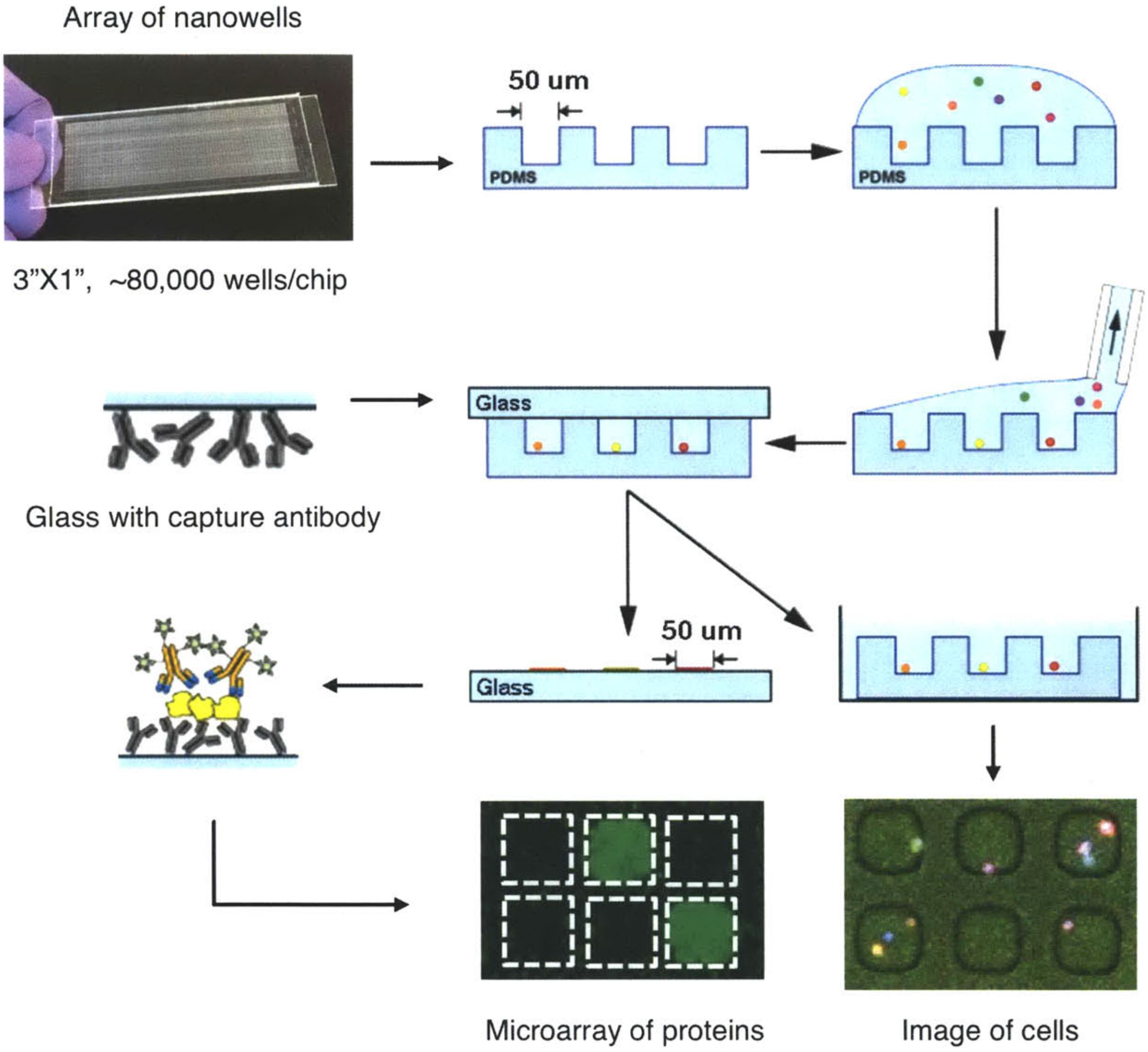

Figure 1.1. Scheme showing the process of microengraving.

Chapter 2. Materials and Methods

2.1 Microengraving

2.1.1 Fabrication of arrays of nanowells

Arrays of nanowells were manufactured by injecting a silicone elastomer (PDMS; 10:1 base:catalyst; Dow Corning) into a custom-built mold and cured at 80 °C for at least 2 h. Each array comprising 72×24 blocks of wells are 1 mm thick and adhered directly to a 3"×1" glass slide. In this study, two designs of blocks of wells were used: blocks of 7×7 nanowells with dimensions of 50 μm × 50 μm × 50 μm (center-to-center distance is 100 μm) for a total of 84,672 wells per array, and blocks of 12×12 nanowells with dimensions of 30 μm × 30 μm × 30 μm (center-to-center distance is 60 μm) for a total of 248,832 wells per array (76).

2.1.2 Preparation of poly-lysine slides

Poly-lysine slides were prepared according to published protocols available online (http://cat.ucsf.edu/pdfs/PolylysineSlides.pdf). Briefly, 3"×1" glass slides (Corning) were cleaned by soaking in solution with 2.5 M NaOH and 60% ethanol for at least 2 h. After thoroughly washing with deionized water, slides were submerged in 0.001% poly-L-lysine solution (diluted in 0.1×PBS) for 1 h with gentle shaking. Coated slides were further washed with water, spun dry, and stored in a desiccator until use.

2.1.3 Immobilization of capture antibodies

Antibodies for capturing secreted proteins were diluted in a buffer comprising 50 mM sodium borate, 8 mM sucrose, and 50 mM NaCl (pH 9.0) (85), deposited on the surface of poly-lysine slides (80 μL), spread by lifterslip (Electron Microscopy Sciences), and incubated for 1 h at 25 °C. Coated slides can be used directly or stored in 4 °C until use. Slides were then blocked in non-fat milk (3% w/v in PBS) for 30 min at 25 °C, washed three times with PBS, dipped in water, and spun dry.

2.1.4 Cell loading and printing

The array of nanowells was first exposed to oxygen plasma for 30 s (Harrick PDC-32G) to turn the surface to hydrophilic. Then, single-cell suspension ($\sim 2\times10^5$ cells/mL) was placed on the surface of the array, and the cells were allowed to settle into the wells by gravity at a density of ~1 cell per well. It is better to include serum in the loading media or pre-block the array with 0.5% BSA solution to prevent cells sticking on the outer surface of the wells. After washing excess cells from the surface of the array with serum-free media, a glass slide coated with capture antibodies was placed onto the loaded array. The array and glass slide was held together under sufficient compression in a hybridization chamber (Agilent Technologies, G2534A) to avoid media leakage and contamination between wells, and incubated at 37 °C with 5% CO_2. After incubation, the glass slide was separated from the array and placed in PBS.

2.1.5 Processing printed microarrays

After microengraving, slides were washed and probed with fluorescent detection antibodies in slide washer (Tecan). Briefly, slides were first blocked with 1% non-fat milk in PBST (PBS with 0.05% (v/v) Tween 20) for 15 min, washed with PBST twice, and then incubated with detection antibodies (1 μg/mL for each antibody) for 45 min at 25 °C. After that, the slides were washed with PBST and PBS three times, respectively, rinsed briefly with water, and dried under nitrogen. A reference slide for quantification of fluorescence intensity was prepared after the experiments: a gradient of individual detection antibody was prepared by diluting stock antibody in H_2O, and then spotted on a poly-lysine slide in triplicates (1 μL/spot) and vacuum dried. Slides with printed proteins and reference slides were scanned by Genepix 4200AL microarray scanner (Molecular Devices) with the same settings of gain and power. Genepix Pro 6.1 software was used for image analysis (refer to Chapter 4 for details).

2.1.6 Cell imaging and enumerating

Cells were stained for viability or surface markers either in bulk before distributed on the array or on-chip after microengraving. Cell images were acquired on an automated inverted epifluorescence microscope (Zeiss) equipped for live-cell imaging (temperature and CO_2 control). The arrays were mounted face-up on the microscope with a lifterslip placed on top of the array.

Transmitted light and epifluoresence micrographs were collected block-by-block (7×7 or 12×12 nanowells per block) automatically. Images were then analyzed using a customized software program to determine the number of cells present in each well and the corresponding mean fluorescence intensity in each fluorescent channel.

2.2 Estimation of the binding sites on the glass

To estimate the number of total binding sites available on a glass slide after adsorbing a capture antibody from solution, we used a fluorescent, sandwich-style assay to evaluate the saturating quantity of analyte immobilized on the surface. Briefly, a capture antibody (50 μg/mL) was spotted on the surface of poly-lysine slides (1 μL/spot) and incubated for 1 h at 25 °C. After blocking and washing the surface, the slide was placed in 96-well Microplate Microarray Hardware (ArrayIt, MMH96) and 100 μL of recombinant antigen (100 ng/mL; e.g., IFNγ) was added on each spot. The dose was selected to saturate the capture antibody fully, as determined by serial dilution on similar arrays. After 2-h incubation at 37 °C, the slide was washed, and a fluorescently labeled detection antibody (10 μg/mL) was applied at 25 °C. The labeled slide was then scanned, and the amount of detection antibody was calculated by comparing with data collected from a standard slide on which known amounts of the detection antibody were spotted.

2.3 Hybridoma culture and IgG detection

Hybridoma cells HYB 099-01 (Anti-ovalbumin, Statens Serum Institute) were cultured at 37 °C in a 5% CO_2 incubator in DMEM Media (Mediatech) supplemented with 10% FBS (PAA Laboratories), 100 U/mL penicillin, 100 mg/mL streptomycin, 10 mM HEPES, 50 μM 2-mercaptoethanol, 1 mM sodium pyruvate, and 0.1 mM nonessential amino acids. The cultures were split every 2-3 days to maintain a density of 10^5-10^6 cells/mL. Poly-lysine slides were coated with a mixture of two antibodies: goat anti-mouse IgG from Zymed (81-6500) and Southern Biotech (1010-01), 50 μg/mL of each (77). Three arrays were loaded with hybridoma from the same culture in parallel, and IgG secretion were measured by microengraving for 15, 30, and 45 min. After microengraving, live cells were stained by adding 1 μM of Calcein violet AM

(Invitrogen) on top of the arrays for 20 min; exposure to light was minimized during this step. The arrays of cells were then imaged for cell counting. Anti-ovalbumin IgG captured on the glass slides were detected by ovalbumin-Alexa 555 (Invitrogen, 2 μg/mL).

2.4 Isolation and culture of human PBMCs

Venous blood was drawn from healthy controls into green-capped, lithium heparin tubes (Kendall) with institutional Internal Review Board Approval. PBMCs were separated using density centrifugation on Ficoll-Paque PLUS (GE Healthcare), frozen at a concentration of 1×10^7 cells/mL in 10% dimethylsulfoxide (Sigma-Aldrich)/90% fetal calf serum (Atlanta Biologicals), and stored in liquid nitrogen until use. Before experiment, frozen PBMCs were thawed, washed, and resuspended at 10^6 cells/mL in RPMI 1640 medium (Mediatech), supplemented with 10% FBS, 2 mM L-glutamine, 10 mM HEPES, 100 U/mL penicillin, 100 mg/mL streptomycin, 0.1 mM non-essential amino acids, and 1 mM sodium pyruvate. Before stimulation, PBMCs were rested at 37 °C with 5% CO_2 over night. In kinetics study, $CD3^+$ T cells were isolated from thawed PBMCs by negative selection (EasySep®, STEMCELL technology) according to manufacture's instructions. Isolated T cells were suspended in HL-1 media supplemented with 10% FBS, 2 mM L-glutamine, 10 mM HEPES, 100 U/ml penicillin, 100 mg/ml streptomycin, 0.1 mM non-essential amino acids, and 1 mM sodium pyruvate. T cells were also rested over night before use.

2.5 Multiplexed detection of cytokines

For capture, 10 μg/ml of each capture antibody (IFNγ, IL-17, IL-2, and TNFα) was used to coat poly-lysine slides. PBMCs were stimulated by PMA (10 ng/mL) and ionomycin (1 μg/mL) in bulk for 6 h, stained with Calcein violet AM, loaded onto the array, and imaged in media containing the applied stimuli. The array was then washed with serum-free media and immediately applied onto a glass slide pre-coated with capture antibodies. After printing for 2 h, a mixture of labeled antibodies was used for detection (1 μg/ml for each antibody). All detection antibodies were labeled by Alexa Fluor-NHS esters according to manufacturer's instructions

(Invitrogen): IL-17-Alexa Fluor 488, IFNγ-Alexa Fluor 555, IL-2-Alexa Fluor 594, and TNFα-Alexa Fluor 647.

2.6 Kinetic measurements of cytokine secretion

For TCR-independent stimulation, resting T cells were stained with anti-CD8-Alexa Fluor 488 (Biolegend), anti-CD45RA-Alexa Fluor 568 (Biolegend), anti-CCR7-Alexa Fluor 647 (Biolegend), and live cell marker (Calcein violet AM). Labeled cells were washed and loaded into an array of 50 μm nanowells from a suspension (500 μL) with a density of 4×10^5 cells/mL. The array of nanowells was imaged and then cultured in serum-free HL-1 complete media supplemented with 10 ng/ml PMA and 1 μg/ml ionomycin, at 37 °C with 5% CO_2, for stimulation. Purified human IgG_1 (150 ng/ml) was added into the culture media to create an independent background to facilitate accurate determinations of positions for each well in the microarrays resulting from microengraving. Kinetic measurements of cytokine secretion started 2 h after stimulation and repeated every 2 h. The stimuli were included throughout both culture and microengraving. During each cycle, cytokine secretion was detected by microengraving for 1 h followed by culturing the nanowells in a large reservoir of media (30 mL) for another hour. Each round of interrogation used fresh media prepared from the same stock to allow detection of the current state of activity by individual cells. After eight consecutive microengravings, cells were stained in situ with a live cell marker Calcein and a dead cell marker SYTOX green (Invitrogen), and then imaged. For the comparison with TCR stimulation, five consecutive microengravings were performed (2-10 h).

Stimulation via the TCR was achieved by co-culturing of T cells with anti-CD3/CD28 Dynabeads® (Invitrogen). T cells were stained and loaded as described above, except that an array comprising 30 μm nanowells was used to improve the contact between T cells and beads, and to increase the number of events scored per array. The array with T cells alone was imaged first for cell staining, then beads were loaded onto the array and the array was imaged again to quantify the number of beads in each well. Kinetic measurements of cytokine secretion were performed as described above with PMA/ionomycin stimulation, except that only five cycles were performed (2-10 h). After serial microengraving, cells were stained in situ with Calcein violet and SYTOX green for viability evaluation.

In all kinetics experiments, three Th1 cytokines were measured: IFNγ, IL-2, and TNFα. For capture, 10 μg/ml of each capture antibody was used. Detection antibodies were labeled by Alexa Fluor-NHS esters: IFNγ-Alexa Fluor 555, IL-2-Alexa Fluor 594, TNFα-Alexa Fluor 647, and IgG-Alexa Fluor 700.

2.7 IL-6 measurement from PBMCs

To stimulate IL-6 secretion, LPS (10 μg/mL), PHA (5 μg/mL), or PWM (5 μg/mL) was added to human PBMCs in round bottom 96-well microtiter plates and then incubated at 37 °C with 5% CO_2. Poly-lysine slides were coated with 40 μg/mL mouse anti-human IL-6 (MAB206, R&D) and 10 μg/mL goat anti-human IgG (81-7100, Invitrogen). PBMCs were stained with Calcein violet before loading onto the array. After depositing cells onto the array, the cells were imaged under temperature and CO_2 control. During image collection, stimuli were included in the media and the array of wells was covered with a lifterslip. The array of wells was then rinsed gently with media containing a trace amount of human serum (1:40,000) and immediately applied onto a glass slide pre-coated with capture antibodies for 2 h. Alexa Fluor 488 (A20000, Invitrogen) labeled goat anti-human IL-6 (AF-206-NA, R&D) and Alexa Fluor 700 (A20010, Invitrogen) labeled goat anti-human IgG (109-175-098, Jackson Immune Research) were used for detection. To assess surface-expressed markers present on the cells after microengraving, 10 μg/ml of CD3-Alexa Fluor 488, CD11b-Alexa Fluor 568, and CD14-Alexa Fluor 660 were added on the array of wells. After incubation at 4°C for 30 min, the array of wells was washed by PBS and re-imaged.

Another portion of the LPS-stimulated PBMCs were collected for mRNA quantification by real-time PCR at intervals matched to the microengraving. RNA from PBMCs was purified using the absolutely RNA microprep kit (Stratagene). cDNA was made using a Taqman kit with supplied random hexamers (Applied Biosystems). The *β2-microglobulin* (*B2M*) and *IL-6* primers and probe were obtained from Applied Biosystems and used according to recommended methodologies. The *IL-6* gene expression is shown relative to *B2M.*

2.8 Primary cell retrieval and cloning

Memory T cells and monocytes were isolated using negative selection (Miltenyi Memory $CD4^+$ T Cell Isolation Kit and Monocyte Isolation Kit II). Memory T cells and monocytes were combined in a 1:1 ratio in the presence of LPS (100 ng/mL) and anti-CD3 (OKT3 1 μg/mL) in HL-1 media and 10% fetal calf serum for 3 days before being deposited on the array of nanowells and analyzed for IL-17 and IFN-γ secretion (2 h). The array of nanowells was incubated in culture media supplemented with 20 U/mL IL-2 for 2 days after microengraving. Cells that exhibited IFNγ or IL-17 secretion in individual nanowells were retrieved using an automated system for micromanipulation (CellCelector, AVISO GmbH) equipped with a drawn glass capillary (50-μm diameter). Retrieved cells were deposited into a round bottom 96-well microtiter plate containing irradiated PBMCs used as feeder cells for clonal expansion in the presence of PHA and IL-2. After two weeks, proliferated clones were collected, stimulated with PMA and ionomycin in the presence of monensin (BD GolgiStopT, BD Bioscience) and interrogated for cytokine expression by ICS.

2.9 Data analysis

2.9.1 Matching cell information

Data extracted from both the array of cells and the printed microarrays were matched by customized program using unique identifiers assigned to each well within the array. The matched dataset was filtered to only include the locations in the array that contained desired number of cells (in most cases, single cells) matched to secreted proteins on the corresponding microarray for subsequent analysis. In kinetics study, the combined data set was filtered to include wells occupied with single live cells both pre- and post-microengraving that yielded cytokine secretion at any of the measured time points.

2.9.2 Classification of differentiated cell types

Cytokine expression data was organized into a matrix with *m* rows and *n* columns. The number of rows corresponds to the number of observations (i.e., the number of cells within each differentiated population), and the number of columns reflects the number of variables, $n=24$ in the full data set (i.e., 8 time points×3 cytokines). A training set was defined by randomly sampling 75% of the data. An equal-sized validation set was defined by randomly sampling 75% of the data. Training data were used to identify the unique subspace (defined by select principal components) that best discriminates the given cell subtype from other subtypes. The principal components of the training data set were determined by the princomp() function in MATLAB. The minimum number of components that preserved at least 90% of the variance in each data set was preserved for classification.

Following PCA, we cycled through all combinations of the remaining components to identify the subset that offered the greatest discrimination among differentiated cell types. We preserved the minimum number of components that maximized the score of the algorithm. Then, each observation in the validation data was projected onto the reduced subspace of each differentiated cell type. The observation was classified according to the projection that resulted in the maximum Euclidian norm; the computed classification was compared with the "true" cell type as determined by surface markers. The entire classification process was iterated 10 times with a different random sampling of training and validation data. The reported percent correct classification reflects the mean results over the 10 independent runs.

Integrated secretion profile: Each cell's cytokine secretion profile was integrated into end-point data, reflecting a single measurement of cytokine secretion that spans a specified time window. As such, cytokine expression data was organized into a matrix with *m* rows and 3 columns for PCA analysis and feature selection; the top 2 principal components were used, preserving >95% of the variance.

Time-aligned data: Each cell's cytokine secretion profile was aligned to reflect the onset of cytokine activity in the first time point. When evaluating the full (8-pt) data set, only cells that originally initiated activity at the 2 h time point were preserved; all other cells were omitted from analysis. When evaluating a τ-point data set (where $\tau \leq 8$), we preserved those profiles that reflected cytokine activity within the first $8-(\tau-1)$ time points. Otherwise, the corresponding data was neglected in the given analysis.

Binary classification: In addition to classifying the four cell subtypes simultaneously, we applied the same algorithm to combinations of any two given cell subtypes to determine the accuracy of binary classification. From these results, we also computed the receiver operating characteristic (ROC) curves of the binary classification to determine the relative sensitivity of classification. We report the ROC curve from each of the 10 iterations of the classification algorithm.

2.9.3 Clustering of dynamic secretory profiles

Self-organizing maps (SOM) were used for clustering similar dynamic profiles from individual T cell responses. Analysis was performed using GenePattern (Broad Institute, Cambridge, MA, USA). For each dataset, the first three time points of time-aligned secretory profiles (2-6 h) were first organized into a matrix with m rows and 9 columns; the number of rows corresponds to the number of cells, and the number of columns reflects the number of variables (i.e., 3 time points per cytokine). Mean-centered Z scores of rates of secretion specific to each cytokine were used in the clustering algorithm.

Comparison of profiles among subsets of $CD8^-$ T cells: Dynamic secretion data from each subset were clustered independently. For each cytokine in the cluster, the average rate of secretion was set to 0 when the rate was below the detection limits determined in the experiment. Qualitatively similar clusters were subsequently combined according to the type of cytokine as well as the trajectory across the time. These combined clusters were consistent with the results obtained by a second round of SOM clustering. This analysis yielded 12 different distinct profiles among the $CD8^-$ T cells. The distributions of cells among these 12 profiles were assessed for all four subsets.

Comparison of profiles between PMA/ionomycin and TCR stimulation: An equal number of cells (n=478) were randomly sampled from each population, combined, and used for clustering by SOM. After clustering, the distributions of cells among clusters were compared between the two stimulations. The two distributions were significantly different ($p<0.0001$; chi-square test with confidence interval 0.95).

Chapter 3. A single-cell technology for multiplexed cytokine analysis

3.1 Introduction

Microengraving was first invented to detect IgG secretion from mouse hybridoma cells and later applied to detect cytokine secretion from primary human immune cells. Although these applications share similar principles of measurement, there are still several challenges when adapting this technology to broad functional assays in the immunological field.

First, most of the time, this assay relies on specific antibodies to capture and detect proteins of interests. The cost of high-quality monoclonal antibodies for cytokines is generally much higher than that of mouse IgG and other reagents in the assay. In addition, the rate of secretion of cytokines from primary cells is one or two orders of magnitude lower than the production of IgG from hybridoma cells. Therefore, the general protocol requires optimization to improve the sensitivity while reducing the amount of the reagent needed.

Second, multiplexed analysis is required in most immunological studies to generate a systematic profile of functional molecules, e.g. cytokines and chemokines, from heterogeneous populations. The original implementation was very limited with the number of analytes in a single assay (one or two). Multiple rounds of microengraving with the same set of cells are able to increase the total number of analytes, but it takes more time and labor for experiments. More importantly, the secretion profile may be highly dynamic within hours under certain conditions, and data collected at a neighboring time points may not reflect the same biological process. Therefore, it is difficult to correlate data measured from different time points and characterize multifunctional populations. Instead of multiple manipulations, it would be ideal to detect all the proteins of interest simultaneously from a single assay. To achieve this goal, a high specific, multiplexed detection format is needed.

Third, identification of the locations of wells containing responding cells will be challenging in cytokine assays. High frequencies of events and rates of secretion of IgG from hybridoma cells give strong positive signals on the entire array. These data can easily determine the location of the entire array. The sparse and weak signals of cytokine secretion from human primary cells, however, usually yield large blank areas on the image. Without sufficient events on the entire array, it is difficult to determine the exact location of the sparse signals in the array, and therefore cannot correlate the functional profile to individual cells.

To solve these problems and better adapt microengraving to detect cytokine secretion for immunological research, in this work, we first optimized the concentration of capture antibodies and conditions for antibody immobilization. Then, we expanded the technology to multiplexed assay and created an additional fluorescent channel that registers the entire array to aid data analysis.

3.2 Optimization of antibody immobilization

Standard 3×1 inch glass slides are good substrates to support antibodies in our assay system: 1) They are flat and rigid enough to resist light pressure during microengraving; 2) The standard shape and size is well adapted to many conventional instruments, e.g. microscope, slide washer, and microarray holder; 3) There are multiple choices of surface modification available; 4) They are easy to obtain and cost efficient. There are several types of surface chemistry that are commonly used for immobilizing proteins on the glass surface: epoxy, amine ($-NH_2$), aldehyde (-CHO), thiol (-SH), etc. In the original protocol of microengraving, epoxy group modified surface (Arrayit) was incubated with 100 μg/mL capture antibody in borate buffer at pH=9 (85). Epoxy groups immobilize proteins by covalently reacting with primary amine on the surface of proteins, which results permanent bond to the antibodies on the surface. Previous studies had shown that borate buffer gives the best result on epoxy slides. However, commercialized epoxy slides are relatively expensive for large numbers of measurements. Alternatively, ploy-lysine coated slides are easy to make in the lab and the cost is low. To compare the quality of immobilization of these two types of surface, we titrated the concentration of capture antibody onto glass slides and measured IL-4 using a spot assay (Figure 3.1A). The results showed a higher signal-to-noise ratio when using poly-lysine slides and the concentration of capture antibody can be reduced to as low as 10 μg/mL on this surface. Although borate buffer at pH=9 was validated for epoxy slides, here, it also shows very good results on poly-lysine slides. The binding between poly-lysine slides and protein is through electrostatic force. For pH=9, the antibody is positive charged (pI of antibody is ~7); while poly-lysine is still negative charged (pI of lysine is ~10). Therefore, borate buffer is also a good choice for poly-lysine slides. By using poly-lysine slides, the concentration of capture antibody can be decreased up to 10 times. To balance the cost of antibody and detection sensitivity, in the modified protocol, we use 25 μg/mL of capture antibody for single-cytokine assay and 10 μg/mL for each antibody in a multiplexed format (see section 3.3). We also tested several temperatures at which slides were coated: 4 °C, 25 °C, and 37 °C (Figure 3.1B). Higher temperature and longer incubation time were generally better for immobilization. For convenience in the operation, we coated our slide either at 25 °C for 1 h or 4 °C overnight. We also tested two different blocking buffers: 0.5% BSA solution and 3% non-fat milk. The result shows that blocking with milk is slightly better than BSA. This result may be because that milk powder is a mixture of proteins with diverse molecular weight and properties.

3.3 Multiplexed analysis of secreted cytokines

3.3.1 Experimental approach

The analysis of multiple cytokines concurrently is important for distinguishing different functional responses among lymphocytes and for realizing robust clinical assays where samples are limited in size. In conventional protein microarrays, multiplexed analysis is achieved by spotting different types of capture antibody separately at different locations on slides. Then, a sample is applied to a relative large area, such that all the spotted antibodies have access to the same sample simultaneously. The quantities of different proteins in the sample are identified by the spatial locations of spot on the array. However, in the format of microengraving, it is not feasible to spot different antibodies separately within each sample area, 50 μm × 50 μm, because of the limitation of protein microarrayers and the resolution of scanner. Instead of using spatial information, we use different fluorescent labeling on the detection antibody to distinguish different secretions. Therefore, in our multiplexed detection format, a mixture of capture antibodies is immobilized on the glass surface to capture multiple cytokines. After microengraving, a mixture of detection antibodies is applied and each of these detection antibodies is conjugated with a different fluorophore (Figure 3.2).

By mixing the capture antibodies, all antibodies distribute on the glass surface uniformly. Therefore, the surface density of each capture antibody is diluted by a factor of N, where N is the total number of antibodies, and has lower binding capacity than that of single-cytokine format. However, in most of the cases, where cytokine secretion is not extremely high, this diluted density does not affect the capture efficiency. A detailed quantitative analysis will be discussed in Chapter 4.

3.3.2 Choice of fluorophores

The limitation of the maximal number of cytokines that can be measured in a single assay is the number of fluorophores that match all the combinations of laser and filters in the scanner. Fluorophores that exhibit significant bleed-through of signal into other channels should be avoided. To balance the number of fluorophores and the separation of spectra, we chose five fluorescent dyes (Alexa Fluor 488, 555, 594, 647, and 700) that could be used together in one array (Figure 3.3A).

Meanwhile, implementation of our assay also benefits from resolving different phenotypes of cells in the sample. Most of the cell types are classified by the expression of different sets of surface markers. For surface staining of cells, we chose four dyes (Alexa Fluor 405, 488, 568, 660) that could be used on epifluorescence microscopes simultaneously (Figure 3.3B).

These dyes show minimal bleed-through between each other. However, when one fluorescent signal is very strong, some level of bleed-through can still be observed in neighboring channels. When this happens, we can apply compensation of signals on these channels to correct the bleed-through — a process routinely used in other assays such as flow cytometry. As a result, our system has the capacity of measuring five cytokines and four surface markers from individual cells in a single assay. The multiplicity of cytokine detection can be further extended by perform several microengraving processes consecutively.

3.3.3 Validation of antibody pairs

Besides the bleed-through between fluorophores, the cross reaction between antibody pairs is another potential cause of nonspecific detection. Therefore, in our assay, antibody pairs must have both high sensitivity and specificity. To find appropriate antibodies for our assay, we tested antibody pairs from several vendors and chose the ones that are most sensitive and specific (Table 3.1). We also measured the cross reactivity among these antibody pairs and generated three panels for different purposes: 1) T cell panel: IL-17, IFNγ, IL-10, IL-4; 2) Th1 panel: IFNγ, IL-2, TNFα; 3) Th2 panel: IL-4, IL-5, IL-9, IL-13.

Figure 3.4 shows the standard curves for a panel of T-cell-specific cytokines as an example. These antibodies have lower limit of detection of 100~500 pg/mL in our platform and exhibited no significant (< 3%) cross-reactivity at the concentrations of cytokines relevant for microengraving (~10 ng/mL).

3.4 Generation of background images for array registration

Cytokine-secreting cells generally comprise a very small fraction of total PBMCs, especially under antigen-specific stimulation (less than 1%). With such sparse number of events, it is hard to accurately correlate positive spots to the corresponding wells on the array. If we add some known cells in the sample population, e.g. some hybridoma cells, they may affect the function of the target cells and also decrease the number of single-cell wells. Therefore, we sought to highlight the outline of the array while minimally disturbing the function of cells. One solution was to include a small amount of human IgG in the assay media (~ 100 ng/mL) and meanwhile include anti-human IgG antibody pair in our microengraving process as an extra channel besides cytokines. When the array is sealed by a glass surface, the media above the array will be pushed away, while the media inside well is retained. As a result, the area on the glass surface that faces the wells has access to more media (a depth of 50 μm per area), and therefore, could capture more IgG, resulting a higher intensity of fluorescence on the image (Figure 3.5). In this way, the structure of the whole array on the chip is highlighted by the IgG signal. Since the same media is applied across the whole array, the intensity of this background channel is uniform and independent of the presence and functions of cells in wells. Therefore, this background image not only helps the localization of array, but also serves as a quality control for the assay.

Addition of human IgG in the printing media does not affect the cell function and cytokine detection. Most of our assays apply to human samples. Human IgG has a very high concentration (~10 mg/mL) in human serum and also exists in the culture media when human serum is added as supplement. Therefore, we don't expect that this small amount of human IgG in the assay media will affect the function of human cells. The total amount of IgG in each nanowell is about the same order of magnitude of the total amount of secreted cytokines, so that it can be considered as an extra analyte in the multiplexed format. Quantitative analysis in Chapter 4 shows that adding one more analyte does not affect the detection sensitivity.

3.5 Detection of four cytokines from primary human samples

To demonstrate the ability to multiplex measurements from single cells, we measured the breadth of cytokine responses of IL-17, IFNγ, IL-2, and TNFα from human PBMCs after stimulation with PMA and ionomycin. Cells were stimulated in bulk for 6 h and then loaded on the array to measure the secretion of all four cytokines simultaneously. After measurement, cells were stained in situ for viability and imaged. Figure 3.6 shows several representative images of the cells and corresponding cytokine secreting information. Single live cells in the array exhibit a range of functional profiles comprising one, two, or three cytokines. Fluorescent images from single secretors also demonstrate that different cytokines can be detected separately and distinguished clearly. With the quantitative tool we developed, these fluorescent signals can be further converted to the rate of secretion for individual cells. The method of quantification will be discussed in Chapter 4.

3.6 Recovery of single cells after measurements

Microengraving is a nondestructive process so individual cells remain viable and can be retrieved afterwards from the nanowells. To demonstrate this, we first measured IL-17 and IFNγ secretion from single cells, then retrieved cells secreting either IL-17 or IFNγ from 50-μm wells after microengraving and cultured them. After two weeks, most of the retrieved cells had proliferated (>80 % efficiency). The cytokine profiles of these clones were then analyzed by intracellular staining for IL-17 and IFNγ. After expansion, the majority of cells in each population retained their original profiles of cytokine production (Figure 3.7). These results demonstrate that incubation of primary T cells in closed nanowells for a short time (~1-2 h) does not change their viability, and that those cells can be specifically retrieved for expansion and for subsequent characterization by other analytical methods. This is helpful in screening certain functional cells and retrieving interested cells from clinical samples.

3.7 Discussion

3.7.1 Detection sensitivity

In microengraving, analytes are detected by pairs of antibodies on a solid substrate, which is similar to sandwich ELISA. One major advantage of microengraving compared with ELISA is that cells are confined in a small volume (0.125 nL per well), which results higher (~8 times) density of cell in nanowell than bulk culture (~ 10^6 cell/mL). In fact, not all the cells in culture are secreting at a given period of time, and therefore the actually concentration of active cells in bulk culture will be even lower. By confining cells in a small volume, the concentration of cytokine can reach pg/mL-ng/mL within 1-2 h, while, the concentration in bulk culture is very dilute highly depending on how many cells in the population actually secrete. However, unlike enzyme amplification in ELISA, direct labeling of fluorophore in microengraving does not amplify signal, which decreases the sensitivity in the detection step. As a result, the overall detection sensitivity is a trade-off between the concentration of analytes and the limit of signal detection.

Although direct labeling lacks sensitivity, it has advantages in quantification. Without amplification, fluorescent signal can vary linearly with the amount of molecules, which allows direct calculation of the amount of detection antibody from the fluorescent intensity (will discuss in Chapter 4). If the quantification of molecules is not necessary, there are still ways to amplify signals in the microengraving system. For instance, Choi et al. applied a hybridization chain reaction to amplify signals and improved the limits of detection and sensitivity by an average of 200-fold (86).

3.7.2 Loading efficiency

In the current protocol for microengraving, cells settle into wells randomly. The number of cells per well follows a Poisson distribution. In theory, the highest efficiency of single-cell loading by Poisson distribution is 36.8% and multiple loadings do not help increase this ratio. In our assay, by using an optimal cell concentration and loading time, we could achieve ~36% single-cell wells in a total of ~84,000 wells, which results ~30,000 single-cell loading (Figure 3.8). In order to get more single-cell events, an alternative way is to use wells with smaller diameter, such as 30 or 20 μm, to increase the total number of wells on the array. In experiments that require more cells per well, increasing the loading concentration of cells, allows us to selectively obtain more wells with multiple cells.

3.7.3 Alternative ways to increase multiplicity

The advantages for current strategy are: 1) Capture antibodies are uniformly immobilized across the slide so that there is no restriction on the alignment of array to the slide; 2) Signals from all fluorescent channels are at the same location and with the same shape, which makes analysis easy. However, the disadvantages are that the multiplicity is limited by the type and spectra of fluorescent dyes and the capability of instruments available.

To further increase the multiplicity, there are several ways that can be considered: 1) Using a combination of both shape and fluorescence to create more diverse coding for different analytes; 2) Using cleavable or reversible labeling to process the detection steps multiple times; 3) Using advanced instrument that has more choices of laser and filters to increase the number of fluorophore that can be used simultaneously.

3.8 Figures

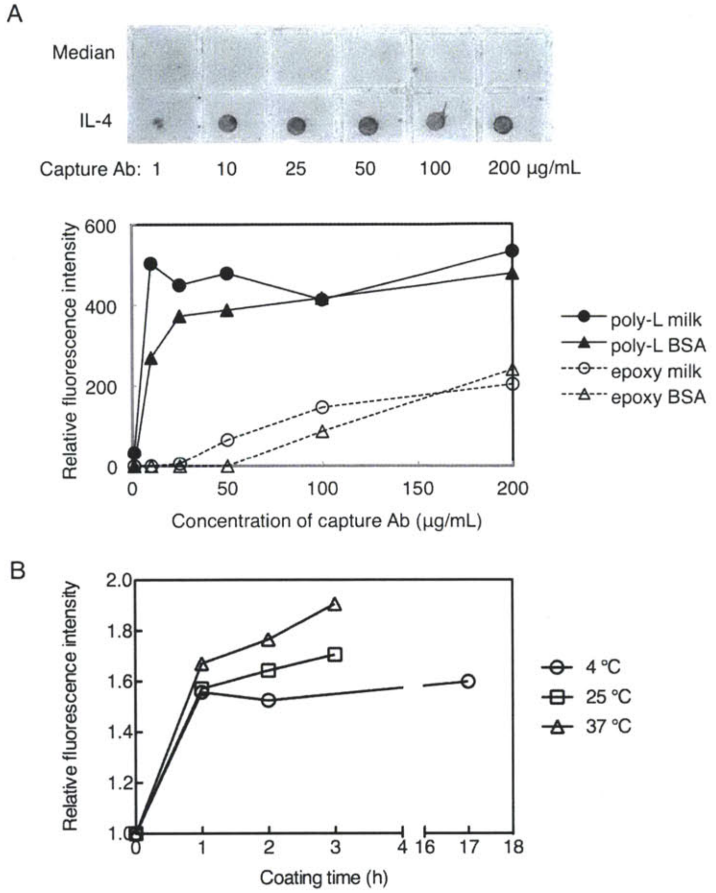

Figure 3.1 Optimization of conditions in immobilization of capture antibody. (A) A gradient of IL-4 capture antibody was spotted on the surface of glass slides (either poly-lysine or epoxy surface), 2 µL/spot. After incubation at 25 °C for 2 hours, the slides were blocked with either 1% BSA or 3% non fat dry milk in PBS for 30 min. Standard IL-4 (500 pg/mL) were added to each spot and incubated for 1 h at 37 °C. Then, 1 µg /mL of IL-4 detection antibody conjugated with fluorescent dye was applied as detection reagent. For the control (background), no IL-4 standard was added. (B) Capture antibody of IL-4 (25 µg/mL) was spotted on poly-lysine glass slides and incubated at 4°C, 25 °C, and 37 °C for several incubation periods. Slides were then blocked with 3 % non fat milk, incubated with 500 pg/mL IL-4 standard for 1 h at 37 °C, and detected by 1 µg/mL detection antibody.

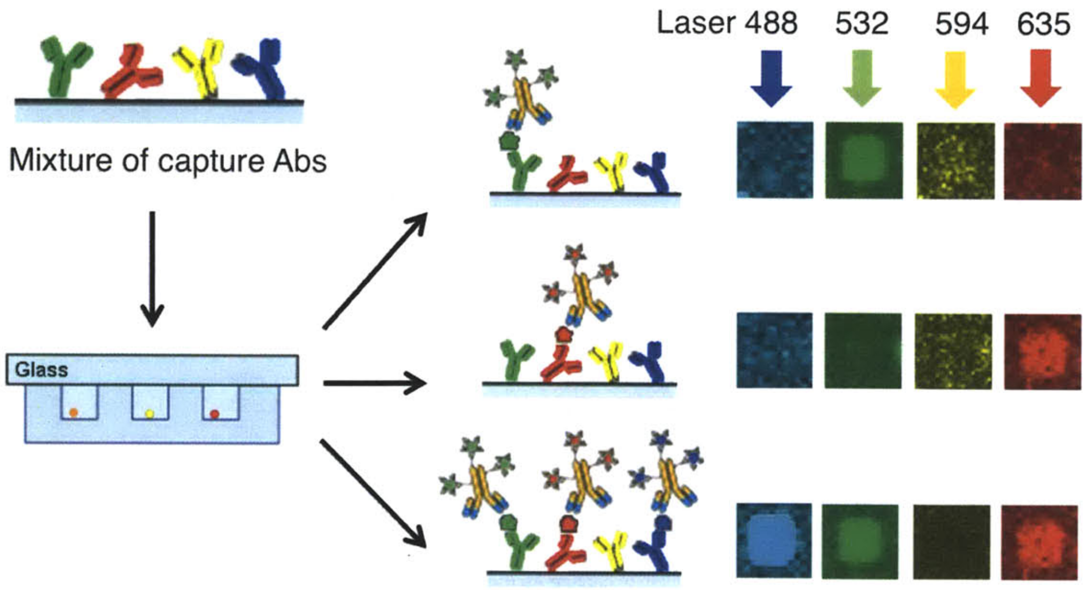

Figure 3.2. Strategy of multiplexed detection of cytokines. A mixture of capture antibodies is immobilized on poly-lysine slide with equal concentration so that different secretory analytes can be captured simultaneously during incubation. After microengraving, all detection antibodies are applied on the slide at one time, where each type of detection antibody is conjugated with a different fluorophore. Images are acquired and analyzed in all fluorescent channels separately.

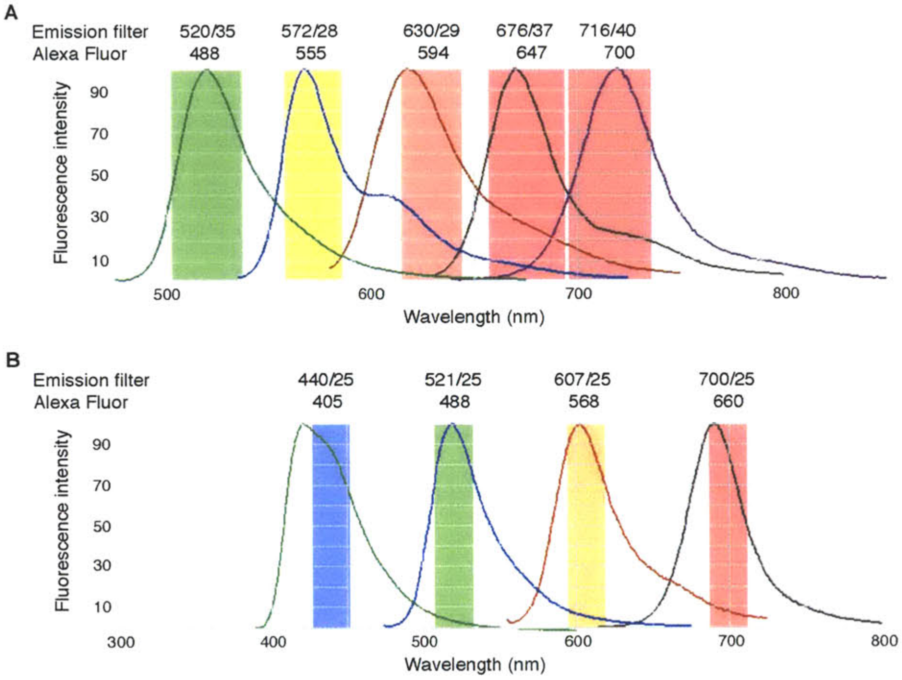

Figure 3.3 Emission spectra of fluorophores and filter sets. (A) Five Alexa Fluor dyes was chosen for different filter sets in microarray scanner. Alexa Fluor 488, 555, and 594 was excited by laser at 488 nm, 532 nm, 594 nm, respectively. Alexa Fluor 647 and 700 are excited by the same laser 635 nm, but the emission signals are acquired through different filters. (B) Four Alexa Fluor dyes are used for microscope and each of them was excited by separate lasers.

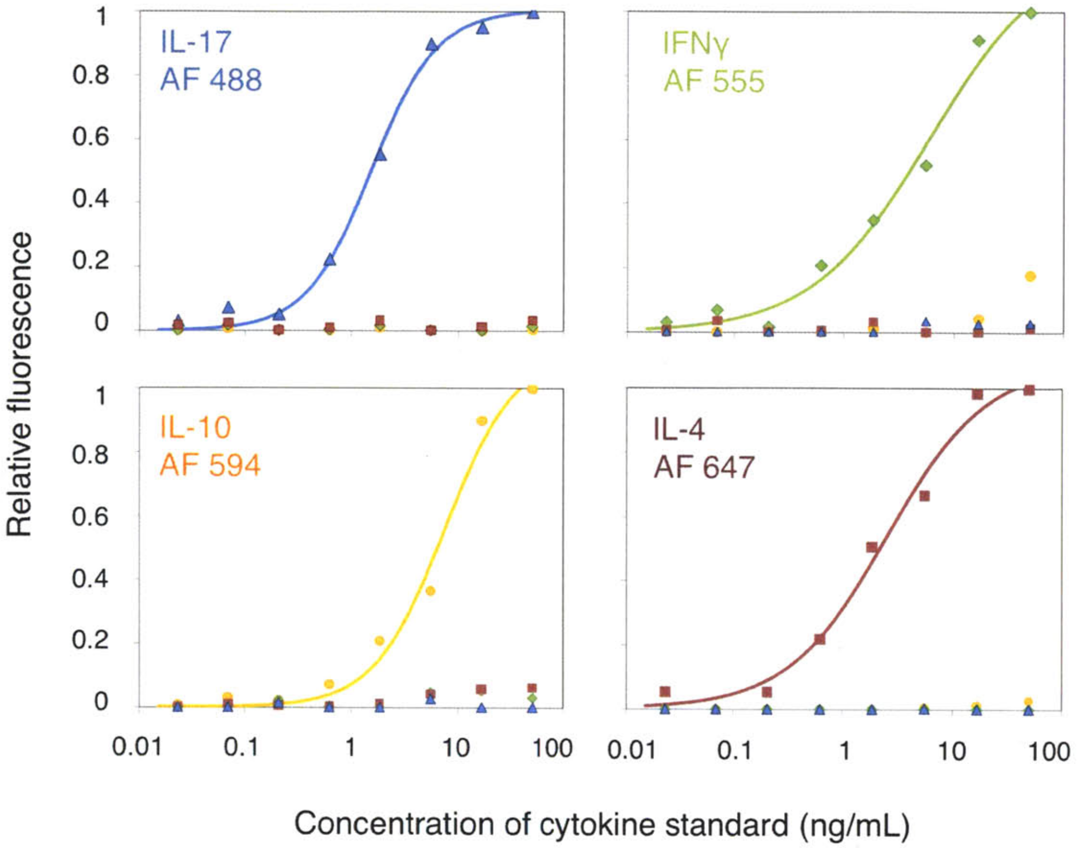

Figure 3.4 Sensitivity and specificity of four cytokines from T cell panel. Mixture of four capture antibodies (IL-17, IFNγ, IL-10, and IL-4) were spotted on poly-lysine glass, 25 ug/mL per antibody, 1 μL per spot. For each standard curve, gradient of single cytokine standard was added. Then a mixture of detection antibody was applied to all curves, where each detection antibody was labeled by different fluorescent dye. For each curve, fluorescence signals from all the four channels were recorded and plotted in the same graph, e.g. slide using IL-17 standard was scanned at IL-17 channel shows the standard curve (blue curve in IL-17 panel), while IL-17 signals from other channel show the noise of IL-17 in other cytokine detection (blue curves in other three panels).

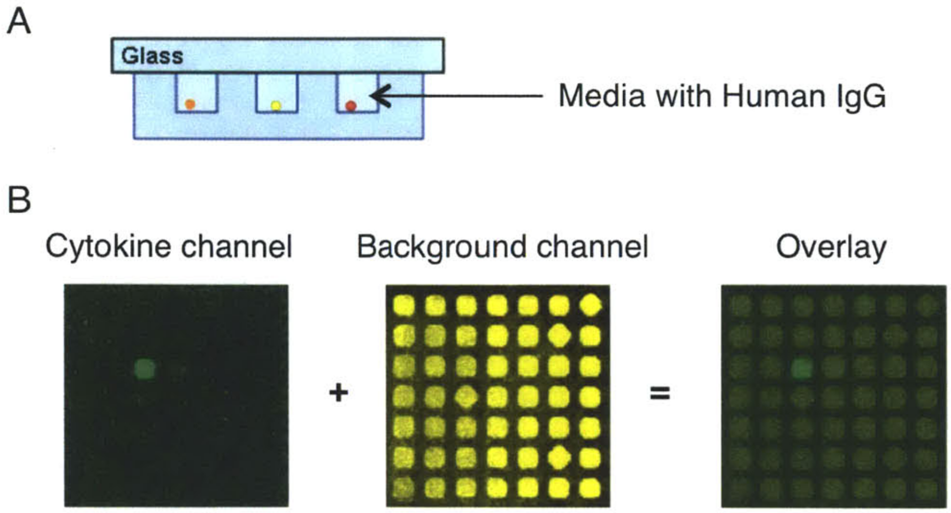

Figure 3.5 Generating background of the entire array. (A) Human IgG is included in the printing media to create an outline of array. (B) Amount of IgG captured on the glass slide was scanned using a separate channel from cytokine signals. By merging two images, the location of positive secretion spot was highlighted on the background grid.

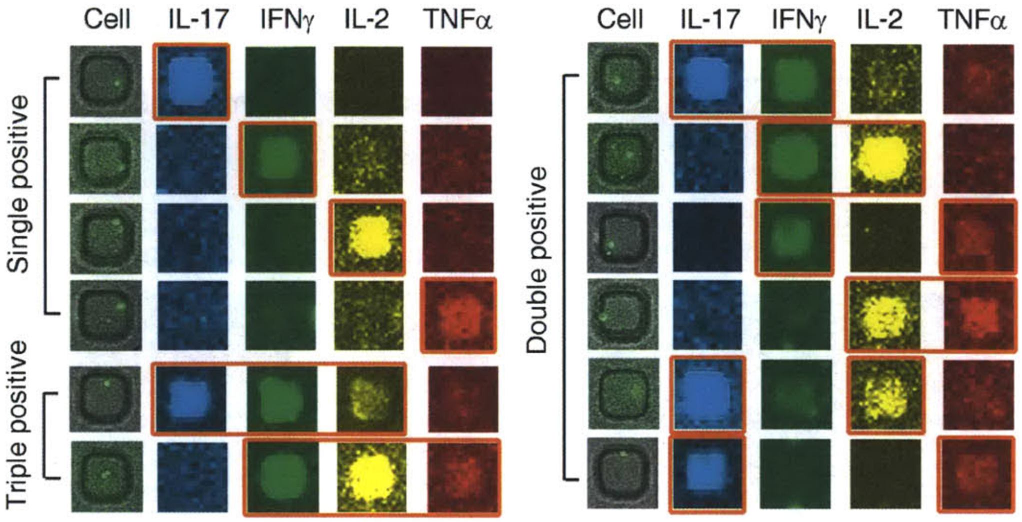

Figure 3.6 Multiplexed detection of cytokine secretion from PBMCs. Human PBMCs were stimulated with PMA and ionomycin for 6 h, followed by microengraving for 2 h. Representative images of individual cells in microwells matched with micrographs from the corresponding microarray of cytokines (arranged in rows) are shown. The first column shows composite micrographs of microwells (phase contrast) and viable cells (Calcein AM). The remaining four columns are micrographs extracted from the matching location on the printed microarray for each of four cytokines (IL-17, blue; IFNγ, green; IL-2, yellow; TNFα, red). Orange boxes outside the images indicate the positive spots in each row (MFI > background + 3SD).

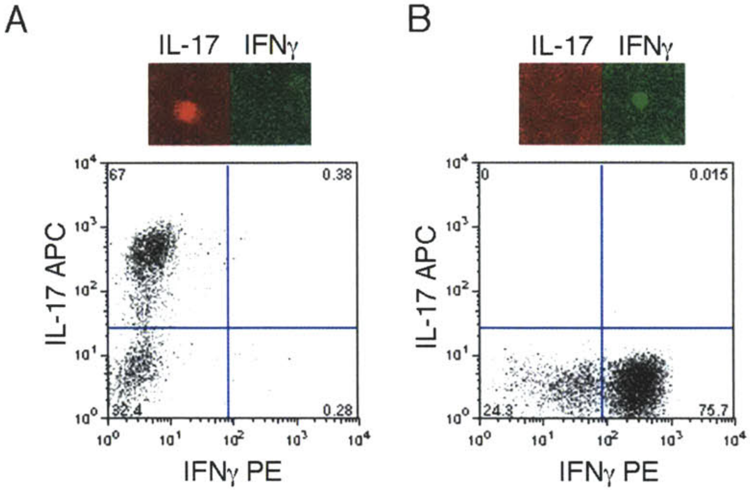

Figure 3.7 Recovery and expansion of T cell lines selected by their cytokine profiles. T cells were stimulated with LPS-activated monocytes and anti-CD3 for 3 days, and then their cytokine profiles were determined by microengraving (2 h). The cells were cultured in the microwells for 48 h after microengraving, and then recovered by micromanipulation. The selected cells were expanded on irradiated PBMCs for 2 weeks, and then characterized by flow cytometry and intracellular staining. Fluorescent micrographs (top panels) indicate the cytokine profile measured by microengraving for (A) IL-17 secreting cells and (B) IFNγ-secreting cells. The number of cells present in both wells at the time of retrieval was four. The scatter plots (bottom panels) show the results of intracellular cytokine staining detected by flow cytometry. The expanded cells were stimulated with PMA/ionomycin in the presence of monensin, then fixed, permeabilized, and stained with antibodies against IFNγ (labeled with phycoerythrin (PE)) and IL-17 (labeled with allophycocyanin (APC)). Cytometry data were plotted in the graph according to the fluorescence intensities measured from both channels.

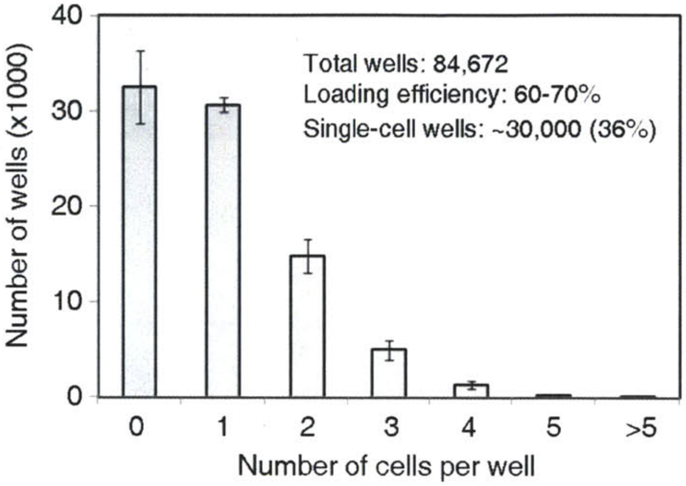

Figure 3.8 Distribution of cells in nanowells. By controlling cell density and loading time, normally ~30,000 single-cell wells can be achieved on one array. Data were collected from 5 independent experiments.

3.9 Tables

Cytokine	Clone	Vendor
IL-2	Cap. 5355	R&D
	Det. Polyclonal	R&D
IL-4	Cap. 8D4-8	BD, Biolegend
	Det. MP4-25D2	BD, Biolegend
IL-5	Cap. JES1-39D10	BD
	Det. JES1-5A10	Biolegend
	Cap. TRFK5	Mabtech
	Det. 5A10	Mabtech
IL-6	Cap. 6708	R&D
	Det. Polyclonal	R&D
	Cap. MQ2-13A5	BD
	Det. MQ2-39C3	Biolegend
IL-9	Cap. MH9A4	BD
	Det. MH9A3	Biolegend
IL-10	Cap. 127107	R&D
	Det. Polyclonal	R&D
	Cap. JES3-19F1	BD
	Cap. JES3-9D7	BD
	Det. JES3-12G8	BD, Biolegend
IL-13	Cap. 32116	R&D
	Det. Polyclonal	R&D
IL-17	Cap. eBio64CAP17	eBioscience
	Det. eBio64DEC17	eBioscience
IFNγ	Cap. 1-D1K	Mabtech
	Det. 7-B6-1	Mabtech
TNFα	Cap. MAb1	BD, Biolegend
	Det. MAb11	BD, Biolegend

Table 3.1 Antibody pairs used in microengraving.

Chapter 4. Analytical characterization of microengraving process

4.1 Numerical simulation of system with single analyte

4.1.1 Model

To understand the dynamic distribution of secreted analytes in a nanowell during microengraving, we developed a numerical model that accounts for the secretion of proteins from cells, the diffusion of those proteins in a confined volume, and the binding of those proteins onto a surface bearing antibodies with specific affinities for the secreted analytes. The geometry of this model derives from one well in the array: a single cell is confined in a cubic container (50 μm in each linear dimension) that comprises a bottom and four sidewalls manufactured in poly(dimethylsiloxane) (PDMS) and a top defined by a glass surface. In the simplest embodiment of the model, the cell only secretes one type of protein and top surface of the reactor only supports capture antibodies specific for this analyte (Figure 4.1A).

We made three assumptions that simplified the model and subsequent numerical simulations. First, the transport of analytes in the media results only from diffusion, because there is no active flow or exchange of fluids in the sealed nanowells during incubation. Second, PDMS surface is impermeable to analyte and the adsorption of analyte on these surfaces is negligible. In microengraving, the array is typically treated with a buffered solution containing bovine serum albumin (BSA) or culture media with 10% bovine serum prior to depositing cells into the wells. These treatments may not eliminate nonspecific adsorption completely, but nonspecific capture on BSA/serum-treated PDMS should be significantly lower than the specific capture on the glass slide. We, therefore, considered this nonspecific interaction to be negligible in the model. Finally, we assumed that proteins were secreted from the cell at a constant rate (κ). The total quantity of protein released from the cell in the volume of the reactor, therefore, increases monotonically with time:

$$N_{\text{total}}=\kappa t$$

where N_{total} is the total number of molecules secreted from the cell, κ is the rate of secretion, and t is the incubation time. The rate of secretion for a live cell likely fluctuates in time depending on extrinsic factors such as the quality of its environment as well as intrinsic factors such as its secretory capacity and its state in the cell cycle (87). Nevertheless, the assumption of a constant rate in this model is useful for first understanding the relationship between the amount of protein secreted and the amount captured on the glass surface at any point in time.

The model comprises two equations that describe the diffusion of proteins from the secreting cell and their capture onto the functionalized surface, respectively. The equation for the diffusion of protein inside the volume of a closed well is:

$$\frac{\partial C}{\partial t} - D\nabla^2 C = 0$$

where C is the concentration of analyte in the media and D is the diffusion coefficient of analyte. The reaction of the secreted analyte with the capture antibody supported on the glass surface is described by a reversible process:

$$\text{Analyte+Ab} \underset{k_{\text{off}}}{\overset{k_{\text{on}}}{\rightleftharpoons}} \text{Analyte} \cdot \text{Ab}$$

The boundary condition describing the dynamics of adsorption and desorption of the proteins on the glass surface, therefore, is:

$$\frac{\partial C}{\partial t} = -k_{\text{on}} \cdot C \cdot (\theta_0 - C_{\text{s}}) + k_{\text{off}} \cdot C_{\text{s}}$$

where k_{on} is the rate of association, k_{off} is the rate of dissociation, C_{s} is the concentration of analyte-antibody complex on the glass surface, θ_0 is the density of total binding sites on the surface. θ_0-C_{s} describes the density of remaining binding sites available on the surface. In the experimental protocols for microengraving, the surface of the nanowells containing cells is rinsed with fresh media immediately before sealing the array with the glass slide. This process dilutes the preexisting analytes in well by more than 10^5-fold. Therefore, we assume the concentrations of analyte both in solution and on the surface are initially negligible (C=0, C_s=0, and $\theta=\theta_0$ at t=0).

The parameters describing the biophysical properties of the cells and the analytes of interest were determined from typical values reported in the literature. Lymphocytes range in diameter from ~5 μm to 20 μm. Cytokines (~15-45 kDa) and antibodies (~150 kDa) exhibit diffusion coefficients (D) on the order of 10^{-9}-10^{-11} m^2/s (88, 89). In this model, we fixed the diameter of the cell and the diffusion coefficient of the analyte to 10 μm and 10^{-10} m^2/s, respectively. For the binding affinity of the antibody and the rate of secretion, we tested a range of different values in the model based on similar values reported previously in the literature (88, 90, 91). The values of parameters used in the simulations described here are listed in Table 4.1.

4.1.2 Results

COMSOL Multiphysics 3.3 (COMSOL Inc., Stockholm, Sweden) was used to solve the partial differential equations relating the secretion, diffusion, and binding of analytes with a specific capture antibody. The calculation provided the spatial concentration profile of analyte in the confined volume as a function of time. For each time point, we integrated the total quantity of analytes in the media and on the glass surface, respectively (Figure 4.1B). The results suggest that the entire process involves three characteristic temporal regimes. Immediately after sealing the cell inside a well, the quantity of analytes in solution exceeds that present on the surface. After a short time (~30 min for a cell secreting 10 molecules/s), a steady-state distribution of analyte is reached in solution, varying from a high concentration around the cell to a low concentration at the surface of the glass. This steady-state distribution is reached at approximately the same point in time regardless of the change of diffusion coefficient for the analyte (10^{-9}-10^{-11} m^2/s). In the ensuing period of time, the analyte accumulates predominantly on the surface rather than in solution. The quantity of analytes captured on the surface increases at a rate reflecting the rate of secretion from the cell ($dN_{surface}/dt \sim \kappa$), while the concentration of analytes in the media remains nearly constant (~pM). Eventually, the quantity of analytes on the surface approaches the total number of available binding sites on the surface ($C_s \sim \theta_0$). At this point (>27 h), the rate of capture at the surface decreases, and the concentration of analytes in the media increases, rapidly approaching the total concentration of analytes secreted.

4.2 Effects of system parameters on the efficiency of capture

The simulations indicate that the intermediate temporal regime (t~30 min to 27 h) represents the ideal period to measure the average rates of secretion for each cell in the array. The viability of mammalian cells in the sealed nanowells, particularly primary cells, declines significantly after 4-6 h; this constraint establishes a practical upper bound on the length of time that is feasible for microengraving to less than 4 h (77, 78). Within this range of time, we used our model to understand how some of the system parameters influence the efficiency of surface capture in the intermediate regime.

For antibodies with high affinity, e.g. K_D~100 pM, the amount of protein captured on the surface closely approximates the total amount of protein secreted during the incubation ($N_{surface}$~95-99% N_{total}). However, decreasing the binding affinity could significantly affect the total quantity of bound proteins, especially when K_D is higher than 10 nM (Figure 4.2A). The commercial antibodies used in this work have K_D~10-100 pM from ELISA measurements provided by the manufacturers. For these antibodies with high quality, we could reasonably assume that variation of affinity will not introduce significant error to the assumption $N_{surface}$~N_{total} in quantification.

The number of binding sites available on the surface (θ_0) also determines how fast the capture occurs. The calculations show that increasing θ_0 improves the accuracy of the quantification (Figure 4.2B). The optimal range of θ_0 (~10^{-9}-10^{-8} mol/m^2) is consistent with the typical saturating densities of antibodies immobilized on hydrophilic surfaces (glass) from buffered solutions measured by optical reflectometry (92, 93), surface plasmon resonance (94), and spectroscopic ellipsometry (95). Our own measurements indicate that θ_0 on the poly-L-lysine slides is also in the order of 10^{-9}-10^{-8} mol/m^2.

For a cell secreting at a constant rate, the model predicts that the accumulated signal on the binding surface increases linearly with the time. This trend implies that the total amount of analyte captured by microengraving for a given cell over a fixed period of time is a measure of its average rate of secretion. Simulations for the number of analytes accumulated on the surface after a fixed time (2 h) suggest that poor binding affinity of the capture antibody could lead to an underestimation of the absolute rate of secretion by approximately two fold (Figure 4.2C). Together, these calculations imply that there is a relatively large range of the operating parameters that give an accurate estimation of rates of secretion in our system. In the case when some parameters are out of the optimal range, the rough estimation still yields a result with an error no more than two to three fold. However, if values of these parameters are known, it is also feasible to use this model to calculate a coefficient to correct the deviations.

Geometric parameters, such as the size and shape of the well and even the position of the cell in the well, could also impact the distribution of secreted analytes. The design and fabrication of the microarray by replica molding determines the physical geometry of the wells, but the position of the cell in each well can vary. Through experimental observation, cells usually settle randomly on the bottom of each well, but they occasionally adhere to the sidewalls. Therefore, in other models, we placed the cell at different locations in the well. The calculations suggest that the position of the cell within the well influences the rate at which a steady-state distribution of analytes is reached in solution during the initial stages of the process, but that it does not affect the predicted range of time for the quantitative capture on the surface (Figure 4.2D). This result implies that the location of the cell inside the well is not important, and that the signals detected from different wells across the same array are comparable. These results also indicate that changing only the depth of the nanowell within the same order of magnitude does not significantly alter the sensitivity of the assay. Changing the surface area exposed to the confined volume, namely the area of the across section of the well, does not affect the initial rate of binding, however, it changes the total number of binding sites per well, thus alters the time to saturation. For a fixed time of incubation, decreasing the exposed surface area increases the density of captured molecules on the surface and therefore improves the signal-to-noise ratio of spots. For lower secreting proteins, therefore, using wells with smaller cross-sectional area will increase the detection sensitivity.

4.3 Numerical simulation of multiplexed system

The basic model discussed above provides systematic characteristics of analyte capture in the nanowell. In reality, however, the system is more complicated: cells may secrete multiple proteins at different rates and multiple antibodies may be immobilized on the glass surface. To characterize the influence on quantitative analysis by nonspecific binding, in this section, we discuss three expanded models: 1) multiple cytokines vs. single capture antibody, 2) single cytokine vs. multiple capture antibodies, and 3) two cytokines vs. two antibodies. The combinations of these models could cover all experimental scenarios.

In the first model, more than one secreted protein exists in the media while only one type of antibody is immobilized on the glass surface (Figure 4.3A). The nontargeted molecules can be either secreted cytokines that are not of interest in the experiments, metabolic molecules from the cells, or even components in the culture media. For all those nonspecific molecules that may potentially influence our assay, we considered them together as secreted irrelevant molecules to simplify the model. Nonspecific binding might compete with the target analyte for binding on the surface, especially when the quantity of nonspecific molecules is much higher than the target analyte. Here, we first kept the rate of both specific and nonspecific secretion the same and tested a range of K_D for nonspecific binding. The calculations show that when the K_D of nonspecific binding is more than two orders of magnitude higher than the specific ones, nonspecific binding does not affect the specific binding within the practical time window (Figure 4.3B). The nonspecific K_D for most antibodies is in the order of 1μM-10 μM. Within this range, increased nonspecific secretion does not affect the specific binding either, although the total nonspecific binding increases with the increase of nonspecific secretion (Figure 4.3C). Together, when the binding sites are sufficient on the surface, specific and nonspecific binding are independent, and the quantity of specific binding in most cases is more than two orders of magnitude higher than that of the nonspecific binding. In the detection step, detection antibodies selectively bind to target analytes, which further lower several orders of magnitude of the noisy signal from nonspecific bound molecules. Therefore, in this case, the nonspecific binding is negligible.

In the second model, there is only one type of secreted analyte in the media while several types of capture antibodies are immobilized on the surface. Different from the first model, nonspecific binding is defined here as the binding of the target analytes to nonspecific capture antibodies. Once the analytes bind on the surface, no matter whether they are through specific or nonspecific binding, they will be detected by the detection antibody and contribute to the final intensity of fluorescent signal. For good antibodies, e.g. K_D=100 pM, the nonspecific binding normally does not cause large error: <2%, even when only 1/10 of the area is coated with specific antibodies (Figure 4.4A). For antibodies with low affinity, e.g. K_D=10 nM, when nonspecific binding affinity is less than 1000-fold lower, there is a significant increase of the nonspecific binding. Therefore, in this model, when there are both specific and nonspecific antibodies on the surface, analytes prefer to bind on the specific antibody first because of the higher reaction rates. When more types of antibodies are coated, the nonspecific reaction starts to increase significantly because of the increased density of nonspecific antibodies on the surface. Nevertheless, if there is only one type of analyte in the system, the nonspecific binding does not cause significant error in the final quantification, since the sum of specific and nonspecific binding is the same as if there is only specific capture antibody. Therefore, as long as the specific binding sites are not saturated, the total amount of analytes captured is approximately equal to the total secretion. However, nonspecific bound analytes may dissociate from the surface in the later steps of the process, thus still brings error in the quantification.

In the third model, cells secrete two types of cytokines simultaneously and both of the corresponding antibodies are immobilized on the surface. In this case, nonspecific binding possibly exists for both cytokines. However, the calculation shows that the chance of nonspecific binding is very small, even when the secretion rate is 100 times different between the two analytes (Figure 4.4B).

In summary, our calculations indicate that when highly sensitive and specific capture antibodies are used, the nonspecific binding from multiplexed detection is negligible. Most of the time, these criteria for antibodies are easy to be satisfied if selected antibodies are already qualified for quantitative analysis in the basic model. Therefore, all the characteristics of diffusion and surface binding of single analyte in the basic model also apply to multiplexed format and the rate of secretion for each cytokine can be quantified independently.

4.4 Validation of computational results by experiments

Our model suggested that the amount of proteins from individual cells captured on a binding surface should increase monotonically with the time during microengraving. To validate this conclusion experimentally, we measured the quantities of IL-6 released from individual PBMCs after stimulation with a Toll-like receptor agonist, LPS, for 48 h. PBMCs from the same stimulated population were loaded onto three arrays, and then the secretion of IL-6 was measured by microengraving for 1, 2, and 3 h, respectively. Although the MFI of IL-6 secretion captured from individual cells varies largely within each time point, the overall median values of the MFI showed significant and linear increase with time (Figure 4.5). This result matches the response predicted by the numerical simulations.

The simulations also indicate that variations in intensity measured at a fixed period of time for microengraving should increase monotonically with increased rates of secretion. To test this result, we used a mouse hybridoma cell line, which secretes mouse IgG with relatively small heterogeneity among individual cells compared with primary PBMCs. The secretion of IgG was measured by microengraving at three different periods of incubation: 15, 30, and 45 min. For each fixed period, we analyzed the quantity of total captured IgG from wells that contained 1, 2, or 3 cells to mimic the situation where cells from different wells have different rates of secretion. The results were consistent with the prediction that MFI increases linearly as the number of cells increase in the wells (Figure 4.6). The slope of the linear regression also increases as the incubation time increases from 15 min to 45 min, which is again consistent with the previous conclusion that the quantity of captured protein increases with the incubation time. These data demonstrate that the variations in MFI of captured protein at a fixed time point reflect the variations in the amounts of protein secreted by individual cells, and, therefore, in the average rates of secretion per cell.

4.5 Calculation of the rate of secretion from single cells

4.5.1 Identification of positive signals

After microengraving, the background image generated by IgG was first used to align the template of array to determine the locations of wells. Then, the MFI of each fluorescent channel corresponding to cytokine secretion was extracted. Positive spots in individual channels were required to match the following criteria, applied serially: diameter of spots within 100-250% of well size, no saturation pixel (%Sat.=0), degree of foreground covariance (FCV) below 60, signal-to-noise ratio (SNR) above 2, and foreground intensity at least 50% chance greater than 2 standard deviations above the local background around each well (%B+2std). These criteria—analogous to those used in high-throughput screening—flagged wells where one of the channels had signal distinct from the local background that were also uniform in appearance on a scale of ~50 μm × 50 μm.

We also established a second, self-consistent reference for the background MFI of wells in the array with no secretion. Features on the images were flagged as background spots when they met the following criteria: %Sat. =0, FCV < 45, SNR<1, and %B+2std<25%. These wells exhibited no distinct differences from the background signal, and provided a reference independent of regional variations that may have resulted from contact between the PDMS and glass. The mean MFI of all background wells was subtracted from positive spots, and these background-corrected values were used to calculate the rates of secretion (Figure 4.7).

4.5.2 Calculation of the rate of secretion

To convert MFI into a rate of secretion, we used a reference slide comprising known amounts of fluorescent detection antibody to produce a standard curve, which related the MFI to the surface density of each detection antibody. Then, background-corrected MFI of positive spots were converted to the amount of detection antibody on each spot using the standard curve (Figure 4.8). Based on the estimated density of binding sites on the surface, if each capture antibody only binds one cytokine, the average distance between cytokines is ~36 nm, more than twice of the size of IgG (~15 nm). For short periods of incubation (30 min-4 h), the model suggests that the fraction of binding sites occupied with cytokines (κ=10 molecules/s) is less than

10%. This low occupancy makes it reasonable to assume that, under the typical experimental conditions employed for microengraving, the distance between bound cytokines will be large enough to only allow each detection antibody to bind to one cytokine. Therefore, the molar ratio of captured proteins to labeled monoclonal detection antibodies is approximately 1:1, and the total number of cytokine captured on the surface is equal to the number of detection antibody. Dividing this number of molecules by the time of incubation yields the average rate of secretion from a single cell, with a unit of molecules/s.

4.6 Detection limit

The values and variation of the MFI of the non-secreting background spots determine the limit for identifying positive spots from the image. Here, we set our threshold equal to the mean value of the non-secreting wells plus 1~3 standard deviations, depending on how stringent the threshold needs to be in different experiments. This additional cut-off provides a more stringent reference for defining the lower limit of detection for each cytokine. The limits of detection for several cytokines that we have measured in our system normally range from 0.5-4 molecules/s (Table 4.2). These values are at least 10 times lower than those previously calculated for artificial receptor assays, and in most cases, are lower than those for encapsulation assays. Since the detection limit is determined by the distribution of the MFI of the background spots, it largely depends on the quality of the antibody pairs as well as the experimental operation. Therefore, this limit is highly experiment-dependent. Intensities of background spots and other nonspecific staining on the image are unlikely to change with the incubation time. Increasing the time of incubation will help increase the positive signals while keep the background unchanged, which erodes the detection limits. This strategy is important for measurement of proteins with extremely low rate of secretion.

4.7 Discussion

4.7.1 Dynamic capture vs. equilibrium capture

Microengraving is a dynamic capturing process where analytes are fluxing into the system from cell membrane. The concentration of analytes in the media reaches steady-state at some point based on our simulation, but it never reaches equilibrium. This characteristic contrasts other assay, e.g. ELISA, where the total amount of analytes is usually unchanged in the system. After sufficient time of incubation, the distribution of analytes in the media and on the surface will reach equilibrium, governed by the K_D and θ_0. After incubation for 2.8 h (stimulated for 10000 s), 98.99% of the total secreted proteins is captured in microengraving from the model. For the same amount of total analytes, if we convert all of them to an initial concentration in the volume of a nanowell, remove cell from the system, and let the process of capture reach equilibrium, then the maximal binding of protein will be 99.47%, which is the theoretical upper limit of total binding. Although it is never possible for the capture to reach equilibrium in the nanowell because the cell is alive and keeps secreting, these calculations show that the dynamic capture is actually very efficient and the error is only 0.48% compared with equilibrium process, which is below the variations of background fluorescence (~1%).

If this small difference is tolerable in the quantification, theoretically, we could generate a standard curve using equilibrium measurement (similar as the standard curve in ELISA) for quantification of the secretion. The advantage of this method is that all the slides and steps are processed under the same conditions that could minimize any systematic errors. However, the challenge for this method is the scale of the system. In order to directly compare signals between standard curve and samples, it requires that standard curve is made in a setting where the volume of media per unit capture area is the same as that in microengraving, e.g. 50 μm of height per area. Different volume to surface ratio could bring large difference in the status of equilibrium and cause the data incomparable. Because of the difficulty in making comparable equilibrium standard curve, in this study, alternatively, we chose a direct way to estimate the number of bound molecules.

4.7.2 Error of estimation

The overall error in direct estimation of the rate is contributed by both approximations from our simulation and the uncertainties of measurements in the experiment. In the calculation discussed in section 4.5, the rate of secretion is proportional to a combination of several measurable parameters in the system:

$$\kappa \approx \frac{MFI_{\mu E} \times Area_{\mu E} \times C_{std} \times V_{std}}{a_{simulation} \times t \times MFI_{std} \times Area_{std}}.$$

$MFI_{\mu E}$ and MFI_{std} are the mean fluorescence intensity of spots from microengraving and the reference slide, respectively. The uncertainty is ~1.5%, which is determined by the performance of the microarray scanner.

$Area_{\mu E}$ is the area of spots identified in microengraving. The resolution of our scanner is 5 μm, and the typical measured width of each spot is ~60 μm (slightly bigger than that of design). This yields a relative uncertainty of 8% in one dimension and 16% in area. $Area_{std}$ is the area of the spot on reference slide. The diameter of each spot is ~2 mm, which yields an error of 2.5% in diameter and 5 % in area.

C_{std} is the concentration of fluorescent detection antibody spotted on the reference slide. The uncertainty of measurement is 2% based on the accuracy of the spectrometer (Nanodrop).

V_{std} is the volume of the fluorescent detection antibody spotted on the reference slide. The uncertainty of measurement is 2.7% based on the accuracy of the pipette.

$A_{simulation}$ is a constant from simulation. Based on our calculation, the total molecules binding on the surface is approximate to the total molecules secreted from cells (>95%). Therefore, the relative error from the approximation is 5%.

t is the incubation time. The error is about 1% (1-2 min variation in time during operation for 1-2 h incubation).

All these uncertainties of parameters were either estimated by our own measurements or provided by the manufacturers. Based on the rule of error propagation, the uncertainty for the rate of secretion measured from a given cell is about 18%. The uncertainty of the area of individual spots on the microarray (16%) was the dominant source of error. The spatial resolution of the scanner employed (5 μm) significantly limits the precision of this measure.

4.7.3 Optimal incubation time for microengraving

Considering all the calculations through this chapter, we produced a graph describing the upper and lower limits of detection in the system that could guide the design of experiment. The steric crowding of cytokines and antibodies on the capture surface at high occupancy (~95% θ_0) establishes an upper bound of binding capacity, while the minimal detectable density of captured analytes determines the lower limit of detection. Larger cross sectional area per well provides more binding sites, and therefore it takes longer to saturate the surface. For a specific design of well, the total binding site is fixed. Therefore, higher rate of secretion takes less time to saturate the surface. The lower limit is basically determined by the detectable noise of background spots by the scanner, e.g. 3 SD of background signals. Assuming that the detection limit is equal to the amount of cytokines that bind to 50 μm × 50 μm area for 2 h at a rate of 0.5 molecules/s (typical order of magnitude for most cytokines we measured), then we can generate a line for lower limit, where the minimum time required for detection is inverse proportional to the rate of secretion (Figure 4.9). Taken together, the calculations discussed here indicate a more general rule to design a given experiment. The optimal incubation time should consider the rate of secretion of both lower and higher secretors in the population. The incubation time should be longer than the time when the signal acquired from the lowest secretor is above the detection limit, while shorter than the time when the highest secretor saturates the surface. From this graph, for a given experimental time, the dynamic range of rates of secretion that could be detected spans around two orders of magnitude, which indicates that this system is very robust to measure highly heterogeneous populations.

4.7.4 Capture efficiency in different systems

Using simulation tools, we compared the capture efficiency across several formats of assay: 1) closed well with one capture surface, 2) open well with one capture surface, and 3) open well with three capture surfaces (Figure 4.10). Under the same condition, closed system confines all the analytes in the volume and has the highest capture efficiency (98.5%). In both open systems, the large amount of bulk media outside the well forms a constant gradient of concentration that drives the diffusion of analytes away from the well and competes with the surface capture. Open system with one capture surface on the bottom is a model analogous to ELISpot. In this case, only 73% of the analytes bind to the surface and the rest of them diffuse away (Table 4.3). Increasing the area of capture surface, e.g. coating all three surfaces inside the well with capture antibodies, could largely improve the capture efficiency to 90%. However, increased area of capture surface decreases the density of captured analytes. Therefore, compared with a closed system, an open system with three capture surfaces has lower signal per area, which may decrease the sensitivity of detection. In sum, from the calculation, a closed system as used in microengraving is more effective in capturing analytes and this assay format also eliminates the cross-contamination of detection between different wells.

4.7.5 Profile of concentration in the microenvironment

Regarding the microenvironments surrounding cells, microengraving is also a process to deplete the secretory proteins from individual cells. To evaluate how significantly the cell environment is changed during microengraving, we compared the concentration of proteins in the media during microengraving and single-cell culture (Figure 4.11A). For a short time of incubation, e.g. 10 min, there is a similar concentration profile around the cell in both cases. After this short period of time, proteins are predominantly captured by the surface or diffuse into bulk media (>96%). The depletion of secretory proteins by surface antibodies is relative faster than that by passive diffusion of proteins outside the well. Therefore, the concentration of analytes remaining inside the well for 2 h of cell culture is 2-3 folds higher than that during the microengraving. However, in both cases, the absolute concentration is very low (< pM), which is less than effective dosage of most cytokines (~1-100 pM). At this low concentration, switching the same array between microengraving and single-cell culture probably will not cause too much disturbance of the microenvironment around cells. Although we did not include autocrine capture in the model, however, if the autocrine signal exists, it will have the same level of effect in both scenarios and the relative concentration profile will not change between microengraving and single-cell culture. These results provide an evidence that in serial microengraving, where the same array undergoes several cycles of detection and culture, individual cells are surrounded by relatively stable microenvironments and the kinetic responses of cells are mostly from stimulation rather than environmental perturbation.

Since the majority of the secreted proteins diffuse outside the well during cell culture in the array, these diffused proteins may influence the function of other cells in surrounding wells. To evaluate the cross contamination of secretory proteins between wells by diffusion, we calculated the concentration profile of proteins in a larger scale of culture environment (Figure 4.11B). To get a maximal estimation of possible contamination, we chose a high rate of secretion of 50 molecules/s and calculated the cumulative concentration in the media for 24 h (suppose that media can be changed once a day). Through natural diffusion, proteins form a gradient from the cell to the bulk media and surrounding wells. The concentration of protein at the bottom corner of the well containing cell is ~30 pM, while the concentration at the bottom of the next wells is reduced for ~50%. For most cytokines, this concentration is around the same order of magnitude of their ED_{50} (e.g. IL-2, IFNγ, and IL-4). Therefore, for cytokines that have high rates of secretion, it is possible to have certain level of crosstalk between cells in neighbor wells during long-time culture. However, cells most likely do not constantly secrete at this high level for a long time. By increasing the amount of bulk culture media or the frequency of refreshing media, the cross contamination could be minimized.

4.8 Figures

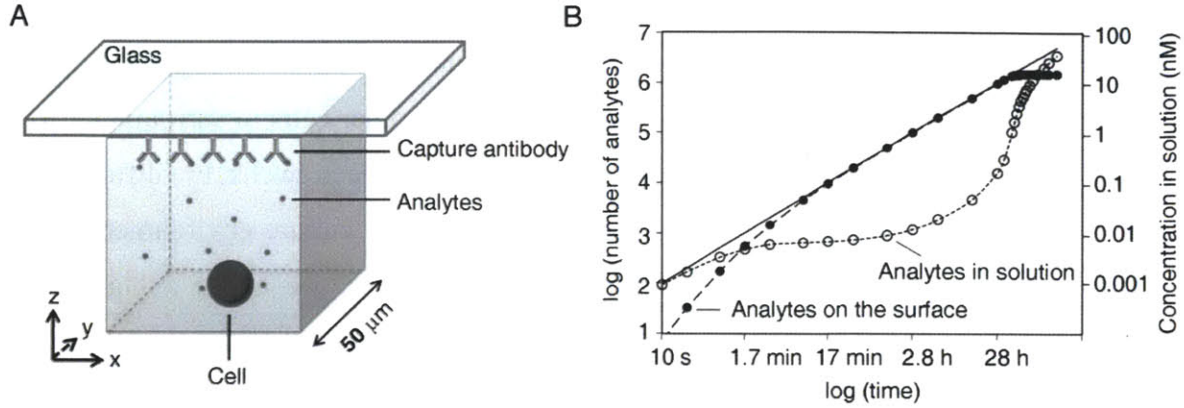

Figure 4.1 Analysis of mass transfer and surface capture of analytes during microengraving using numerical model. (A) Schematic of the configuration of one nanowell containing a single cell. (B) Plot of the calculated quantity of analytes accumulated in the media (○) and on the surface of the glass (●) during microengraving when the cell secretes at a constant rate of 10 molecules/s. The solid line indicates the cumulative quantity of analytes secreted by the cell over time. In this simulation, the affinity of capture antibody was K_D=100 pM, and the density of binding sites on the surface was $\theta_0=10^{-9}$ mol/m^2.

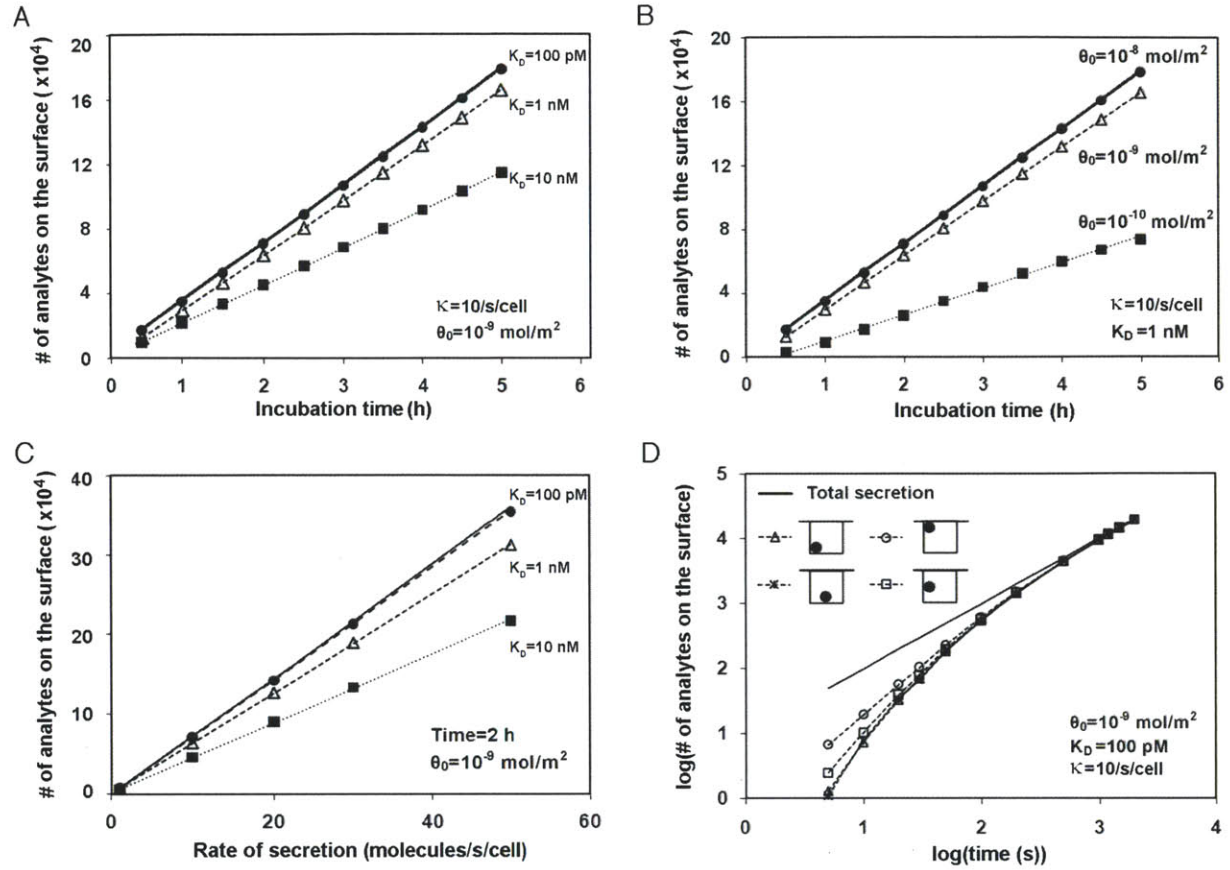

Figure 4.2 Effects of model parameters on the efficiency of surface capture in the linear regime. The number of analytes captured on the glass surface decreases with the increase of (A) the dissociation constant of capture antibody or (B) the decrease of the density of binding sites on the surface. (C) The number of analytes captured on the glass surface for a fixed time period increase linearly with the rate of secretion. (D) Variation of the positions of the cell within the nanowell (relative to the glass) only affects the early stage of capture. Solid lines in all four panels represent the total quantity of analytes secreted with time.

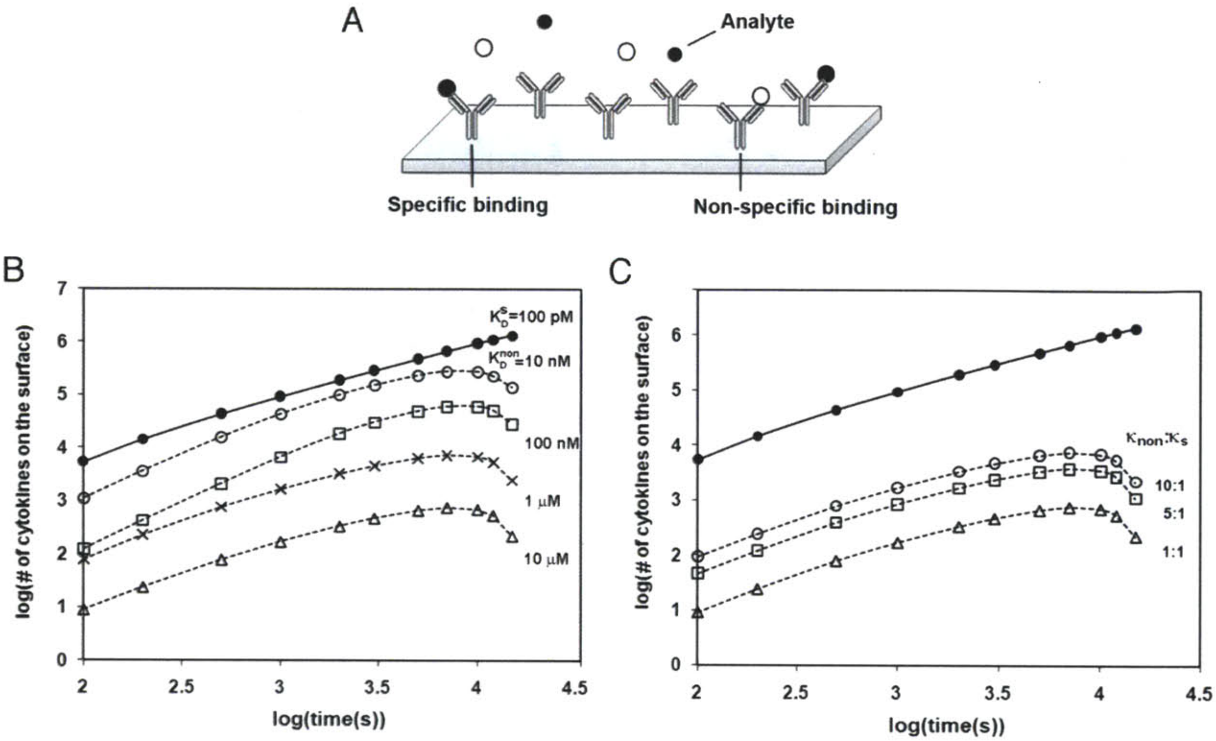

Figure 4.3 Effects of nonspecific capture of molecules secreted from the cell on the detection of target analytes. (A) Schematic illustration of the competition between specific and nonspecific binding to the capture antibodies. (B) Plots of the calculated number of molecules captured in the linear regime for a series of affinities assigned to nonspecific binding (K_D^{non}). For these calculations, the affinity for specific binding was fixed to 100 pM. Open symbols represent the amount of nonspecific binding at the different affinities used in the calculations. The closed circles represent the amount of specific binding when K_D^{non} = 10 nM. The rates of secretion used for both molecules were 100 molecules/s. (C) Plots of the calculated number of molecules captured at different ratios of the rates of secretion of the nonspecific and specific molecules (N_{non}:N_s). The affinities for specific and nonspecific binding were 100 pM and 10 μM, respectively. The rate of secretion of target analyte was fixed to κ=100 molecules/s. Open symbols represent the amount of nonspecific binding at the different ratios of secretion indicated. Closed circles represent the amount of specific binding at N_{non}: $N_{specific}$ =10:1. The solid lines in both (B) and (C) represent total quantity of analytes secreted.

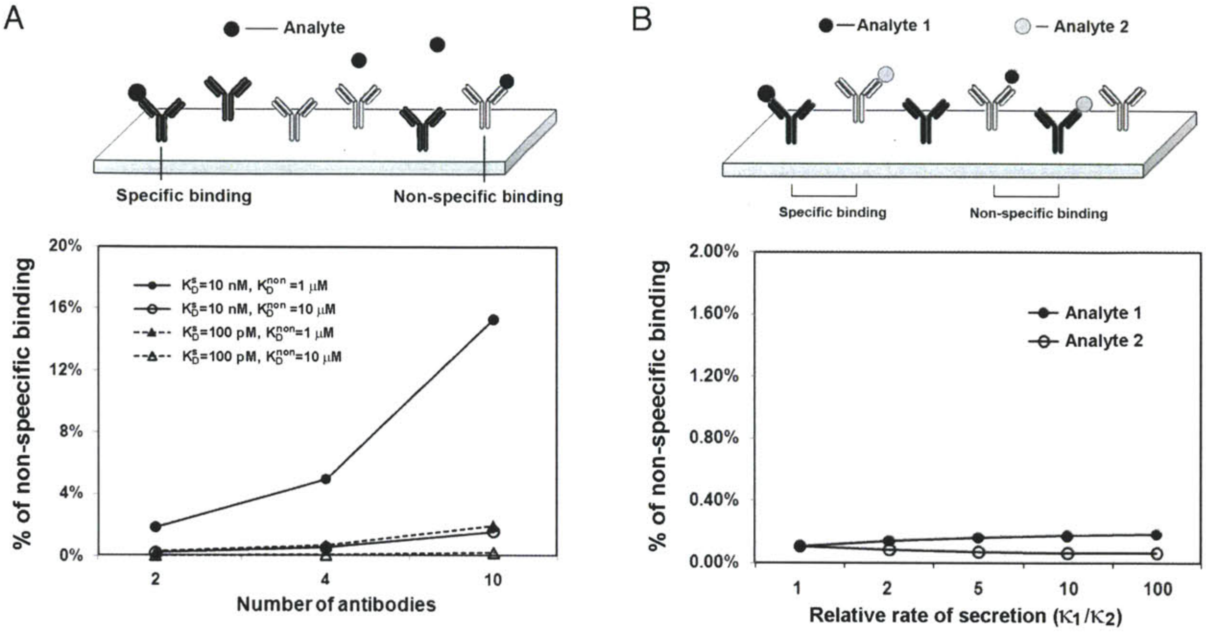

Figure 4.4 Effect of nonspecific binding in models with multiple analytes. (A) Schematic for a single analyte binding to a surface supporting two different capture antibodies (top). Plots of the calculated percentage of nonspecific binding as a function of the number of capture antibodies (bottom). The rate of secretion was 100 molecules/s. The total density of binding sites on the surface was $\theta_0=10^{-9}$ mol/m^2, which is equally divided to each type of antibodies in the calculation. (B) Schematic of two analytes binding simultaneously to a surface supporting two different capture antibodies (top). Plots of the calculated percentage of nonspecific binding as a function of the ratio between two analytes (bottom). The affinity of specific and nonspecific binding was 10 nM and 10 μM, respectively, for both antibodies. The rate of secretion of analyte 1 was fixed to 100 molecules/s. The total density of binding sites on the surface was $\theta_0=10^{-9}$ mol/m^2 and shared equally by these two antibodies.

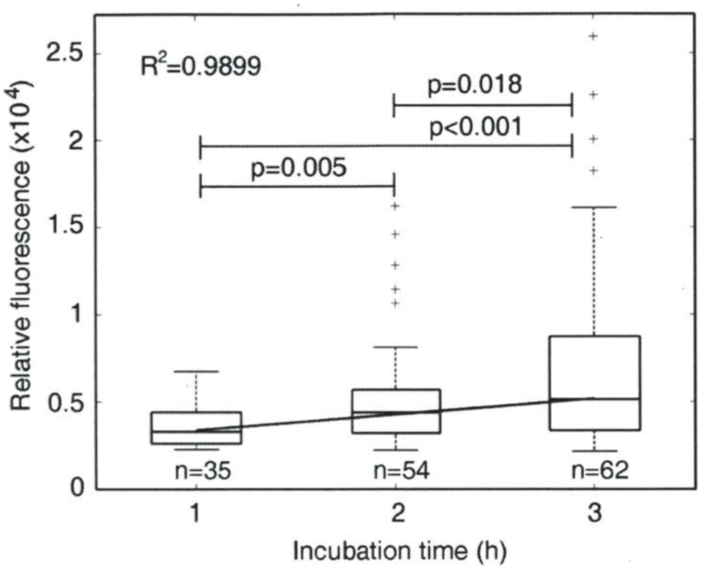

Figure 4.5 IL-6 secretions from individual human PBMCs. Box plots follow Tukey's convention, with the center line representing the median, and the upper and lower edges of the box representing the values of the upper and lower quartiles. Whiskers extending from each end of the box represent the most extreme values within 1.5 times the interquartile range. Relative MFI of captured IL-6 increases linearly and significantly as a function of incubation time. *n* is the number of single-cell events in each box plots. The solid line was fit by linear regression of the median values of MFI at each time (central bar in each box). Statistics were determined by a two-tailed Student's t-test.

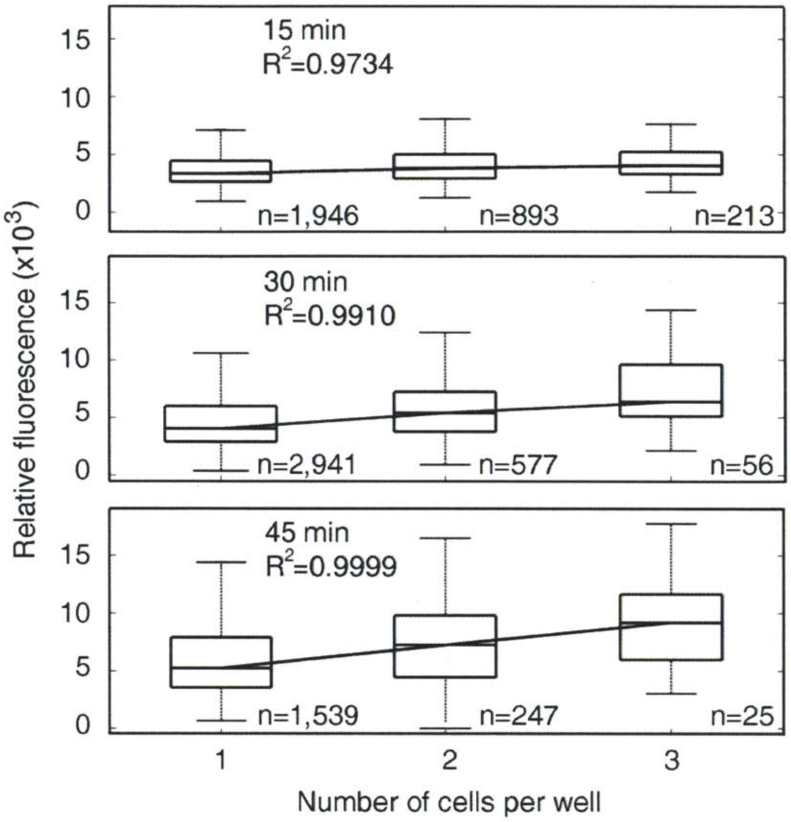

Figure 4.6 Measurement of the secretion of antibodies from mouse hybridoma cells. The relative MFI of the signals were plotted as a function of the number of cells in each well for three different incubation time (15, 30, and 45 min). Solid lines were fit by linear regression. *n* is the number of events in each box.

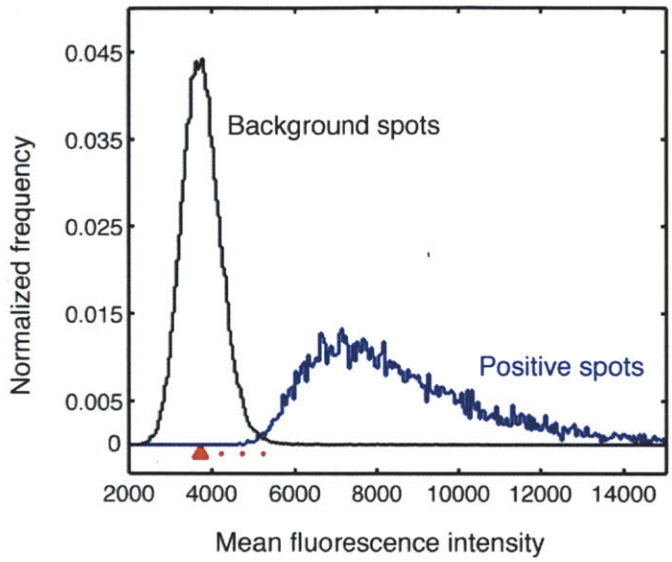

Figure 4.7 The distribution of MFI of background spots and positive spots from the same slide. An representative example from one slide is shown here. The red triangle represents the mean value of the background spots, whereas three red dots represent values that are 1, 2, and 3 standard deviations above the mean value.

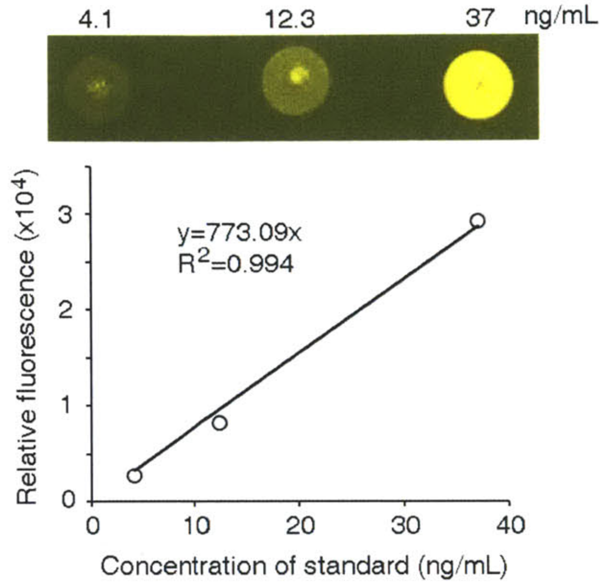

Figure 4.8 Micrograph of a standard reference slide (top) and a sample calibration curve (bottom) used to calculate the rate of secretion from cells. A series of diluted, fluorescently labeled detection antibody was spotted on the glass (1 μL/spot) at the concentrations indicated, and the mean fluorescence intensity of each spot was plotted to generate the calibration curve (solid line).

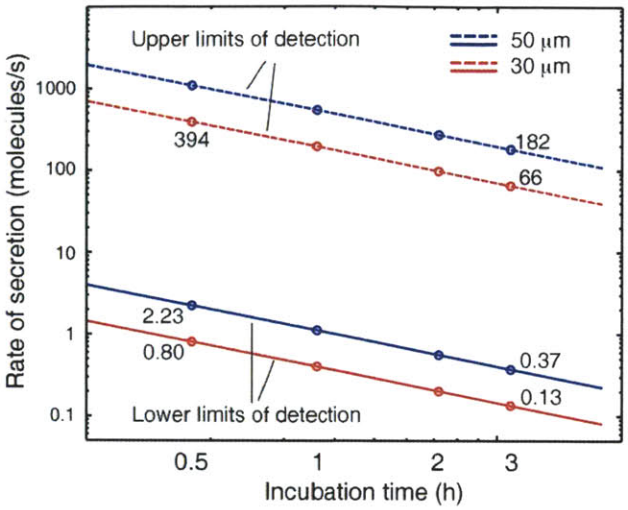

Figure 4.9 Diagram showing the optimal experimental windows for 50 μm (blue) and 30 μm (red) nanowells. For a fixed time period of incubation, the lower limit of detection is the minimal rate of secretion that provides signal above backgound+3SD. This line is determined experimentally and might vary with different antibody pairs and fluorophores. An average result from IL-2 measurement is presented in this graph. The upper limit of linear detection is defined as the rates of secretion at which 95% of the binding sites are occupied by the analytes. Region between lower and upper limits is the dynamical range of rate for quantification. The lower and upper limits of several time points (0.5, 1, 2, and 3 h) are indicated in open circle on the graph along with the corresponding rates of secretion.

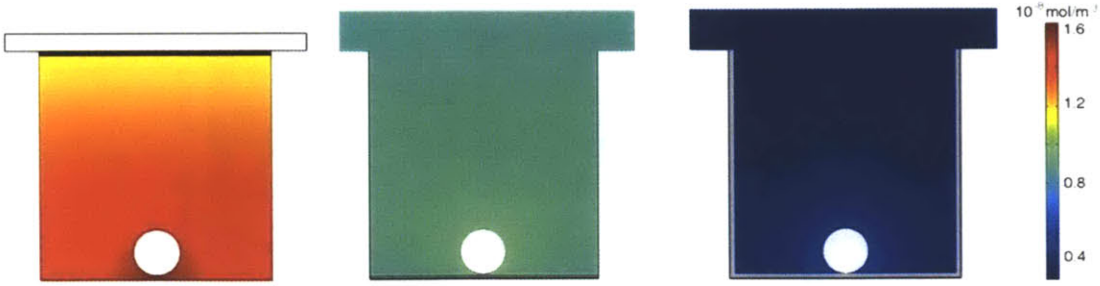

Closed system
One capture surface

Open system
One capture surface

Open system
Three capture surfaces

Figure 4.10 Three two-dimensional models were constructed to compare the capture efficiency in closed and open systems. Left, closed system with one capture surface on the top (black thick line). Middle, open system with one capture surface on the bottom (grey thick line). Right, open system with three capture surfaces on the bottom and two side walls (grey thick lines). All the physical parameters used in simulation are the same as those in Figure 4.1 and the total incubation time is 2 h. For the open system, the media outside the nanowell is 1 mm high. Color map shows the concentration gradient in the media.

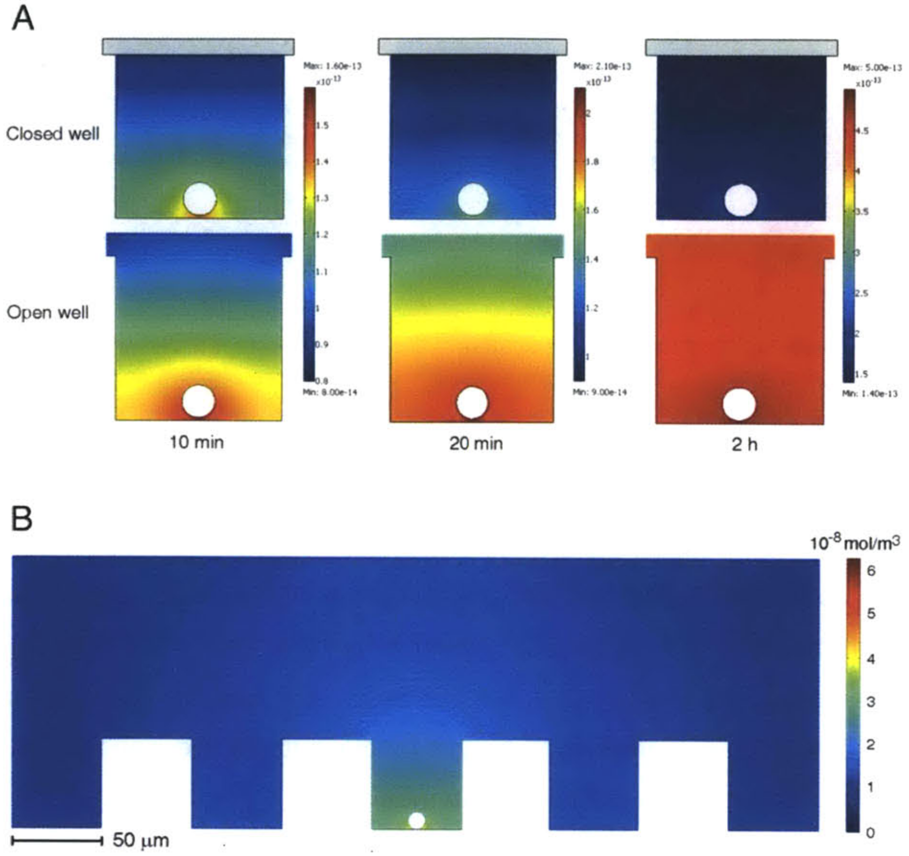

Figure 4.11 Concentration profile of cytokine in the nanowell during microengraving and cell culture. (A) Two-dimensional models were used to compare the change of concentration with or without microengraving. The model of closed well is analogous to the process of microengraving, where the top surface is coated with capture antibodies. In the model with open well, there is no capture surface and only secretion and diffusion of analytes were considered. This model is analogous to the process of single-cell culture in the array. All the parameters for calculation are the same as Figure 4.1 and the bulk median above well was set to 1 mm for simulation. Paired comparison between both models at 10 min, 20 min, and 2 h are shown as examples. (B) Concentration profile of cytokine in bulk media during single-cell culture was calculated using an expanded two dimensional model. The bulk media above wells is 1 mm. The result shows the concentration of secretion in median after 24 h of incubation with a rate of secretion of 50 molecules/s.

4.9 Tables

Parameter	**Value**
Well size	50 μm×50 μm×50 μm
Cell diameter	10 μm
Diffusion coefficient (D)	10^{-10} m^2/s
Association rate constant (k_{on})	10^5-10^6 $M^{-1}s^{-1}$
Dissociation rate constant (k_{off})	10^{-3}-10^{-4} s^{-1}
Rate of secretion (κ)	1-100 molecules/s
Density of total binding sites (θ_0)	10^{-8}-10^{-10} mol/m^2

Table 4.1 Values of parameters used in simulation.

Cytokine	**Fluorophore**	**Limit of detection (molecules/s)**
IL-6	Alexa Fluor 488	0.5-0.7
IL-17	Alexa Fluor 488	0.5-0.6
IFNγ	Alexa Fluor 555	3.8-4.1
IL-2	Alexa Fluor 594	0.8-3.1
TNFα	Alexa Fluor 700	1.8-2.0

Table 4.2 Experimental limits of detection for cytokines.

	Capture surface	**Media inside well**	**Media outside well**
Closed system One capture surface	98.5%	2.5%	-----
Open system One capture surface	73%	1.2%	25.8%
Open system Three capture surface	90.1%	0.4%	9.5%

Table 4.3 Comparison of distribution of analytes in closed and open systems.

Chapter 5. Comparison of microengraving to other technologies

There are several existing tools for measuring cytokine expression from human T cells. ELISpot and ICS are commonly used for measuring the frequency of cytokine secreting cells because of their single-cell resolution. ELISA or Luminex are used for measuring the bulk concentration of cytokines in the supernatant. qPCR is used to measure cytokine gene expression rather than protein production. All these technologies have different mechanisms and characterize different aspects of cytokine production. In this section, we present a have side-by-side comparisons of microengraving to these existing tools to highlight the advantages of microengraving.

5.1 Microengraving vs. qPCR

To compare the kinetics of protein secretion and gene expression, we measured IL-6 production by microengraving and qPCR. PBMCs were stimulated with a toll-like receptor agonist, LPS, for three intervals of stimulation (3, 6, and 12 h), then applied for both assays. In microengraving, the secretion of IL-6 from individual cells was measured for 2 h and scored for both the frequency (number of-secreting cells within the total population) and rates of secretion of IL-6-secreting cells (Figure 5.1A). The results were presented as histograms showing the distribution of the rates at each time point of stimulation. The area under the curve presents the total cell number that had positive secretions. From the distribution, most cells secreted IL-6 at rates below 10 molecules/s, and a few high secretors could secret up to 50-60 molecules/s. The distribution slightly shifts towards higher rates over time: the median rate increased monotonically from 6.5±3.2 (3 h) to 10.6±7.1 (12 h). This range of values is consistent with that estimated by ELISA (using the supernatants from the stimulated cells), and reported values in the literature for cytokine release from primary cells (96). The frequency of secreting cells increased significantly with time, especially from 3 h to 6 h.

To assess whether the most productive cells were derived from a particular subset of cells within the PBMCs, the cells were labeled and then imaged in situ after microengraving. Most of the cells secreting IL-6 were CD11b+CD14- (45%, 10±8.4 molecules/s) and CD11b+CD14+

(27%, 10±7.4 molecules/s), while a small population of cells were CD3+ (4.7%, 12.5±9.4 molecules/s) (Figure 5.1A insert). Since CD11b and CD14 are markers predominantly associated with monocytes, this result is consistent with previous reports that show LPS strongly mediates monocyte responses (97, 98). The median rates of secretion for each class of cells, however, did not differ significantly (two-tailed, unpaired Student's t-test), suggesting the magnitudes of responses to the applied stimulus of LPS for these different lineages of cells are all similar.

The expression of total mRNA encoding IL-6, however, had different kinetics as protein secretion (peaked at 6 h) (Figure 5.1B). This observation indicates, as expected, that the timing of transcription does not necessarily correlate with the timing for secretion of a protein. Besides the kinetics, the amount of mRNA in cells does not necessarily correlate with the amount of final protein product, because the mRNAs and new synthesized proteins sometimes may undergo degradation intracellularly. Because cytokines are extracellular signaling molecules, the actual secretion is more meaningful for the function of cells than gene expression. Therefore, direct measurement of the secretion is useful to assess the responses of samples.

In terms of protein production, the frequency of secretion changed much more dramatically with time than rates of secretion (Figure 5.2B). Similar phenomena has also been observed by studies on antigen-specific CD4+ memory T cells. Waldrop et al. found that certain noncognate costimuli are capable of augmenting the absolute frequency of cytokine-producing CD4+ memory T cells in CMV antigen-stimulated PBMC cultures, but have no significant effect on the amount of cytokine synthesized per responding cell (99). Together with the our observation that different lineages of cells have similar distribution of rates, these results suggest that under the same stimulation condition, the overall cytokine response is regulated primarily by changing the frequency of active cells in the population rather than changing the rates of individual cells.

5.2 Microengraving vs. ELISpot

The major difference between these two technologies is that ELISpot requires longer times of incubation, normally 24 h, and microengraving requires only 1-2 h. Therefore, ELISpot measures integrated signals from a longer period, and cannot tell the kinetics information on when the cells secrete. However, microengraving gives a snapshot of the status of secretion, and reveals whether the cells secrete in this short window of time but may miss other time points when cells are active. To get a parallel comparison of frequency of secretion, we used the same clones of antibodies in both technologies to avoid issues of sensitivity brought by antibodies. In general, microengraving measured higher frequencies of all four cytokines than ELISpot. The relative frequencies of IFNγ, IL-17, and IL-4 secretion were consistent and comparable in both methods. However, frequency of IL-10 is quite different. One possible explanation would be that IL-10 antibody used in microengraving is not suitable for ELISpot or the secretion of IL-10 is too low so that the signal cannot reach the detection limit of ELISpot.

Form our calculations in Chapter 4 (secretion 4.8.4), the efficiency of capture in an open system (ELISpot) is much lower than that in a closed system (microengraving). Therefore, ELISpot only captures part of the secreted proteins on the membrane (70% or less). In addition, in ELISpot, secreted proteins diffuse around the cell and are captured on the surface without a confined area. This type of capture yields a smeared boundary between signal and background, and therefore, to some extent, decreases the signal-to-noise ratio, diluting the signal intensity. The radius of a spot depends on the rate of secretion and the shape of spots may not be ideally round if several cells are close together on the surface. Therefore, the spots are not uniform on the final image, and may contribute to errors in counting. All these technical issues may partially explain the lower sensitivity of ELISpot. Operationally, ELISpot also requires for 2-3 days for the whole process in a standard protocol, while microengraving can be finished within one day. More importantly, ELISpot cannot measure multiple analytes at the same time and cannot retrieve cells after the assay. These aspects are disadvantages when clinical samples are precious and further analysis of interested cells is required.

5.3 Microengraving vs. intracellular staining (ICS)/Luminex

T cells from the same donor were evaluated in parallel by ICS and Luminex to measure the frequency and concentration of cytokine in the supernatant, respectively. For ICS, T cells were stimulated in bulk (2×10^6/ml) with PMA and ionomycin for 3, 7, and 11 h. Brefeldin A was added at 0 h to inhibit the secretion of cytokines extracellularly. Expression of IFNγ, IL-2, and TNFα by individual cells was determined by permeabilizing and staining the cells with fluorescence antibodies; the number of secreting cells were evaluated by flow cytometry. In parallel, another fraction of the T cells (2×10^6/ml) was stimulated under the same conditions as that in ICS except no Brefeldin A was added. Culture supernatants were collected at the end of the stimulation. The concentration of the three cytokines (IFNγ, IL-2, and TNFα) in the supernatants was measured by Luminex. We then estimated the average rates of secretion of each cytokine using the following expression:

$$\bar{\kappa} = \frac{CV}{pNt},$$

where $\bar{\kappa}$ is the average rate of secretion, C is the concentration of cytokine in the supernatant (measured by Luminex), V is the total volume of the culture media, p is the percentage of cytokine secreting cells (measured by ICS), N is the total number of cells being stimulated, and t is the time of stimulation.

For microengraving, T cells from the same donor were stimulated at the same condition and measured for 1 h at the end the stimulations. The mean rates of secretion measured for each cytokine by microengraving were consistent with those estimated from a combination of ICS and Luminex (Figure 5.3A). The rates calculated from ICS and Luminex stand for an average rate in the entire stimulation, while rate measured by microengraving is the average from the last one hour of stimulation. Although the meaning of these two measurements is not exactly the same, however, this is the most closed comparison so far. These results demonstrate that the way we estimate the rate of secretion in microengraving (discussed in Chapter 4) gives comparable results as other methods.

The frequency of secretion measured from ICS is consistently higher than that from microengraving, which is expected because that ICS integrates signal for a longer time than microengraving. In addition, ICS also counts cells that have synthesized cytokine intracellularly but not yet start to secrete. Theses data together well demonstrated that microengraving can get consistent results compared with ICS and Luminex. Most importantly, such multidimensional information is obtained in a single assay.

5.4 Both frequency and rate of secretion improve the characterization of cell responses

Through the comparison above between different technologies, a significant advantage of microengraving is that it provides both the frequency of responding cells and the distributions in their rates of secretion. The combination of both data should facilitate distinguishing differences in the magnitude of functional immune responses after stimulation. To test that, we measured IL-6 secretion from PBMCs after exposing to three different stimuli and also compared these responses between two donors (Figure 5.4). The responses of cells from the same donor exhibited strong variations in both frequency and magnitude (rates) depending on the stimulation, and this combination of responses was unique to the individuals. Both donors exhibited similar frequencies of responding cells when stimulated with PHA, but the distributions in the rates of secretion were quite different. Kolmogorov-Smirnov statistical tests of the distributions indicated that only two conditions of stimulation (LPS and PHA for Donor 2) were similar ($p=0.8622$). These results demonstrate that assays that distinguish immune responsiveness based on multiple, independent measures (frequencies and rates) may be more robust than those relying on single-parameter measures (frequencies). Considering the results from section 5.1, these results suggested that the distribution of the rate of secretion reflects the signature of response to specific stimulation, while the frequency of secreting cells reflects the strength of the responses.

5.5 Figures

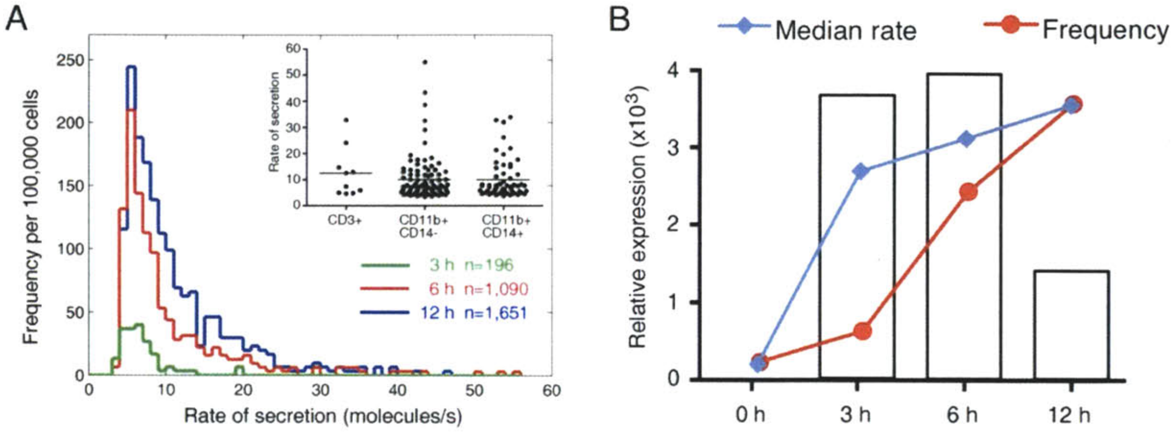

Figure 5.1 Production of IL-6 by human PBMCs following stimulation with LPS for 3, 6, or 12 h. (A) Distributions of rates of secretion of IL-6 measured by microengraving (2 h) was shown as a function of the time allowed for stimulation (3 h, green; 6 h, red; 12 h, blue). Insert: A plot of the specific rates of secretion determined for different subsets of cells within the array after 6 h stimulation. Horizontal bars indicate the mean value for each group. (B) mRNA levels of *IL-6* expression from the same population of stimulated cells in (A) was measured by quantitative PCR (bar graph). Relative level of median rates of secretion (blue curve) and frequency (red curve) of IL-6 measured from microengraving are plotted for comparison.

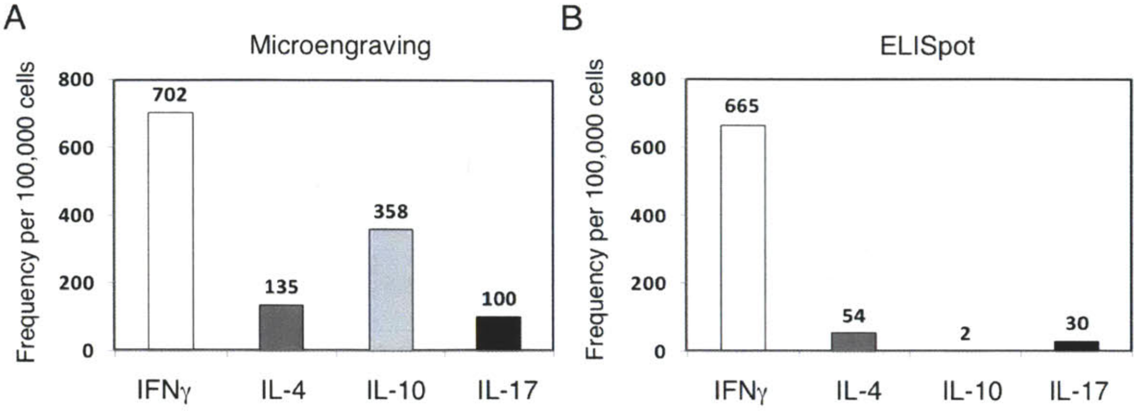

Figure 5.2 Comparison of the frequency of cytokine secretion between microengraving and ELISpot. PBMCs from healthy donor were stimulated by PHA for xx h, then the secretion of four cytokines were measured by multiplexed microengraving for 2 h. For comparison, same PBMCs were loaded in to 96-well plate for ELISpot assay. In each of the well on ELISpot plate, only one type of capture antibody is coated. Therefore four cytokines were detected separately from multiple wells. Cells were stimulated by PHA in the well for 24 h before process the membrane. The frequency of secreting cells was normalized to 100,000 cells for comparison.

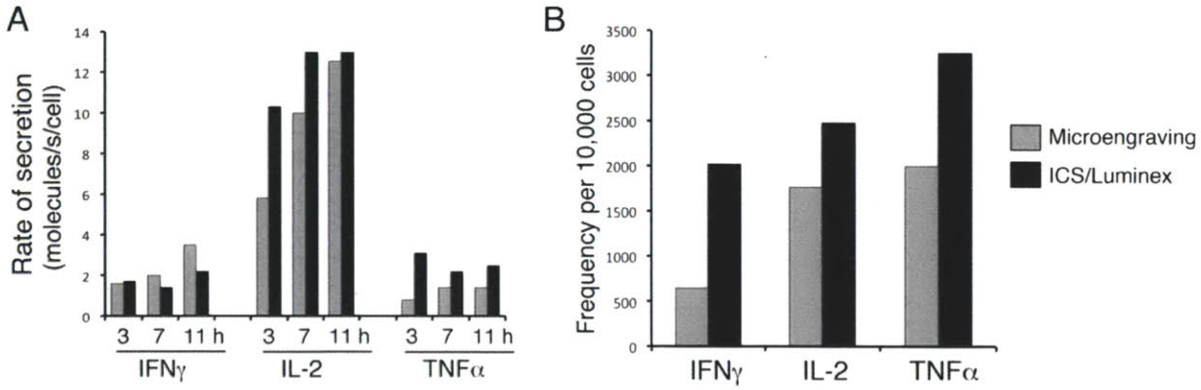

Figure 5.3 Comparison of rates and frequency of cytokine secretion measured by microengraving and intracellular staining (ICS)/Luminex. T cells isolated from the same donor were stimulated in bulk with 10 ng/ml PMA and 1 μg/ml ionomycin for 3, 7, or 11 h. The production of IFN-γ, IL-2, and TNFα cytokines were measured by microengraving, ICS, and Luminex in parallel. For microengraving, cytokine secretion from individual cells was captured only during the last hour of stimulation. For ICS, secretion was blocked during stimulation and intracellular cytokines were stained at the end of each time period. For Luminex, cells were stimulated without secretion inhibitor and culture supernatants were taken at the end of each stimulation period. (A) The average rates of cytokine secretion for microengraving (gray bars) are compared with those estimated from ICS/Luminex (black bars). The average rates from ICS/Luminex were determined by dividing the total amount of cytokine measured in the supernatant (Luminex) by the total number of secreting T cells (ICS) and the time of stimulation. The limits of detection for this set of experiments were as follows: 0.5 ± 0.1 IFNγ molecule per s per cell, 1.1 ± 0.2 IL-2 molecules per s per cell, and 0.7 ± 0.1 TNFα molecule per s per cell. (B) The frequency of cells secreting cytokines after the 7-h stimulation was determined independently for each cytokine, regardless of co-expression. The number of active cells resulting from each experiment is reported relative to 10,000 cells.

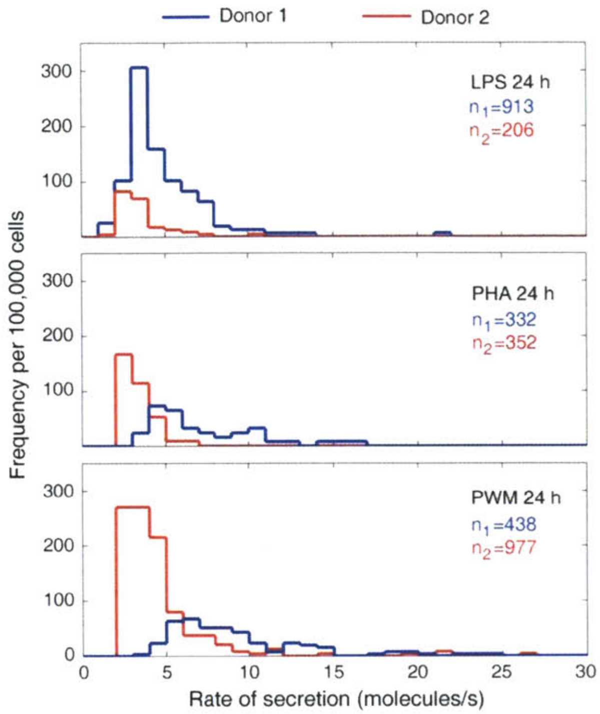

Figure 5.4 IL-6 secretions under different stimulation conditions were measured by microengraving. PBMCs from two donors were processed in parallel. Cells were stimulated with LPS, PHA or PWM for 24 h, then loaded on the array and measured by microengraving for 2 h. The values n are the normalized frequencies of responding cells under each condition. Histograms show the distribution of rates of secretion.

Chapter 6. Dynamic functional responses from single T cells

6.1 Generation of kinetic secretory profiles from single T cells

Functional behaviors of T cells, such as secretion of cytokines, are known to yield complex dynamics following activation, but characterization of the breadth and magnitude of these responses among single cells has been restricted to time-integrated, end-point measures. Serial microengraving, however, provides a non-destructive way to investigate the dynamic cytokine responses of individual T cells. In this work, we applied this technology to measure the secretion kinetics of three Th1-associated cytokines (IFNγ, IL-2, and TNFα) from individual primary CD3$^+$ T cells following polyclonal stimulations. These three cytokines are major and most widely tested functions that define a vaccine-elicited responses against specific infections that require T cells for protection. The heterogeneous secretion patterns of these three cytokines, e.g. single-functional and polyfunctional, bring more complicate problems to our knowledge of T-cell functions, and many studies have been done trying to correlate different secretion profiles with the quality of T cells (1). With our multidimensional technology, we aim to characterize the time-dependent production of these three cytokines, thus expanding our understanding about the polyfunctionality of T cells.

A combination of image cytometry and serial microengraving were used in our assay (Figure 6.1A). First, CD3$^+$ T cells were enriched from healthy donors and stained for their viability (Calcein) and differentiated state (classified by CD8, CD45RA, and CCR7) in bulk. After distributing cells into the array, we imaged each well by automated fluorescence microscopy to determine the occupancy and phenotype of cells in each well. The cells in the array were then activated by PMA and ionomycin on chip at single-cell level. These stimuli bypass cell surface receptors and activate T cells independent of accessory cells or IL-2 (100). Ionomycin induces an increase in [Ca^{2+}] in treated cells by increasing their ability to transport Ca^{2+} across cell membranes, and together with PMA synergistically enhances the activation of protein kinase C, which results in the phosphorylation of a number of cellular proteins (101). Both stimuli are soluble in culture media, and therefore create uniform strength of stimulation across the array, which minimizes the variation of stimulation between cells. We chose this TCR-independent stimulation as our first model system to probe a broad range of responses independent of the heterogeneous thresholds of T cell population. Cytokine secretions were then measured after 2 h of activation by serial microengraving, in which eight cycles of microengraving were performed consecutively. In each cycle, secretion was measured for 1 h and followed by another hour of cell culture on chip. Stimuli were included in all media used throughout the entire process, providing constant stimulation to cells during both culture and measurement. After all these cycles, cells in the array were stained for viability and imaged again. At the end, up to 30 data points were generated per cell over 16 h to describe the temporal release of cytokines from individual cells (Figures 6.1B). Using three surface markers, image cytometry classified total T cells into eight distinct subsets (Figure 6.2). Quantitative analysis of microarray images from microengraving provided rates of secretion for all three cytokines at eight time points (Figure 6.3).

Combining cell phenotype and secretion profile, we generated a heatmap showing the kinetic profile of cytokine secretion from activated, viable single cells (Figure 6.4). The secretions of cytokine were dynamic and highly diverse among individual cells. Aggregation of the responses showed that the number of cells secreting IL-2 and IFNγ increased over time, while those secreting TNFα diminished (Figure 6.5A and B). The secretion of IL-2 was also more prevalent among $CD8^-$ T cells than $CD8^+$ T cells. These basic trends including the order and timing of cytokine responses were consistent with those determined by bulk analysis using ICS and ELISA (29, 33). To confirm that the secretory activity on-chip was not influenced by isolated activation, we also measured secretions from cells stimulated in a bulk culture. The total frequency of secreting cells was consistent when measured by microengraving between 6-7 h after stimulation either in bulk (10.7%) or on-chip (13.6%).

6.2 Initial release of cytokines varies temporally among activated T cells

One interesting observation was that new cohorts of T cells sharply transitioned into active secretion states during each sampling period. These asynchronous, apparently stochastic, events were biphasic, concentrated at ~2-6 h and 12-16 h (Figure 6.5C). Interestingly, there was no statistical association between the timing of initiation and specific subsets, although memory T cells (CD45RA$^-$) tended to respond most often during the first burst of activity (Table 6.1). To test whether such variation of observed timing of initial release came from the diversity of cells in primary human samples, we also measured the kinetics of secretion from an in vitro-expanded human T-cell clone (Figure 6.6). These cells exhibited similar asynchronous release of cytokines under persistent stimulation. Therefore, these observed temporal distributions of initial release implies TCR-independent thresholds for cytokine release by individual cells, which may be influenced by variability in the expression levels of kinases, transcription factors, and other signaling proteins (ERK, NFAT, SHP-1) (102, 103), along with slow epigenetic events such as chromatin remodeling near transcription factor binding sites that promote production of cytokines (104, 105).

6.3 Simultaneous release of multiple cytokines is transient

Although ICS enumerates cells that produce multiple cytokines over a fixed time period, it cannot reveal the lifetime, persistence, or concomitance of these productions. Our experiments here demonstrated that most cells (~90%) first initiate secretion in a monofunctional manner, releasing only a single cytokine. Further, the frequency of multifunctional cells during any single sampling period was significantly lower than that seen by integrating these data across time (Figure 6.7). These observations suggest T cells are more likely to secrete multiple cytokines sequentially rather than simultaneously.

We found that cells secreting multiple cytokines simultaneously were more likely to change their functional states than those releasing individual cytokines (Figure 6.8A). Only cells that secreted IFNγ or IL-2 showed significant persistence of their functional states. The average lifetimes of states in which two or more cytokines were secreted simultaneously were 1.5- to 2-fold shorter than those of IFNγ or IL-2 alone (Figure 6.8B). TNFα single producing state was short-lived but with relatively higher preservation of function within 16 h. This is consistent with the observation that some cells started to secrete TNFα early after stimulation and then quickly turn off. Unlike TNFα single-functional state, multifunctional states were short-lived and not functional persistence. These results implied that the simultaneous secretion of two or more Th1-associated cytokines likely occurs as a transition between states, and that the secretory responses by T cells evolve dynamically during sustained, TCR-independent activation. Cells that initiated secretions within four hours of stimulation were more likely to produce multiple cytokines in total, either simultaneously or sequentially (Figure 6.9), indicating a lower threshold of activation for polyfunctional cells.

6.4 Transitions between functional states

The transient nature of multifunctional states brought up a question regarding the directions of transitions between states. To identify the most common transitions among functional states, we quantified the likelihood that a cell in a secretory state at time t_N would transition to another state 2 h later, t_{N+2h} (Figure 6.10A). The most probable outcomes observed here were that cells either retained the current state (diagonal positions) or downgraded the number of cytokines secreted (upper triangle area). Secretion of TNFα was found more likely to be lost in the downgradation of multifunctional states, which implies a direction of functional evolution from TNFα to other cytokines. For example, the release of TNFα in combination with either IFNγ or IL-2 commonly resolved to the secretion of IFNγ or IL-2 alone. These analyses further confirm that cytokine secretion by individual cells occurs in a predominantly sequential manner, with multifunctional release arising as a transient state.

To statistically evaluate the significance of these transitions, we then computed the corresponding Z scores for these state transitions relative to randomly-permuted datasets to evaluate whether certain transitions occurred more or less commonly than expected by chance (Figure 6.10B). As anticipated, persistence of individual secretory states was significant, confirming that cells actively sustain specific functional states. Some transitions were significantly underrepresented. For instance, observed transitions between IFNγ and IL-2 single producing states occurred less frequently than expected by chance. This result is consistent with observations that IFNγ expression, controlled by the transcription factor Tbet, suppresses the bulk production of IL-2 by lymphoma cells activated by PMA/ionomycin (106). We anticipate that identifying dominant individual-cell secretory transitions may offer new insights on the regulation of cytokine signaling and provide a way to predict T-cell responses.

6.5 T cells exhibit programmatic trajectories of cytokine secretion

The global transition matrices suggested that the trajectories of secretory states among cells evolve with identifiable, deterministic programs, rather than stochastic or idiosyncratic courses. That is, the set of trajectories observed is small relative to the number of all possible trajectories for the three cytokines ($>10^7$). To test this hypothesis, we investigated the cytokine trajectories derived from the first three time-aligned data points by self organizing maps (SOMs) (Figure 6.11). For each CD8$^-$ T-cell subset, the optimal number of clusters was determined by evaluating the explained variance using elbow criterion (107) (Figure 6.12). Metaclusters were then determined by further SOMs and qualitative alignment of similar clusters (Figures 6.13 and 6.14).

The dominant trajectories exhibited either persistent secretion of individual cytokines (e.g., IL-2, IFNγ) or a transition from a single functional state to another (e.g., TNFα→ IL-2; TNFα→ IFNγ). Memory T cells (CD45RA$^-$) used the most diverse sets of states, with a small, but significant, bias toward TNFα-secreting states among the effector memory (CCR7$^-$) cells, whereas CD45RA$^+$ cells predominantly exhibited a short burst of IFNγ. These results support models for T-cell differentiation where T cells maintain transient memory for gene expression resulting from chromatin remodeling (105), and also suggest that some subsets of T cells from all differentiated populations can release limited bursts of IFNγ within 2 h of initial activation.

6.6 Classification of T-cell subsets using dynamic profile

We next considered whether the observed sequential cytokine trajectories could distinguish different subsets of cells (effector memory, central memory, effector, and naïve) more effectively than time-integrated data, which may fail to resolve differences in how multifunctional responses are reached. Using principal component analysis (PCA), in combination with feature selection, we identified unique subspaces that best segregated subsets in specified training data. These subspaces were subsequently used to classify cells based on their dynamic cytokine profiles. Using raw CD8- T-cell data, we could discriminate among the four subsets more accurately (41 ± 1%, percent correct classification) than random assignment (25%) (Figure 6.15A). Integrating the data over 6 h (i.e., approximating ICS) reduced the accuracy of classification to 33 ± 1%. Remarkably, aligning the trajectories of individual cells according to the initial time of cytokine release dramatically improved the accuracy of classification to 58 ± 4%. We also found that classification using time-aligned data improved monotonically with the temporal length of the trajectories, especially for naïve and effector cells (Figure 6.15B and 6.16). Sensitivity analysis for the binary classification of subsets (based on receiver operating characteristic curves) confirmed that effector memory and central memory cells were challenging to discriminate based on their functional profiles (Figure 6.17), suggesting that there are limited differences between the ranges of dynamic cytokine responses for these two subsets, and that local microenvironments along with receptor-mediated signaling likely modulate context-specific responses. Further resolution of the phenotypic diversity within memory cells may also improve their classification (10).

6.7 TCR-dependent activation induces similar programed responses

Whereas the stimulation of T cells in a TCR-independent manner provided a view of the accessible trajectories of secretory states, activation of T cells in vivo occurs through the engagement of TCRs with cognate antigens presented in class I or II major histocompatibility complexes (MHC) and costimulatory molecules such as CD28 (108). To determine whether the dynamics of cytokine secretion after PMA/ionomycin stimulation were consistent with TCR-dependent stimulation, we compared the responses of primary T cells subjected to each condition during the period in which all functional states and transitions were most prevalent (2–10 h). We coincubated $CD3^+$ T cells with beads bearing anti-CD3 and anti-CD28 antibodies as a homogeneous surrogate for antigen-presenting cells (APCs) and monitored the dynamic evolution of their secretory states. These beads partially mimics APCs to across link TCR on the cell surfaces by surface bound anti-CD3 antibody, and also provides CD28 costimulatory signals that facilitate the initiation of T-cell responses and help sustain proliferation (3). Therefore, this stimulation provides a more physiologically relevant mechanism of activating T cells than PMA/ionomycin. To compare the cytokine responses between two stimuli directly, we monitored the cytokine secretion from T cells isolated from the same subjects. Qualitatively, the responses measured from TCR-dependent stimulation were similar to those observed during

TCR-independent stimulation (Figure 6.18A). Different subsets of cells again initiated secretion stochastically throughout the period of observation, and most cells did not begin in a multifunctional state.

Since stimulation beads were randomly loaded into each well and might not initially contact with cells, this TCR-dependent stimulation cannot provide perfect uniform strength of stimulation to individual cells as soluble stimuli did. Using video imaging to monitor cell behavior in nanowells, we observed that T cells were able to move around the well and most of the time they contacted beads within 1 h. Once contacted, most of the cells maintained contact throughout the measurements. Therefore, although the timing of initial contact was not absolutely synchronized at the beginning of our assay, the variations of the delay for cells contacting beads were shorter than the time scale of functional responses (> 4 h for most of the secretion). To confirm that on-chip beads stimulation was as efficient as bulk stimulation to activate cells, in another parallel experiment, we stimulated T cells in bulk with the anti-CD3/CD28 beads for 6 h and then loaded them on chip to measure the same cytokines. The results showed that 3.2% and 2.6% of cells were secreting after bulk and on-chip stimulation, respectively. We also scored the number of beads in wells where cells initiated secretion at different time points, and found there was not specific correlation showing the more beads in well the faster of activation (Table 6.2). These data suggest that the activation of T cells is more determined by intrinsic thresholds than the extracellular availability of the beads.

Detailed analysis further revealed that TCR-dependent stimulation induced more cells secreting IL-2, and fewer secreting TNFα, than those stimulated with PMA/ionomycin (Figure 6.18B). TCR-dependent activation also favored fast, limited bursts of secretion rather than sustained release, despite under persistent stimulation (Figure 6.18C). This response is qualitatively consistent with the finite temporal persistence of phosphorylated ERK observed by flow cytometry in mouse T cells after activation (109). Regulation of persistent TCR-dependent signals to allow only transient release of cytokines suggests another mechanism for limiting the effects of indiscriminate activation and supports in vivo observations that multiple serial encounters are often required to induce activation (110).

For both stimulations, cells secreting a single cytokine were more likely to preserve that functional response than cells releasing multiple cytokines (Figure 6.18D). The number of cells preserving functions was generally higher after TCR-dependent stimulation and may be a consequence of the limited bursts of activity (Figure 6.18E). Surprisingly, both stimuli induced similar trajectories, differing only in the frequencies of observed states (Figure 6.18F). Although stimulation via the TCR appears to alter the timing and persistence of specific secretory states, the programmatic trajectories of secretory states after activation do not appear to depend strongly on TCR-mediated signaling.

6.8 Correlation of cell proliferation with cytokine profile

Effective stimulation does not only induce cytokine secretion at early time but also induce proliferation of T cells, which is important in the immune defense to generate more effector cells and memory cells. Proliferation of T cells however takes longer time (normally 2-3 day) to be observed. By culturing T cells on-chip with anti CD3/CD28 beads, we have previously observed cell proliferation after 3 days. However, how this late time proliferation correlates with early cytokine profile, specifically with dynamic profile, at single-cell level is not clear. Here, we cultured single cells in nanowell array after serial microengraving with TCR-stimulation, and then evaluated their proliferation after 3 days. Although there were many cells proliferated, surprisingly, there was little correlation between the cytokine activity within 11 h after stimulation and proliferation after 3 days. Among the population of cells that showed cytokine secretion, only a small fraction proliferated, and this observation was not selective to specific cell types (Figure 6.19A). However, cells with proliferation did bias, although not largely, to earlier initiation of secretion and more IL-2 production (Figure 6.19B).

6.9 Discussion

6.9.1 Effect of activation strength on the secretion profile

TCR can detect subtle differences in the strength of interaction with pMHC ligand and transmit this information to influence downstream events in T cell responses. The strength of signal can be manipulated by changing the amount, density, and potency of pMHC ligands, and also influenced by the duration of interactions between T cell and APCs (111). Any changes relate to the quality and quantity of pMHC ligands might induce distinct cytokine profiles of T cells. The MHC binding affinity of antigenic determinants, leading to differential interactions at the T cell-APC interface, can be crucial for the differential development of cytokine patterns in T cells (112). Chaturvedi et al. reported that cells primed with high-affinity peptide are committed to differentiate into Th1 irrespective of the priming dose and affinity of challenge antigen; while the differentiation of cells primed with low-affinity peptide depends upon the dose of immunization and binding affinity of the challenge antigen for MHC (113). The hierarchical organization of TCR signaling thresholds exists in individual cells, and the strength of stimulation could induce distinct cytokine responses, e.g. more TCR signaling is needed to elicit IL-2 than to evoke IFN-γ synthesis (114). Antigen-specific memory CD4$^+$ T cells also vary in their costimulatory requirements. Under different thresholds, the secretion frequency may vary not necessarily proportionally with the increase of co-stimulation. For instance, in response to CMV, IL-2 synthesis is relatively more dependent on co-stimulation as compared with IFNγ (99). Therefore, even for the same set of cells, different strength of stimulation might result different functional profiles.

In this study, we applied both TCR-specific and nonspecific stimulation in this study and showed some commonality and specificity in cytokine profiles of T cells. We found that most of these profiles commonly existed in different stimulations but biases differently. Although engagement of TCR with anti-CD3/CD28 antibody stimulates T cells much gently compared with PMA/ionomycin, however, it is still orders of magnitude stronger than cognate recognition of pMHC and therefore is limited to absolutely mimic physiological TCR stimulation through peptide ligands presented by MHC (111). To better characterize physiologically responses of T cell activation, surface modification of the nanowell with pMHC would be an alternative way to create an APC-free stimulation environment (115). It will be promising to apply this multidimensional tool to resolve different profiles for various stimulation strengths and understand the downstream signaling pathways.

6.9.2 Evolution of functional states of T cells

Sequential acquisition of TNFα, IFNγ, and IL-2 function in subpopulations of T cells has been observed from previous studies at the population level. ICS studies following T cell stimulation revealed that expression of TNFα alone was the dominant function at 1 h of stimulation. Coexpression of IFNγ and TNFα rapidly became the most prevalent phenotype, followed by IL-2, IFNγ, and TNFα triple expression at later time points (33). However, because of the limitation of technology, for multifunctional states with low frequency, it is unclear whether they are developed from existing active states in early time or recently generated from a new subpopulation at later time. In this work, we followed the functional profile from the same single cells over time, and got directly evidence showing that single cells was capable of functional transition within short period of time (<16 h) and that multifunctional states were transient. More importantly, because of the time resolution, we observed how these functional states transitioned between each other and clustered multiple transition patterns. The dynamic responses also initiated at different time of stimulation, which added in one more parameter for the T-cell population to adjust systematically the overall functional strength. These asynchronous, dynamic responses may shed light on our understanding of the way that immune system uses to regulate the functional networks.

Our findings also raise a question on how to appropriately name the function of a T cell. Since the function of single cells may change over time, it may be a single producer at one time but become a double producer at another time. Therefore, it is not comprehensive to define a cell's function only based on the function at one time point and it also hard to decide which time point should be set as the standard reference time. In the end-point measurement, such as ICS, integrated cytokine production for a longer period of time, so that 'multifunctional states' cannot distinguish whether these cytokines have been secreted simultaneously or sequentially. Further more, the longer of the time of integration, the more frequent of multifunctional cells will be (Figure 6.7). Even in our kinetic assay, the secretion was not measured absolutely in a real-time fashion and the measurement only lasted 16 h. There may be more features of T-cell functions existing beyond the scope of our measurements. Nevertheless, this study discloses some novel characteristics of multifunctional T cells that may guide more research on these questions.

6.9.3 Correlation of cytokine secretion

For multifunctional cells, the correlation between cytokines is normally defined by a static view of the function. The magnitude of IFNγ secretion was found to associate with the number of cytokines produced by a T cell, e.g. IFNγ showed higher MFI in ICS when it was coexpressed with IL-2 and/or TNFα than when it was single-expressed (25, 27). Therefore, it was proposed that MFI of IFNγ could be used as a first approximation of the quality of a T cell response when multiplexed analysis was limited (1). Here, our kinetic data provided some mechanistic interpretation of this observation. We found that the rates of IFNγ secretion increased with time once the cell was initially activated, no matter whether IFNγ was secreted alone or together with other cytokines (Figure 6.20). The rates were very consistent in IFNγ single-producers and double/triple-producers if they have been activated for the same length of period. In this aspect, MFI was not informative to indicate the state of function. However, single-functional state existed more frequently at early time points after stimulation while multifunctional states were prevalent at later time point, therefore the average or apparent rates of secretion, which considered both the frequency and rates of single cells, showed differences between single-functional and polyfunctional populations. In conventional single-cell measurement, the temporal information for when individual cells have been activated is unavailable; therefore, it cannot reveal this underlying phenomenon.

Sequential release of different cytokines from multifunctional cells implies that the correlation of multiple cytokines may be dynamic. At the transcriptional level, different cytokines may be activated through different pathways or have different thresholds for TCR signaling or co-stimulation, therefore they may have different kinetics of mRNA expression. If some cytokines share the same transcriptional pathway and their genes are highly linked, the expression of mRNA may have higher chance to be correlated, for example, the Th2 cytokine genes (*IL4*, *IL5* and *IL13)* (116). Besides the stimulation signaling, autocrine or paracrine signals from cytokines may bring feedbacks to the cell, thus results in a more complex and dynamic correlation. For instance, IL-2 production in T helper cells is high at the early time of stimulation and then is limited by a negative feedback of itself or in collaboration with other common γ chain (IL-4 and IL-7) and IL-6/IL-12 family cytokines that is mediated by several signal transducer and activator of transcription (STAT) family transcription factors (117).

Secretory pathways of proteins may add additional spatial and temporal control to regulate the release of cytokines. In the classic canonical secretion pathway, cytokines or its subunits are synthesized in cytoplasm and pass through endoplasmic reticulum (ER) and Golgi. Some cytokines are released through non-canonical pathway in which they do not pass ER and Golgi (118). IL-2 is secreted through conventional ER and Golgi routes and no major additional secretion-regulatory check-points have so far been defined, therefore it is considered as a transcriptionally-regulated cytokine (118). TNFα is secreted through a different model of canonical pathway. It first moves through Golgi to the cells membrane, and then is cleaved by tumor necrosis factor-α converting enzyme (TACE) (119). In mouse T helper cells, IFNγ and IL-2 are secreted into immunological synapse sharing similar pathway, while TNFα is released multidirectionally (120).

Due to these multiple levels of the regulation, a better way to describe the correlation of cytokine functions should consider the relationship of multiple cytokines dynamically rather than simply consider which two or three cytokines are coexpressed at one time point. In this work, we characterized the correlation of functions using a transition matrix for adjacent time points and using trajectories of function at three consecutive time points. This kind of visualization may not be the best for such complex dynamic data, however, conceptually it provides a new way to view the correlations.

6.9.4 New tool to classify T cell groups

In our analysis, we first predefined several groups of cells based on surface markers that corresponding to the antigen-engagement history and homing capacity, then compared the cytokine function among these groups. The huge diversity of functional trajectories within each subset indicated much more classes of T-cell populations than what had been classified by three surface markers. Limited surface makers available in T cell study may not be sufficient to classify every population or T-cell subsets classified by those markers may not necessarily consistent with distinct functional profiles. Instead of from phenotype to function, our approach for classification using dynamic secretion data suggests an alternatively way to group cells only based on their functions, especially by time-aligned profiles. From the function-based groups, we then could go back to characterize other properties of those cells, such as genomic information, surface markers, cytolytic actively, etc. This classification can be very sensitivity when more time points are included, however, the extent of classification can be flexible and adjustable by choosing appropriate time length, depending on how complex the function profiles are. This function-oriented approach is very useful and straight forward for screening cells with novel or different secretory functions when there is no particular knowledge a priori of their phenotype or genotype.

6.9.5 Proliferation vs. cytokine activity

IL-2 is a T cell growth factor, principally produced by CD4$^+$ T cells (121). It plays a central role in the expansion and differentiation of CD4$^+$ and CD8$^+$ effector T cells both in vivo and in vitro (122, 123). IL-2 signal at early time point is important for proliferation. Bulk experiment found that after stimulation IL-2 responses was peaked during the first 24 h of culture, then the secretion declined gradually at later days and most of the cells proliferated (117). However, our proliferation assay following cytokine measurement showed little correlation of cytokine secretion, especially IL-2, with cell growth. These results seemed inconsistent with other studies on the biology of IL-2.

Although high concentrations and chronic exposure to IL-2 can negatively impact T-cell stimulation by sensitizing T cells to activation-induced cell death and tolerance induction (124-127), our quantitative model suggests that in our single-cell culture system, the concentration of IL-2 normally does not maintain at a high level over a few days (Chapter 4). Therefore, the proliferation is unlikely inhibited by too much IL-2 in the culture media. One notable difference in our assay is that cells were isolated on the array. There is work showing that paracrine delivery of IL-2 through synaptic contact region increase proliferation of CD8$^+$ T cells in vitro much higher than observed with equivalent amount of bulk IL-2 (128). We speculate that the low correlation of proliferation with IL-2 and other cytokine secretion in this work may be caused by the lack of cell-cell contact.

6.9 Figures

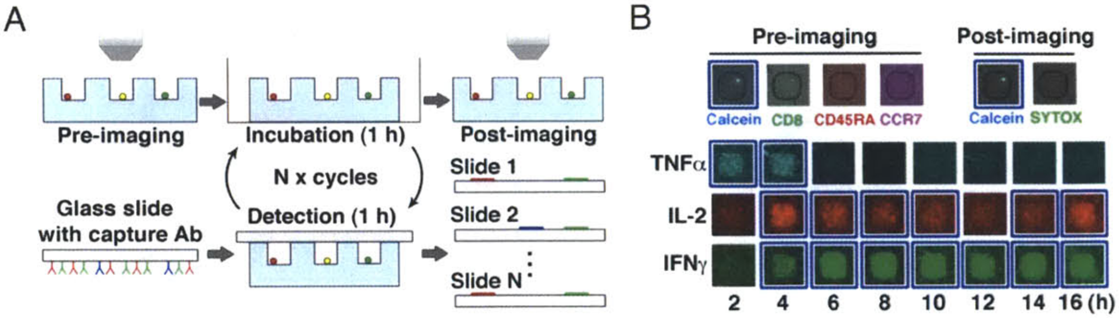

Figure 6.1 Kinetics of cytokine secretions were measured by serial microengraving. (A) Illustration of serial microengraving to monitor cytokine secretion by viable single T cells in time. (B) Representative micrographs of data evaluating viability (Calcein and SYTOX); phenotype (CD8, CD45RA, and CCR7); and TNFα (blue), IL-2 (red), and IFNγ (green) secretion. Blue squares outline positive events.

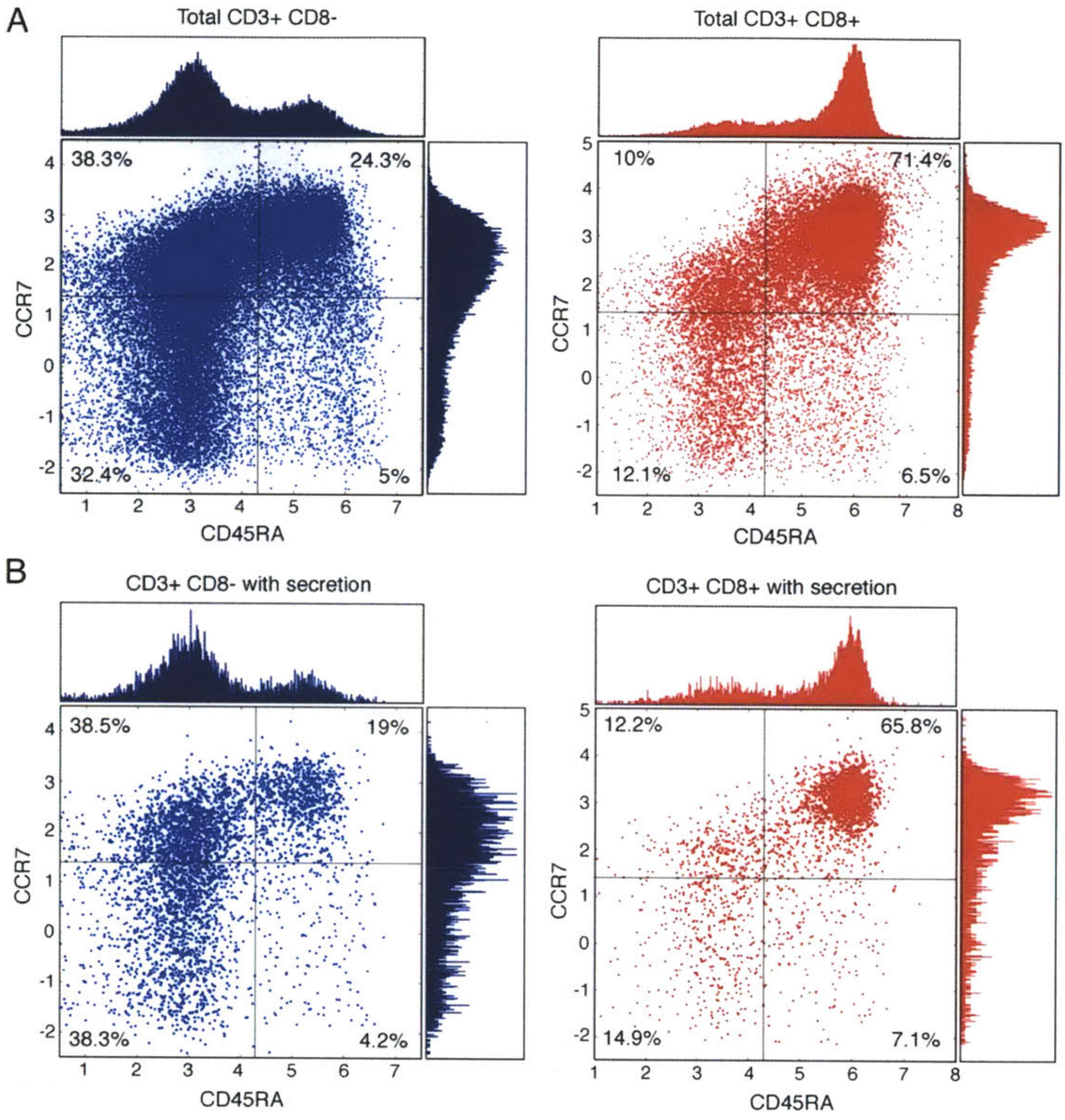

Figure 6.2 Classification of T-cell differentiations by imaging cytometry. Representative scatter plots and corresponding histograms of total individual viable CD3$^+$ T cells in nanowells (A) and individual viable CD3$^+$ T cells with cytokine secretion (B). T cells were stained with fluorescent surface markers: CD8, CD45RA, and CCR7. Raw fluorescence intensities acquired from individual cells were processed by logical transformation with a cofactor of 5 before analysis using FLAME within GenePattern (Broad Institute). Thresholds for positive events were set based on the distribution of data from the histograms of each fluorescence channel.

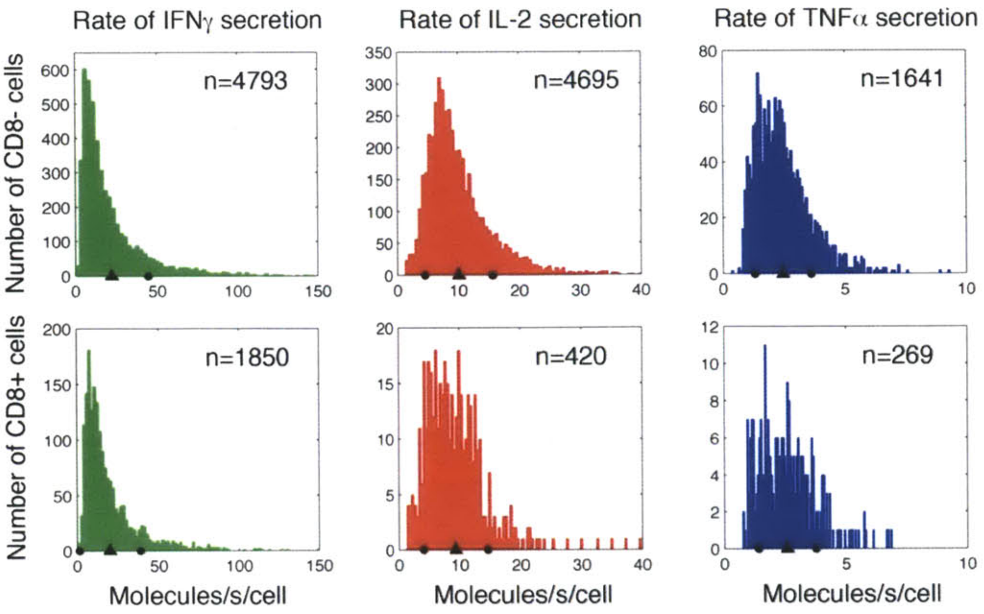

Figure 6.3 Distributions of rates of secretion of individual cytokines from $CD8^+$ (upper) and $CD8^+$ (lower) T cells. All nonzero secretion rates of each cytokine (positive secretion based on our criteria) were included. The total number of events (n) in each histogram was indicated in the graph. Mean and mean ±1 SD of each distribution are indicated on the x axis by triangles and dots, respectively. In this set of kinetic measurements, the average limits of detection were 3.2 ± 0.6 IFNγ molecules per s per cell, 1.8 ± 0.9 IL-2 molecules per s per cell, and 0.8 ± 0.3 TNFα molecule per s per cell.

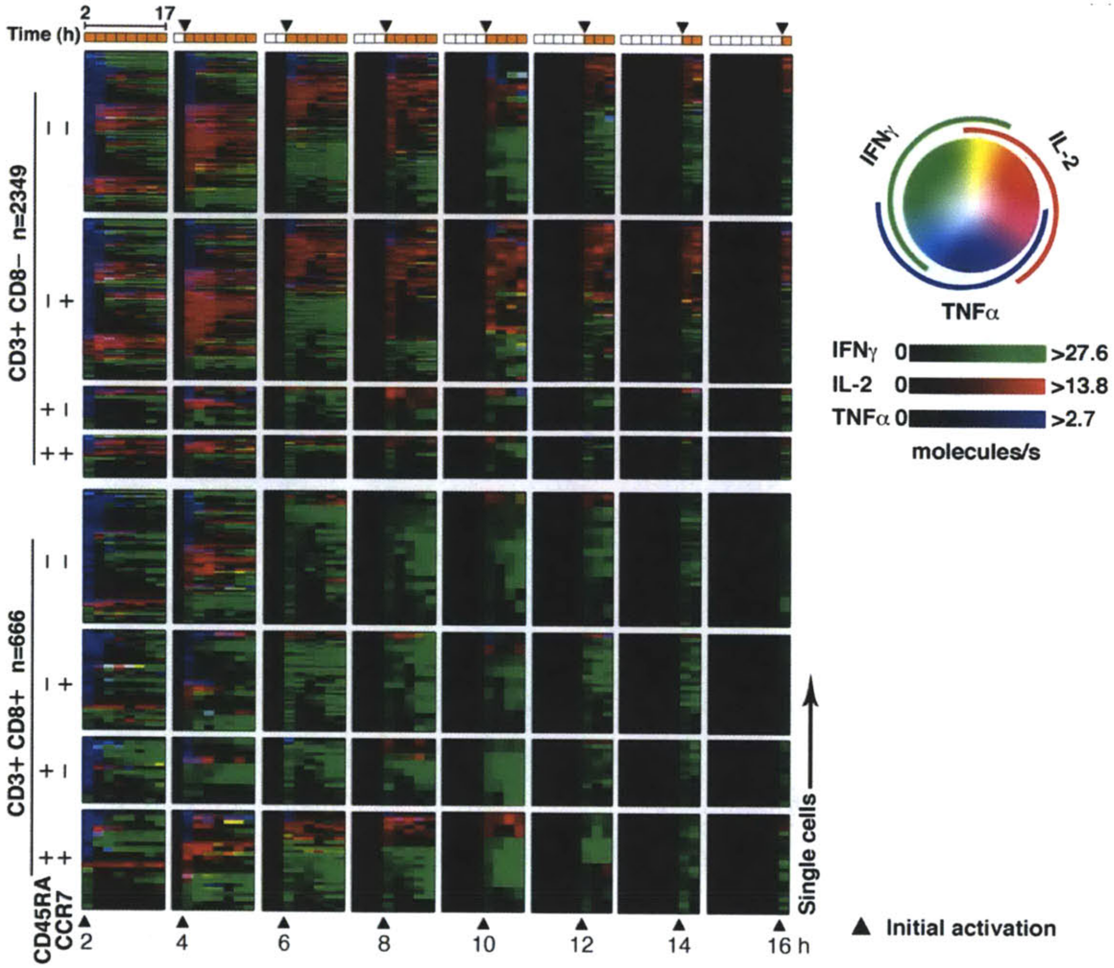

Figure 6.4 Cytokine secretion kinetics of 3,015 viable T cells. Each row within each block reflects the dynamic activity of an individual T cell over time. The color wheel illustrates the type and relative magnitude of secreted cytokines; inactivity is black. Block columns and block rows organize cytokine profiles by initial time of activity and differentiated cell types, respectively. Kinetic profiles are ordered within each block according to cytokine function. These data are representative from three independent experiments.

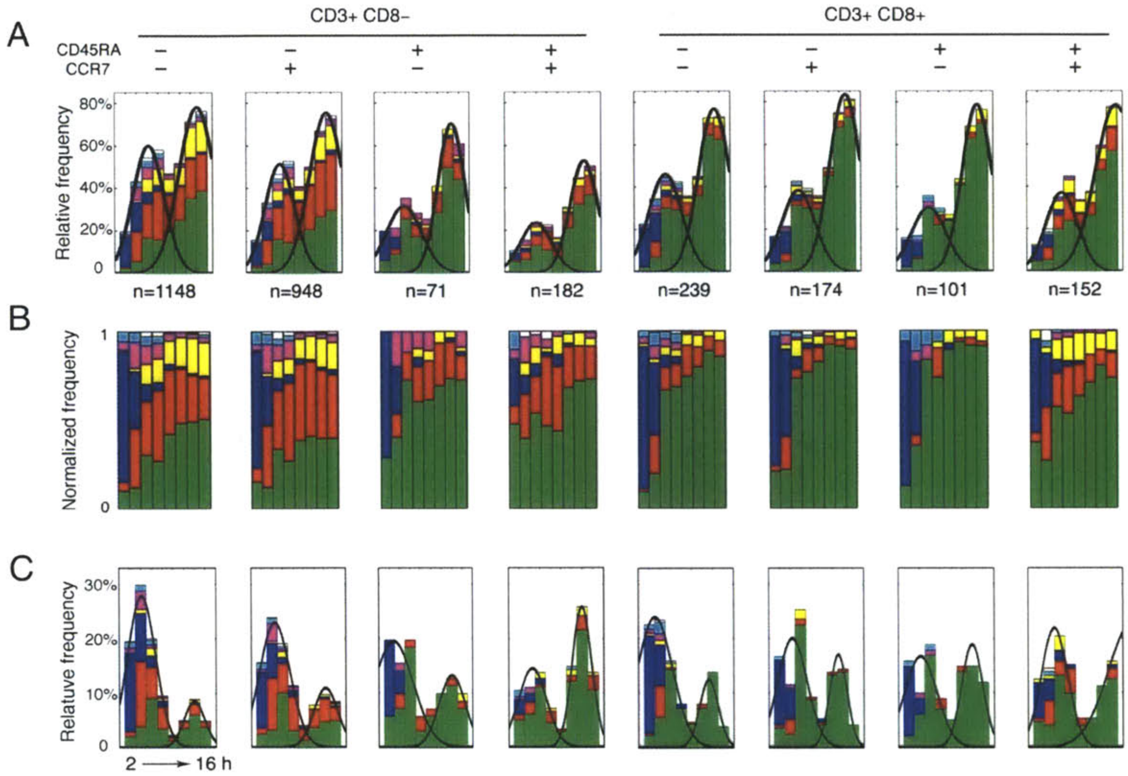

Figure 6.5 Temporal distribution of secretory states of activated T-cell subsets during constant stimulation with PMA/ionomycin. Histograms of the total percentage of actively secreting cells (A) and their corresponding normalized frequencies are shown as a function of time (B). The colors correspond to the observed secretory states according to the legend. The size of each subset population, n, is indicated below each plot. (C) Histograms of the percentage of cells that initiate secretion and their corresponding secretory states are shown as a function of time. Early and late responses are observed in both cytokine activity and initiation (A and C, respectively). Black solid lines superimposed on the bar graphs reflect fitted Gaussian curves.

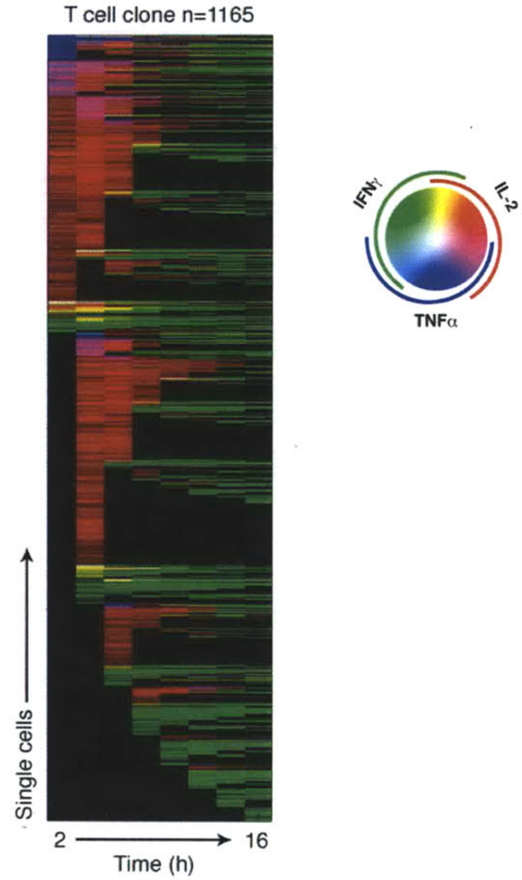

Figure 6.6 Cytokine secretion dynamics for individual cells of a T-cell clone upon activation. T cells expanded from an individual IFNγ-secreting cell were used to measure the functional variation from isogenic cells. Cytokine secretion was measured under the same protocol as Figure 6.1. The heat map illustrates the dynamic cytokine secretion profiles from 1,165 viable single cells. The limits of detection for this set of experiments were 1.0 ± 0.2 IFNγ molecule per s per cell, 0.4 ± 0.2 IL-2 molecule per s per cell, and 0.9 ± 0.3 TNFα molecule per s per cell.

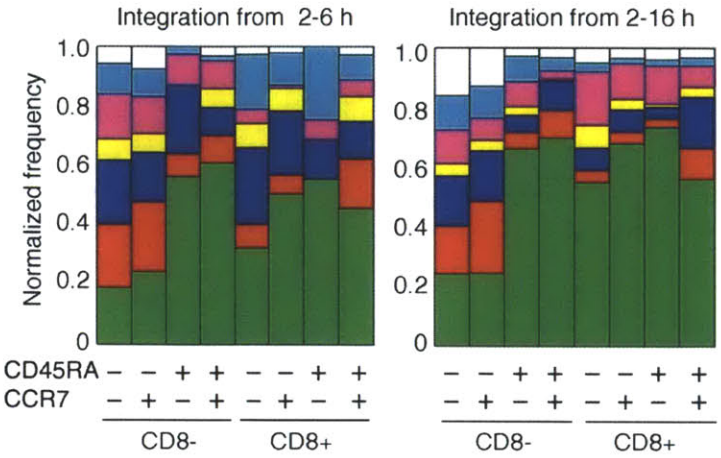

Figure 6.7 Bar graphs representing the integrated cytokine profile of T cells. Cytokine secretions from individual cells were integrated over 2-6 h (left) and 2–16 h (right). This integration yields one aggregate state for each cell. The relative frequency of functional states is normalized with a given subtype of cells.

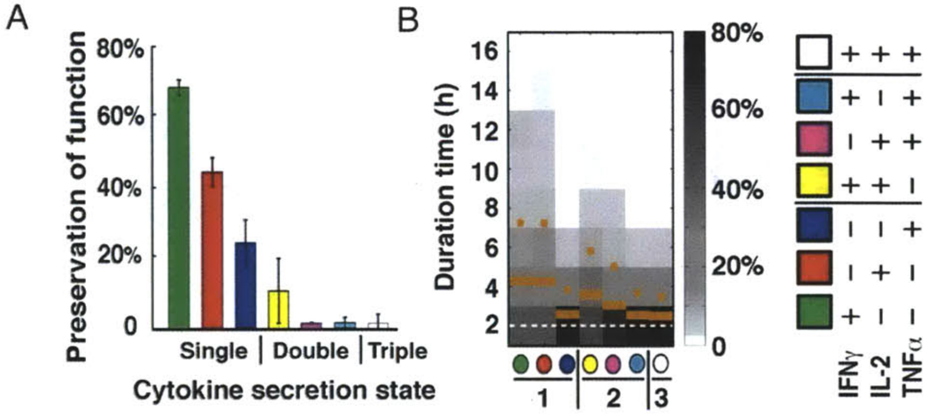

Figure 6.8 Stabilities of functional states. (A) Bar graph of the probability that a given cell preserves its functional state in 16 h. The secretory states for cells at 4, 6, and 8 h were used as independent reference points. Error bars indicate SD. (B) Heatmap indicating lifetime of secretory states. Solid orange lines reflect mean lifetime; orange dots reflect the mean plus 1 SD; white dashed line reflects the lower limit of detection, 2 h. All subtypes of T cells were included.

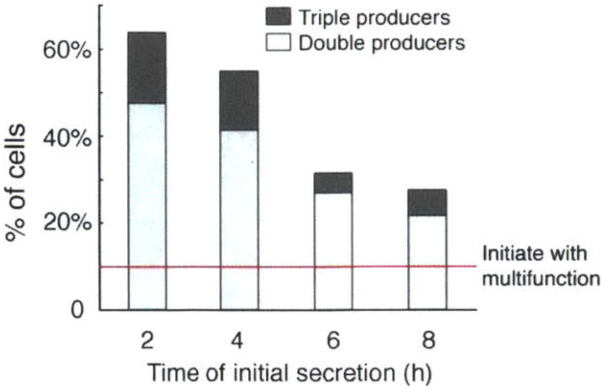

Figure 6.9 Multifunctionality correlates with early initiation of cytokine activity. The bar graph indicates the frequency of cells that produced two (light gray) or three (dark gray) cytokines within 10 h of initiating cytokine secretion. The total number of cells in each bar corresponds to those in Figure 6.3, and the analysis includes all subtypes. The solid red line marks the basal percentage of cells that initiated with multifunctional activity.

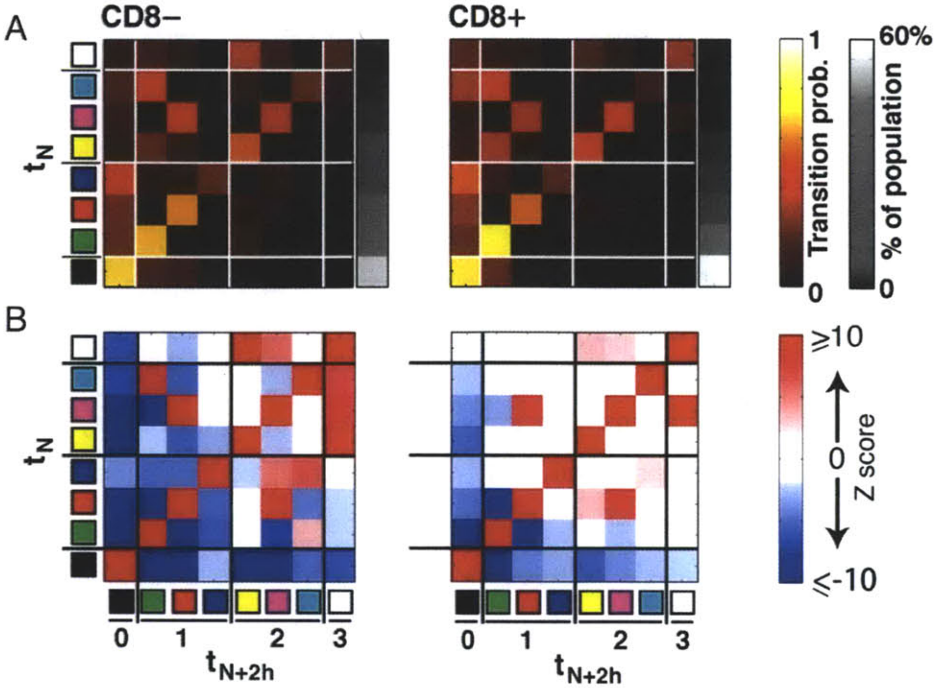

Figure 6.10 (A) Transition matrices for CD8$^-$ and CD8$^+$ T cells. Frequencies of transitions were normalized across each row to show the likelihood that a cell in any given state would transition to a new state in the next sampling period. The adjacent gray scale bar reflects the relative frequency of each state over 16 h. (B) Z scores highlight transitions that occur with significantly more/less frequency than expected by chance. Z scores indicate significant transitions (>2, red; <2, blue); insignificant values (within ±2) are white.

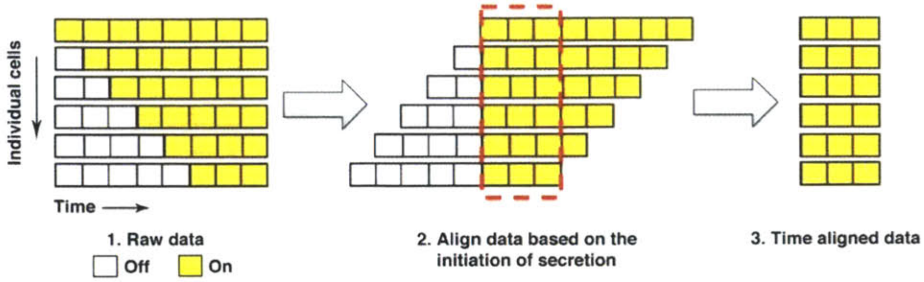

Figure 6.11 Illustration showing the procedure for time-aligning kinetic profiles. The length of individual time-aligned profiles varied with different analyses. If the time length after cell initiation was shorter than the desired length of time, that cell is not included in the analysis. For instance, in a three-point time aligned dataset, cells that initiated secretion at the seventh or eighth time points are not included.

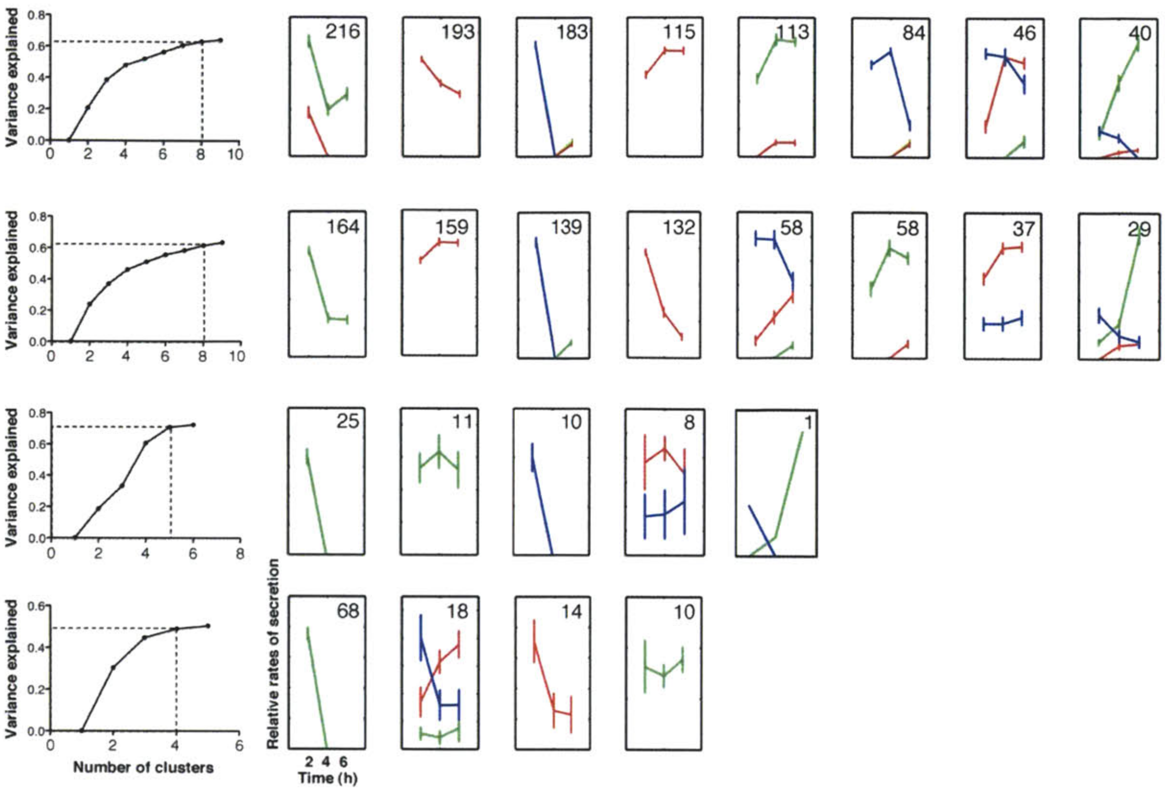

Figure 6.12 Clustering of cytokine trajectories within CD3$^+$CD8$^-$ T-cell subsets. The first three time-aligned data points specific to each subset were clustered, independently, by self-organizing maps (SOM). The optimal number of clusters for each subset was determined by the elbow criterion, where the marginal increase of the variance began to level. The explained variance for the clustering of each subset was plotted as a function of the number of clusters (left). The average rates of secretion in each cluster were plotted separately, ordered by the number of cells clustered in each pattern. The cytokines are indicated by color: IFNγ (green), TNFα (blue), and IL-2 (red). Error bars indicate SE. We use the following abbreviations for cell subtypes: EM: effector memory, CD45RA$^-$CCR7$^-$; CM: central memory, CD45RA$^-$CCR7$^+$; E: effector, CD45RA$^+$CCR7$^-$; N: naïve, CD45RA$^+$CCR7$^+$. The number of cells in each cluster is reported in the upper right corner of the plot.

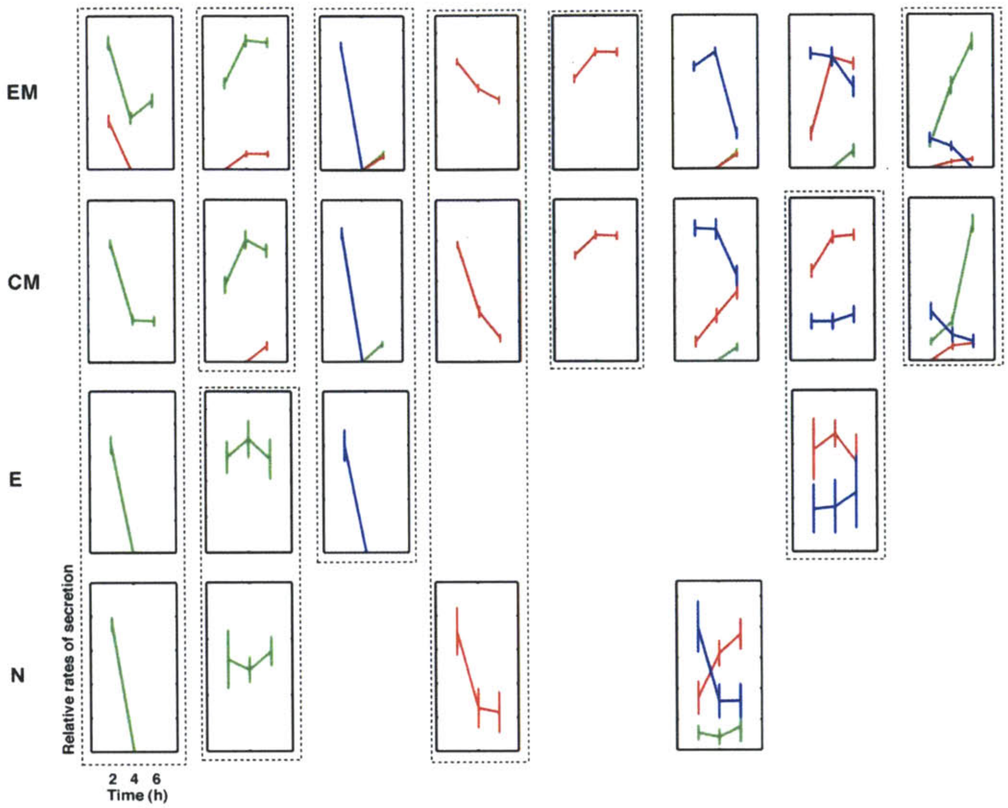

Figure 6.13 Metaclustering of similar trajectories across subsets was determined by a second round of SOM. The number of combined clusters across all subsets was selected for 95% of the variance explained (12 combined clusters). Qualitative alignment of clusters from each subset of T cells are highlighted and grouped according to the dashed boxes.

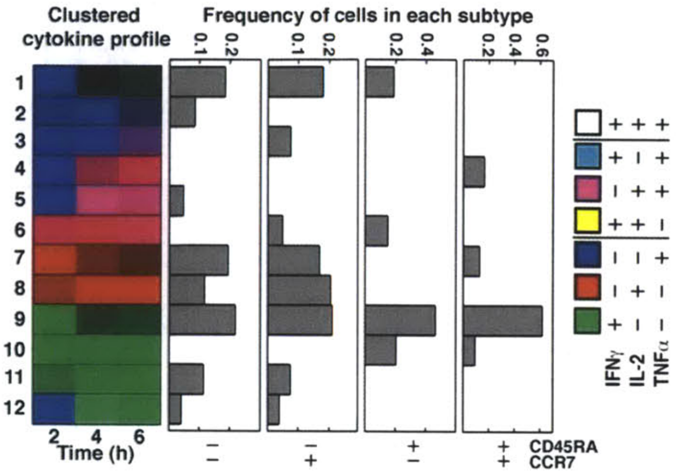

Figure 6.14 Common time-aligned cytokine secretion profiles of CD8$^-$ T cells (determined by SOM) and their relative percent distribution within each differentiated subset of T cells. Colorimetric representation of cytokine states is consistent with Figure 6.3.

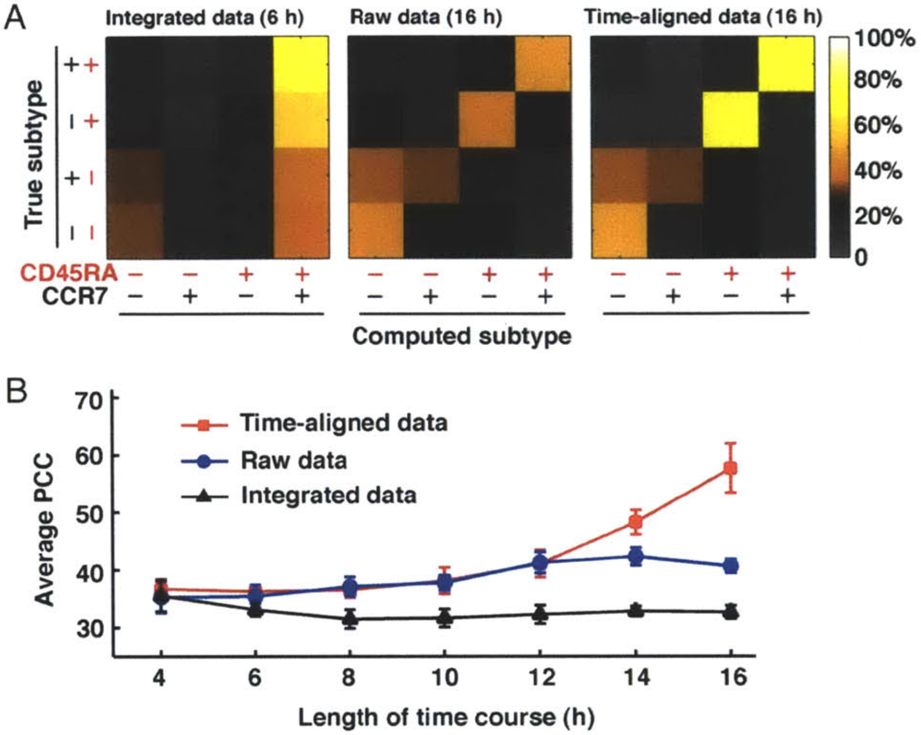

Figure 6.15 T cells can be classified by their dynamical functional profiles. (A) Matrices depicting the accuracy of classification of CD8$^-$ T-cell subtypes based on dynamic secretion profiles. These "confusion matrices" quantify the percent of accurately classified cell types (defined by surface cell markers) computed by PCA relative to the true subtypes (identified by their cell surface markers). The color bar reflects the percentage of cells classified as a certain subtype; uniform random assignment (25%) and below is denoted in black and gray scale, respectively. (B) Average percent correct classification (PCC) of CD3$^+$CD8$^-$ T-cell subtypes over 10 independent, randomly sampled iterations as a function of the length of dynamic trajectory. Error bars indicate SD.

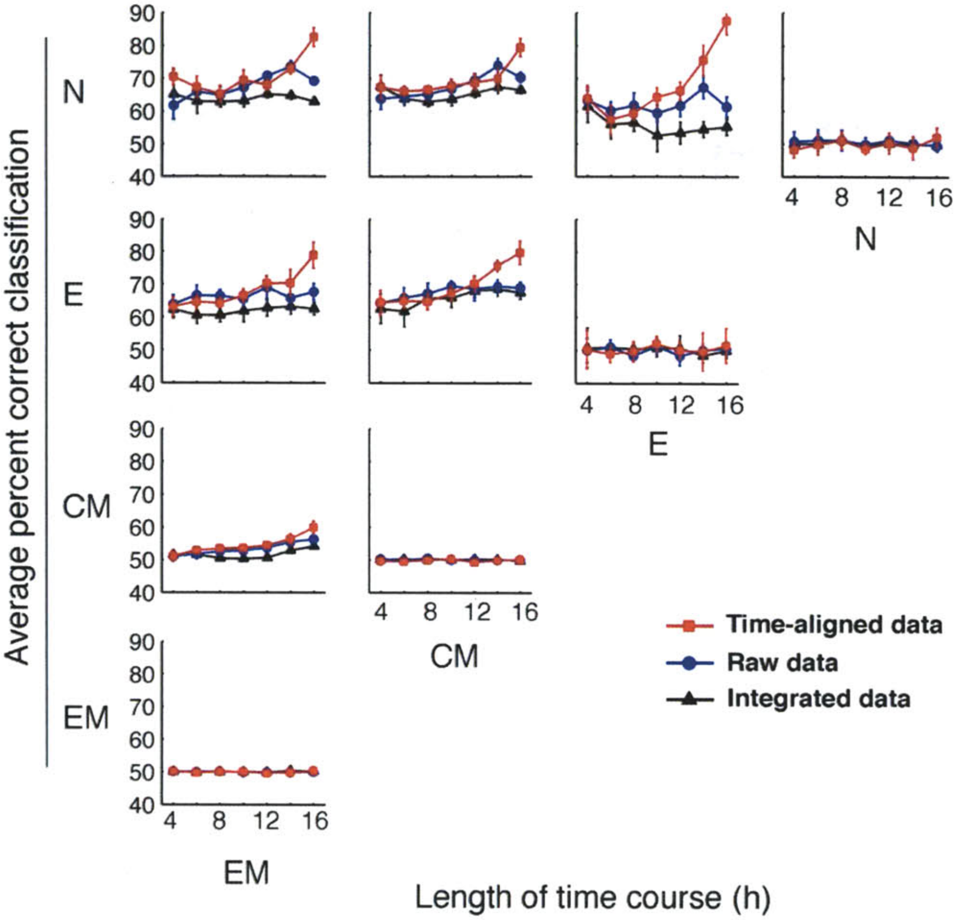

Figure 6.16 Classification of each binary combination of cell subtypes. The reported percent reflects the mean over 10 iterations of the classification algorithm as a function of the length of time course for integrated, raw, and time-aligned data.

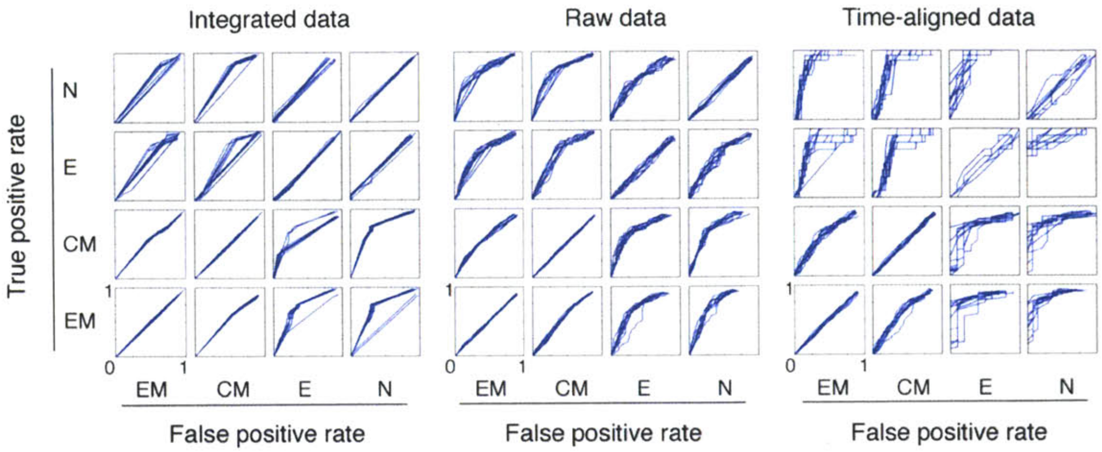

Figure 6.17 The receiver operating characteristic (ROC) curves for each binary combination of classification corresponding to the full 16-h time course. Each line (blue) corresponds to an independent iteration of the algorithm. The first block of 16 ROC curves corresponds to integrated data, the second to raw data, and the third to time-aligned data. A steep step-like curve indicates accurate and sensitive classification.

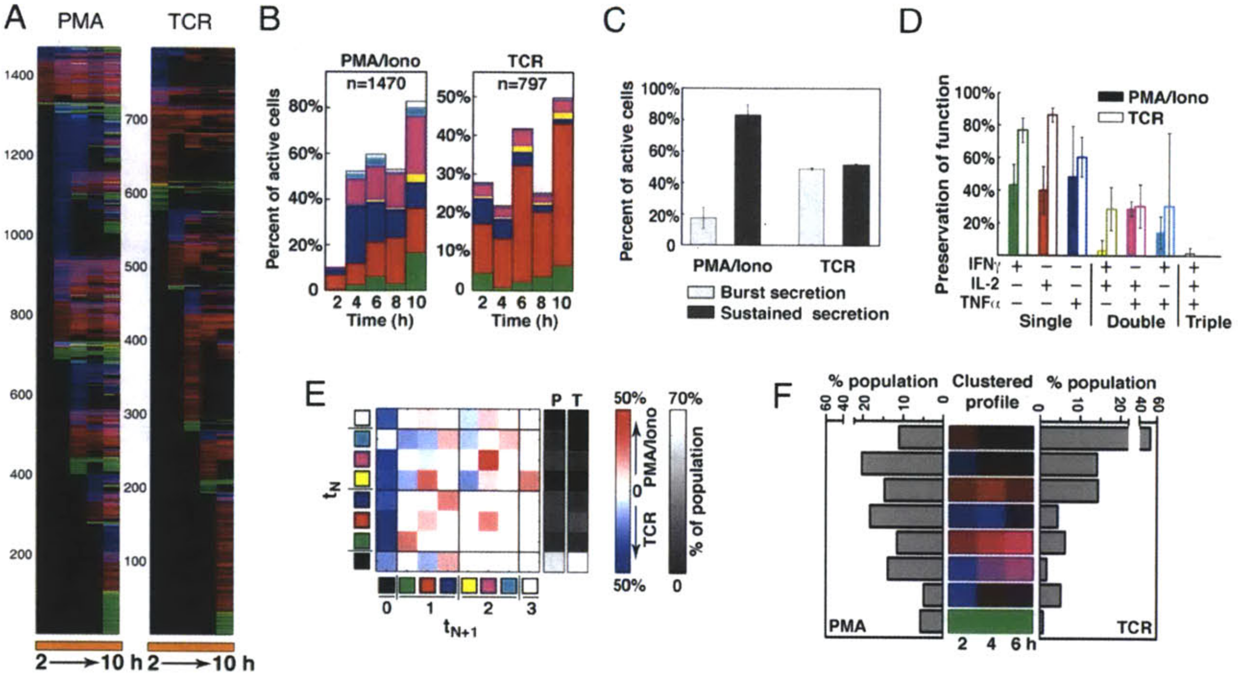

Figure 6.18 T-cell receptor-dependent stimulation and corresponding dynamic T-cell responses. (A) Temporal cytokine profiles from viable T cells stimulated over 10 h with PMA/ionomycin and anti-CD3/CD28. (B) Comparison of the frequencies of cytokine-secreting cells from the same subject stimulated with PMA/ionomycin (left) and anti-CD3/CD28 (right). (C) Bar graph of the normalized average distributions of sustained (>2 h) or burst-like (2 h) secretions by activated T cells as a function of stimulation. Error bars indicate SD. (D) Bar graph depicting the probability that a given cell preserves its functional state in the 10-h period upon stimulation with PMA/ionomycin (filled bars) and anti-CD3/CD28 (open bars). Error bars indicate SD. (E) Matrix reflecting the differential normalized probabilities of T-cell state transitions upon PMA/ionomycin (red, P) and anti-CD3/CD28 (blue, T) stimulation. Cells were randomly sampled from each dataset to compare equal population sizes (n=797). Gray scale bars reflect the relative frequencies of states within each dataset. (F) Common trajectories that are accessed by PMA/ionomycin and TCR-dependent stimulated T cells. An equal number of cells (n=478) were randomly sampled from each population, combined, and used for SOM clustered. The distributions of accessibility for cells to these trajectories are shown in adjacent histograms. Data are representative from experiments for three different donors. All T-cell subtypes were included in A–E; only $CD3^+CD8^-$ T cells were included in F.

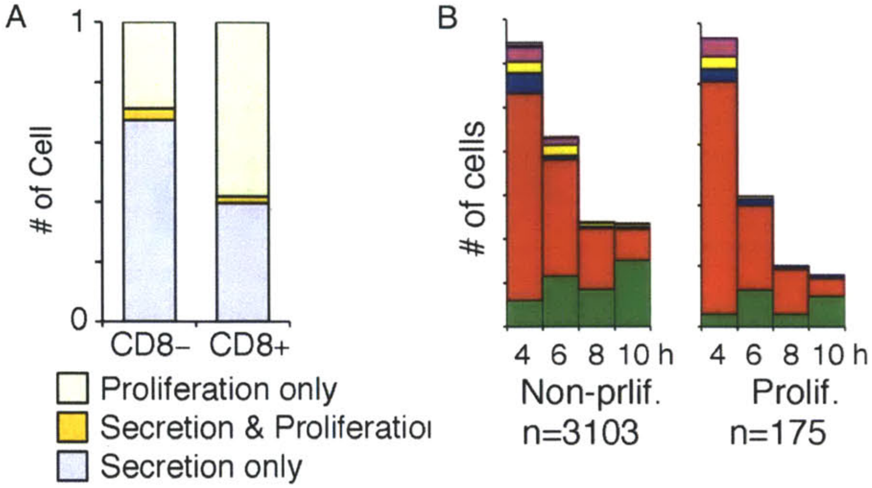

Figure 6.19 Cytokine secretion at early time point after secretion does not correlate with cell proliferation. (A) Only a small population of cells that secreted cytokine within 10 h after TCR-specific stimulation finally proliferated after 3 days. (B) Cells that proliferated have higher potential to secretion IL-2 as the initial functional state after stimulation.

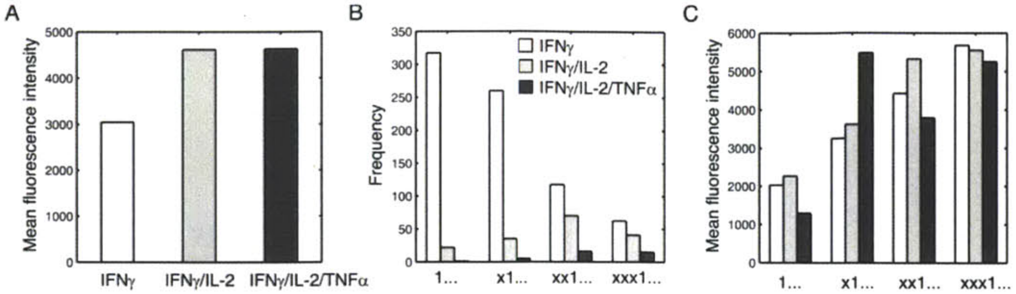

Figure 6.20 Comparison of IFNγ secretion between single producers and multifunctional cells. (A) Multifunctional cells have higher secretion level of IFNγ than single producers. (B) Distribution of cytokine state as a function of time length after initiation. (C) Mean fluorescence intensity of IFNγ secretion from different cytokine states as a function of time length after initiation. In B and C, x, presents any secretory states and 1 presents specific functional state as indicated in the legend. The order of x and 1 is counted after initial secretion. For example, x1... in white bar means single-IFNγ state was observed at the second time point after initial activation.

6.10 Tables

Initial secretion of cytokines

Subtype	CD8	CD45RA	CCR7	t_1	t_2	A_1/A_2
CD8- EM	–	–	–	4.2	14.0	3.27
CD8- CM	–	–	+	4.6	14.2	2.10
CD8- E	–	+	–	2.8	14.0	1.48
CD8- Naïve	–	+	+	4.6	14.0	0.56
CD8+ EM	+	–	–	3.0	13.4	1.92
CD8+ CM	+	–	+	4.4	13.2	1.17
CD8+ E	+	+	–	4.2	14.0	0.89
CD8+ Naïve	+	+	+	5.0	20.0	0.95

Total activity of cytokine-secreting cells

Subtype	CD8	CD45RA	CCR7	t_1	t_2	A_1/A_2
CD8- EM	–	–	–	6.2	15.2	0.77
CD8- CM	–	–	+	6.4	15.0	0.68
CD8- E	–	+	–	5.6	14.6	0.45
CD8- Naive	–	+	+	6.0	15.0	0.45
CD8+ EM	+	–	–	6.0	15.0	0.60
CD8+ CM	+	–	+	6.4	15.2	0.46
CD8+ E	+	+	–	6.2	15.2	0.38
CD8+ Naive	+	+	+	6.6	16.8	0.47

t_1, mean time of the first peak; t_2, mean time of the second peak; A_1/A_2, ratio of the height of the first peak to the second one; EM, effector memory cells (CD45RA-CCR7-); CM, central memory cells(CD45RA-CCR7+); E, effector cells(CD45RA+CCR7-); Naïve, naïve cells(CD45RA+CCR7+).

Table 6.1 Fitting parameters calculated for Gaussian distributions.

Time of initial secretion	4 h	6 h	8 h	10 h	No secretion
Number of wells	1389	907	496	486	31928
Number of beads per well	3.8±1.9	3.9±1.9	3.9±1.8	3.9±1.9	3.9±2.0

Table 6.2 Average number of anti-CD3/CD28 beads per well in TCR-specific stimulation.

Chapter 7. Conclusions

In this work, we optimized and expanded microengraving technology to a sensitive, multiplexed, quantitative, and high-throughput single-cell assay for characterizing functional diversity of heterogeneous cell populations. In a single assay, 10^5-10^6 single cells can be measured for their secretory functions simultaneously, such as cytokine secretion from T cells and antibody secretion from B cells. Confining secreting cells in small volumes significantly reduces the time required to detect specific analytes and enhances the sensitivity of the assay. Numerical simulations of the microengraving process indicate an operating regime between 30 min-4 h that permits quantitative analysis of the rates of secretion. In the multiplexed assays, both theoretical calculations and experiments demonstrated that up to four different analytes could be detected simultaneously and quantified independently from individual viable primary immune cells. The limits of detection for several cytokines that we have measured in our system range from 0.5-4 molecules/s, which are at least 10 times lower than those previously calculated for artificial receptor assays, and in most cases, are lower than those for encapsulation assays. Meanwhile, the array with isolated cells is compatible with imaging system, so that phenotype and viability of individual cells can also be measured by image cytometry. Therefore, in a typical functional measurement, populations of viable cells are categorized on the basis of three independent attributes: 1) surface-expressed markers indicating their immunophenotypes, 2) the frequencies of cells with secretion, and 3) the rates of secretion of secretory products.

Multidimensional analysis by microengraving provides higher resolution and greater sensitivity to characterize cell responses than conventional single-parameter assays. We showed that cells from different donors exhibited distinct responses based on both the frequency and magnitude of cytokine secretion when stimulated under different activating conditions. These results imply potential application of multidimensional profile to evaluate vaccine responses and understand the pathology of chronic diseases. Besides, array of nanowells makes the approach especially well suited for characterization of clinical samples where the number of cells available may not be sufficient for analysis by independent conventional methods (e.g., infants, tissue biopsies).

The results from the analytical model, confirmed by experimental data, also emphasize a technical advantage associated with temporarily confining cells into small volumes that contain appropriate capture reagents for one or more analytes of interest. In contrast to ELISpot and related adaptations of these conventional immunoassays implemented in open arrays of microwells, the closed system improves capture efficiency and decreases cross contamination of analytes between individual wells.

The nondestructive nature of microengraving makes it suitable for integrative single-cell analysis that is not possible by conventional ELISpot or ICS. Primary T cells can be identified and recovered based on their functional attributes for subsequent expansion in vitro, which enables further evaluation of the heterogeneities among various clonotypes.

Integration of multiple cycles of microengraving (serial microengraving) could explore the dynamics of cell response; especially resolve the evolution of functions in multifunctional T cells. For the first time, we reported a detailed characterization of dynamic secretions of three Th1 cytokines (IFNγ, IL-2, TNFα) from individual human primary T cells. The data showed that the timing of initial activation and the kinetics of secretion after that were highly diverse among T cells. Asynchronous release of cytokines under persistent stimulation was observed in both primary T cells and T-cell clones, which is independent of the differentiation states of cells and the type of stimulation. The release of individual cytokines from single cells could be burst-like or sustained; the release of multiple cytokines could be simultaneously or sequential. Multifunctional cells are normally believed to indicate higher effector functions; however, our data showed that multifunctional states were normally short-lived and occurred as transitions between states.

Computational analysis of these dynamical data indicated that the transitions between different functional states were not stochastic. In the adjacent time points, the most probable outcomes observed were that cells either retained the current state or downgraded the number of cytokines secreted. Time-aligned data showed that there were limited types of trajectories of cellular responses and the accessibility of certain trajectories varied among differentiated subsets. These results suggested that the evolution of functions in a single cell was programmatic and differentiation-dependent. We further showed that sequential trajectories of secretions, especially time-aligned trajectories, distinguished different subsets of cells more effectively than time-integrated data. Together, this work highlights how incorporating kinetic timing within multidimensional data enhances the resolution of phenotypic and functional diversity among T cells and suggests new approaches to define functional signatures of immune responses associated with specific clinical conditions.

Implication for future directions

Our preliminary work comparing cytokine secretions from the same population of T cells under single-cell and bulk stimulation indicated that cell-cell interaction influenced cytokine secretion. For example, IFNγ secretion was inhibited when cells were isolated, while TNFα was promoted when cells were cultured in bulk. These interactions are probably from paracrine signals between T cells. The transitions between two functional states observed in the dynamics study also imply certain connections between the regulatory pathways of different cytokines. Therefore, perturbation experiments could be designed to investigate how autocrine and paracrine signals affect the kinetic expression of other cytokines and cytokine receptors on the cell surfaces, as well as the trajectories of function. These studies may inform models on the intracellular regulatory networks of cytokines.

Although PMA/ionomycin stimulation is artificial and may not provide the true responses of cells, the timing to add it and its strength can be easily controlled in the assay. In this work, we only focused on cytokine dynamics under constant stimulation. Analogous to the way commonly used in control theory, it will be interesting to give individual cells (system) different types of stimulation (input), such as pulse or ramp signal, and analyze how cell-response (output) changes. Using mathematical methods, we may be able to identify types of regulation machinery of cytokine expression in T cells.

The multiplexed assay system we established in this work has broad application potentials in various cell-based assays. Similar kinetics measurements could be applied on other functional subsets of T cells, such as Th2, Th17 cells, to reveal a broader view of the way that different cytokine functions are regulated. Incorporating APCs in a single-cell co-culture system would further refine our dynamic single-cell measures to reveal the effects of both antigen-specificity and cell-cell interactions on the evolution of paracrine responses. Apply multidimensional analysis on immune cells from clinical samples could help identify signatures of immune responses associated with certain diseases, such as allergy, autoimmune disease, HIV infection etc. The dynamic single-cell analysis of cellular functional responses should also help evaluate the nature and evolution of intercellular interactions present in other biological systems such as tumor microenvironments and stromal niches for stem cells.

References

1. Seder RA, Darrah PA, & Roederer M (2008) T-cell quality in memory and protection: implications for vaccine design. *Nat Rev Immunol* 8(4):247-258.
2. Sallusto F & Lanzavecchia A (2009) Heterogeneity of CD4+ memory T cells: functional modules for tailored immunity. *Eur J Immunol* 39(8):2076-2082.
3. Lenschow DJ, Walunas TL, & Bluestone JA (1996) CD28/B7 system of T cell costimulation. *Annual Review of Immunology* 14:233-258.
4. Viret C & Janeway CA, Jr. (1999) MHC and T cell development. *Reviews in immunogenetics* 1(1):91-104.
5. Kaech SM, Wherry EJ, & Ahmed R (2002) Effector and memory T-cell differentiation: Implications for vaccine development. *Nature Reviews Immunology* 2(4):251-262.
6. Seder RA & Ahmed R (2003) Similarities and differences in CD4(+) and CD8(+) effector and memory T cell generation. *Nature Immunology* 4(9):835-842.
7. Lanzavecchia A & Sallusto F (2000) Dynamics of T lymphocyte responses: Intermediates, effectors, and memory cells. *Science* 290(5489):92-97.
8. Hamann D, *et al.* (1997) Phenotypic and functional separation of memory and effector human CD8(+) T cells. *Journal of Experimental Medicine* 186(9):1407-1418.
9. Sallusto F, Lenig D, Forster R, Lipp M, & Lanzavecchia A (1999) Two subsets of memory T lymphocytes with distinct homing potentials and effector functions. *Nature* 401(6754):708-712.
10. Appay V, van Lier RAW, Sallusto F, & Roederer M (2008) Phenotype and Function of Human T Lymphocyte Subsets: Consensus and Issues. *Cytometry Part A* 73A(11):975-983.
11. Sallusto F, Geginat J, & Lanzavecchia A (2004) Central memory and effector memory T cell subsets: Function, generation, and maintenance. *Annual Review of Immunology* 22:745-763.
12. Campbell JJ, *et al.* (2001) CCR7 expression and memory T cell diversity in humans. *Journal of Immunology* 166(2):877-884.
13. Zhou L, Chong MMW, & Littman DR (2009) Plasticity of CD4+ T Cell Lineage Differentiation. *Immunity* 30(5):646-655.
14. Veldhoen M, *et al.* (2008) Transforming growth factor-beta 'reprograms' the differentiation of T helper 2 cells and promotes an interleukin 9-producing subset. *Nature Immunology* 9(12):1341-1346.
15. Mosmann TR & Coffman RL (1989) TH1-CELL AND TH2-CELL - DIFFERENT PATTERNS OF LYMPHOKINE SECRETION LEAD TO DIFFERENT FUNCTIONAL-PROPERTIES. *Annual Review of Immunology* 7:145-173.
16. Suzuki Y, Orellana MA, Schreiber RD, & Remington JS (1988) INTERFERON-GAMMA - THE MAJOR MEDIATOR OF RESISTANCE AGAINST TOXOPLASMA-GONDII. *Science* 240(4851):516-518.
17. Williams MA, Tyznik AJ, & Bevan MJ (2006) Interleukin-2 signals during priming are required for secondary expansion of CD8(+) memory T cells. *Nature* 441(7095):890-893.

18. Weaver CT, Harrington LE, Mangan PR, Gavrieli M, & Murphy KM (2006) Th17: An effector CD4 T cell lineage with regulatory T cell ties. *Immunity* 24(6):677-688.
19. Sakaguchi S (2004) Naturally arising CD4(+) regulatory T cells for immunologic self-tolerance and negative control of immune responses. *Annual Review of Immunology* 22:531-562.
20. Zhu J & Paul WE (2008) CD4 T cells: fates, functions, and faults. *Blood* 112(5):1557-1569.
21. Betts MR, *et al.* (2006) HIV nonprogressors preferentially maintain highly functional HIV-specific CD8(+) T cells. *Blood* 107(12):4781-4789.
22. Duvall MG, *et al.* (2008) Polyfunctional T cell responses are a hallmark of HIV-2 infection. *European Journal of Immunology* 38(2):350-363.
23. Caccamo N, *et al.* (2010) Multifunctional CD4(+) T cells correlate with active Mycobacterium tuberculosis infection. *European Journal of Immunology* 40(8):2211-2220.
24. Precopio ML, *et al.* (2007) Immunization with vaccinia virus induces polyfunctional and phenotypically distinctive CD8(+) T cell responses. *Journal of Experimental Medicine* 204(6):1405-1416.
25. Darrah PA, *et al.* (2007) Multifunctional TH1 cells define a correlate of vaccine-mediated protection against Leishmania major. *Nat Med* 13(7):843-850.
26. Lindenstrom T, *et al.* (2009) Tuberculosis Subunit Vaccination Provides Long-Term Protective Immunity Characterized by Multifunctional CD4 Memory T Cells. *Journal of Immunology* 182(12):8047-8055.
27. Kannanganat S, Ibegbu C, Chennareddi L, Robinson HL, & Amara RR (2007) Multiple-cytokine-producing antiviral CD4 T cells are functionally superior to single-cytokine-producing cells. *Journal of Virology* 81(16):8468-8476.
28. Lagrelius M, Jones P, Franck K, & Gaines H (2006) Cytokine detection by multiplex technology useful for assessing antigen specific cytokine profiles and kinetics in whole blood cultured up to seven days. *Cytokine* 33(3):156-165.
29. Mascher B, Schlenke P, & Seyfarth M (1999) Expression and kinetics of cytokines determined by intracellular staining using flow cytometry. *J Immunol Methods* 223(1):115-121.
30. Hess K, *et al.* (2004) Kinetic assessment of general gene expression changes during human naive CD4(+) T cell activation. *International Immunology* 16(12):1711-1721.
31. Rogers WO, *et al.* (1997) Visualization of antigen-specific T cell activation and cytokine expression in vivo. *Journal of Immunology* 158(2):649-657.
32. Sojka DK, Bruniquel D, Schwartz RH, & Singh NJ (2004) IL-2 secretion by CD4(+) T cells in vivo is rapid, transient, and influenced by TCR-specific competition. *Journal of Immunology* 172(10):6136-6143.
33. Sandberg JK, Fast NM, & Nixon DF (2001) Functional heterogeneity of cytokines and cytolytic effector molecules in human CD8(+) T lymphocytes. *Journal of Immunology* 167(1):181-187.
34. Divekar AA, *et al.* (2006) Protein vaccines induce uncommitted IL-2-secreting human and mousle CD4 T cells, whereas infections induce more IFN-gamma-secreting cells. *Journal of Immunology* 176(3):1465-1473.

35. Maheshri N & O'Shea EK (2007) Living with noisy genes: how cells function reliably with inherent variability in gene expression. *Annu Rev Biophys Biomol Struct* 36:413-434.
36. Ross DT, *et al.* (2000) Systematic variation in gene expression patterns in human cancer cell lines. *Nat Genet* 24(3):227-235.
37. Urenjak J, Williams SR, Gadian DG, & Noble M (1993) Proton nuclear magnetic resonance spectroscopy unambiguously identifies different neural cell types. *J Neurosci* 13(3):981-989.
38. Ferrell JE, Jr. & Machleder EM (1998) The biochemical basis of an all-or-none cell fate switch in Xenopus oocytes. *Science* 280(5365):895-898.
39. McAdams HH & Arkin A (1997) Stochastic mechanisms in gene expression. *Proc Natl Acad Sci U S A* 94(3):814-819.
40. Elowitz MB, Levine AJ, Siggia ED, & Swain PS (2002) Stochastic gene expression in a single cell. *Science* 297(5584):1183-1186.
41. Kamme F, *et al.* (2003) Single-cell microarray analysis in hippocampus CA1: demonstration and validation of cellular heterogeneity. *J Neurosci* 23(9):3607-3615.
42. Sims CE & Allbritton NL (2007) Analysis of single mammalian cells on-chip. *Lab Chip* 7(4):423-440.
43. Woods NM, Cuthbertson KS, & Cobbold PH (1986) Repetitive transient rises in cytoplasmic free calcium in hormone-stimulated hepatocytes. *Nature* 319(6054):600-602.
44. Fink L, Kwapiszewska G, Wilhelm J, & Bohle RM (2006) Laser-microdissection for cell type- and compartment-specific analyses on genomic and proteomic level. *Exp Toxicol Pathol* 57 Suppl 2:25-29.
45. Bodey B (2002) The significance of immunohistochemistry in the diagnosis and therapy of neoplasms. *Expert Opin Biol Ther* 2(4):371-393.
46. Streeck H, Frahm N, & Walker BD (2009) The role of IFN-gamma Elispot assay in HIV vaccine research. *Nat Protoc* 4(4):461-469.
47. Czerkinsky CC, Nilsson LA, Nygren H, Ouchterlony O, & Tarkowski A (1983) A solid-phase enzyme-linked immunospot (ELISPOT) assay for enumeration of specific antibody-secreting cells. *J Immunol Methods* 65(1-2):109-121.
48. Boulet S, *et al.* (2007) A dual color ELISPOT method for the simultaneous detection of IL-2 and IFN-gamma HIV-specific immune responses. *J Immunol Methods* 320(1-2):18-29.
49. Gazagne A, *et al.* (2003) A Fluorospot assay to detect single T lymphocytes simultaneously producing multiple cytokines. *J Immunol Methods* 283(1-2):91-98.
50. Harriman WD, *et al.* (2009) Multiplexed Elispot assay. *Journal of Immunological Methods* 341(1-2):127-134.
51. Perfetto SP, Chattopadhyay PK, & Roederer M (2004) Seventeen-colour flow cytometry: unravelling the immune system. *Nat Rev Immunol* 4(8):648-655.
52. Ornatsky O, *et al.* (2010) Highly multiparametric analysis by mass cytometry. *Journal of Immunological Methods* 361(1-2):1-20.

53. Bendall SC, *et al.* (2011) Single-Cell Mass Cytometry of Differential Immune and Drug Responses Across a Human Hematopoietic Continuum. *Science* 332(6030):687-696.
54. Newell EW, Sigal N, Bendall SC, Nolan GP, & Davis MM (2012) Cytometry by Time-of-Flight Shows Combinatorial Cytokine Expression and Virus-Specific Cell Niches within a Continuum of CD8(+) T Cell Phenotypes. *Immunity* 36(1):142-152.
55. Manz R, Assenmacher M, Pfluger E, Miltenyi S, & Radbruch A (1995) Analysis and sorting of live cells according to secreted molecules, relocated to a cell-surface affinity matrix. *Proc Natl Acad Sci U S A* 92(6):1921-1925.
56. Powell KT & Weaver JC (1990) Gel microdroplets and flow cytometry: rapid determination of antibody secretion by individual cells within a cell population. *Biotechnology (N Y)* 8(4):333-337.
57. Frykman S & Srienc F (1998) Quantitating secretion rates of individual cells: design of secretion assays. *Biotechnol Bioeng* 59(2):214-226.
58. Nagrath S, *et al.* (2007) Isolation of rare circulating tumour cells in cancer patients by microchip technology. *Nature* 450(7173):1235-1239.
59. Zheng S, *et al.* (2007) Membrane microfilter device for selective capture, electrolysis and genomic analysis of human circulating tumor cells. *J Chromatogr A* 1162(2):154-161.
60. Talasaz AH, *et al.* (2006) Cell trapping in activated micropores for functional analysis. *Conf Proc IEEE Eng Med Biol Soc* 1:1838-1841.
61. Kraeft SK, *et al.* (2004) Reliable and sensitive identification of occult tumor cells using the improved rare event imaging system. *Clin Cancer Res* 10(9):3020-3028.
62. Krivacic RT, *et al.* (2004) A rare-cell detector for cancer. *Proc Natl Acad Sci U S A* 101(29):10501-10504.
63. Zhu H, *et al.* (2009) Detecting Cytokine Release from Single T-cells. *Analytical Chemistry* 81(19):8150-8156.
64. Tokilmitsu Y, *et al.* (2007) Single lymphocyte analysis with a microwell array chip. *Cytometry Part A* 71A(12):1003-1010.
65. Sasuga Y, *et al.* (2008) Single-Cell Chemical Lysis Method for Analyses of Intracellular Molecules Using an Array of Picoliter-Scale Microwells. *Analytical Chemistry* 80(23):9141-9149.
66. Revzin A, Sekine K, Sin A, Tompkins RG, & Toner M (2005) Development of a microfabricated cytometry platform for characterization and sorting of individual leukocytes. *Lab on a Chip* 5(1):30-37.
67. Rettig JR & Folch A (2005) Large-scale single-cell trapping and imaging using microwell arrays. *Analytical Chemistry* 77(17):5628-5634.
68. Ostuni E, Chen CS, Ingber DE, & Whitesides GM (2001) Selective deposition of proteins and cells in arrays of microwells. *Langmuir* 17(9):2828-2834.
69. Ochsner M, *et al.* (2007) Micro-well arrays for 3D shape control and high resolution analysis of single cells. *Lab on a Chip* 7(8):1074-1077.
70. Kovac JR & Voldman J (2007) Intuitive, image-based cell sorting using optofluidic cell sorting. *Analytical Chemistry* 79(24):9321-9330.

71. Chin VI, *et al.* (2004) Microfabricated platform for studying stem cell fates. *Biotechnology and Bioengineering* 88(3):399-415.
72. Park MC, Hur JY, Kwon KW, Park S-H, & Suh KY (2006) Pumpless, selective docking of yeast cells inside a microfluidic channel induced by receding meniscus. *Lab on a Chip* 6(8):988-994.
73. Henn AD, *et al.* (2009) Modulation of single-cell IgG secretion frequency and rates in human memory B cells by CpG DNA, CD40L, IL-21, and cell division. *J Immunol* 183(5):3177-3187.
74. Kannanganat S, Ibegbu C, Chennareddi L, Robinson HL, & Amara RR (2007) Multiple-cytokine-producing antiviral CD4 T cells are functionally superior to single-cytokine-producing cells. *J Virol* 81(16):8468-8476.
75. Darrah PA, *et al.* (2007) Multifunctional TH1 cells define a correlate of vaccine-mediated protection against Leishmania major. *Nat Med* 13(7):843-850.
76. Ogunniyi AO, Story CM, Papa E, Guillen E, & Love JC (2009) Screening individual hybridomas by microengraving to discover monoclonal antibodies. *Nat Protoc* 4(5):767-782.
77. Love JC, Ronan JL, Grotenbreg GM, van der Veen AG, & Ploegh HL (2006) A microengraving method for rapid selection of single cells producing antigen-specific antibodies. *Nature Biotechnology* 24(6):703-707.
78. Story CM, *et al.* (2008) Profiling antibody responses by multiparametric analysis of primary B cells. *Proceedings of the National Academy of Sciences of the United States of America* 105(46):17902-17907.
79. Love KR, Panagiotou V, Jiang B, Stadheim TA, & Love JC (2010) Integrated Single-Cell Analysis Shows Pichia pastoris Secretes Protein Stochastically. *Biotechnology and Bioengineering* 106(2):319-325.
80. Bradshaw EM, *et al.* (2008) Concurrent detection of secreted products from human lymphocytes by microengraving: Cytokines and antigen-reactive antibodies. *Clinical Immunology* 129(1):10-18.
81. Gong Y, Ogunniyi AO, & Love JC (2010) Massively parallel detection of gene expression in single cells using subnanolitre wells. *Lab on a Chip* 10(18):2334-2337.
82. Varadarajan N, *et al.* (2011) A high-throughput single-cell analysis of human CD8(+) T cell functions reveals discordance for cytokine secretion and cytolysis. *Journal of Clinical Investigation* 121(11):4322-4331.
83. Varadarajan N, *et al.* (2012) Rapid, efficient functional characterization and recovery of HIV-specific human CD8(+) T cells using microengraving. *Proceedings of the National Academy of Sciences of the United States of America* 109(10):3885-3890.
84. Love JC (2010) Integrated Process Design for Single-Cell Analytical Technologies. *Aiche Journal* 56(10):2496-2502.
85. Ronan JL, Story CM, Papa E, & Love JC (2009) Optimization of the surfaces used to capture antibodies from single hybridomas reduces the time required for microengraving. *Journal of Immunological Methods* 340(2):164-169.
86. Choi J, Love KR, Gong Y, Gierahn TM, & Love JC (2011) Immuno-Hybridization Chain Reaction for Enhancing Detection of Individual Cytokine-Secreting Human Peripheral Mononuclear Cells. *Analytical Chemistry* 83(17):6890-6895.

87. Bird JJ, *et al.* (1998) Helper T cell differentiation is controlled by the cell cycle. *Immunity* 9(2):229-237.
88. Frykman S & Srienc F (1998) Quantitating secretion rates of individual cells: Design of secretion assays. *Biotechnology and Bioengineering* 59(2):214-226.
89. Gutenwik J, Nilsson B, & Axelsson A (2004) Determination of protein diffusion coefficients in agarose gel with a diffusion cell. *Biochemical Engineering Journal* 19(1):1-7.
90. Day YSN, Baird CL, Rich RL, & Myszka DG (2002) Direct comparison of binding equilibrium, thermodynamic, and rate constants determined by surface- and solution-based biophysical methods. *Protein Science* 11(5):1017-1025.
91. Foote J & Eisen HN (1995) KINETIC AND AFFINITY LIMITS ON ANTIBODIES PRODUCED DURING IMMUNE-RESPONSES. *Proceedings of the National Academy of Sciences of the United States of America* 92(5):1254-1256.
92. Buijs J, White DD, & Norde W (1997) The effect of adsorption on the antigen binding by IgG and its F(ab')(2) fragments. *Colloids and Surfaces B-Biointerfaces* 8(4-5):239-249.
93. Buijs J, vandenBerg PAW, Lichtenbelt JWT, Norde W, & Lyklema J (1996) Adsorption dynamics of IgG and its F(ab')(2) and Fc fragments studied by reflectometry. *Journal of Colloid and Interface Science* 178(2):594-605.
94. Chen SF, Liu LY, Zhou J, & Jiang SY (2003) Controlling antibody orientation on charged self-assembled monolayers. *Langmuir* 19(7):2859-2864.
95. Xu H, Lu JR, & Williams DE (2006) Effect of surface packing density of interfacially adsorbed monoclonal antibody on the binding of hormonal antigen human chorionic gonadotrophin. *Journal of Physical Chemistry B* 110(4):1907-1914.
96. Otto NM, *et al.* (2008) Hyperosmotic stress enhances cytokine production and decreases phagocytosis in vitro. *Critical Care* 12(4).
97. Guha M & Mackman N (2001) LPS induction of gene expression in human monocytes. *Cellular Signalling* 13(2):85-94.
98. Davtyan TK, Harutyunyan VA, Hakobyan GS, & Avetisyan SA (2008) Heightened endotoxin susceptibility of monocytes and neutrophils during familial Mediterranean fever. *Fems Immunology and Medical Microbiology* 52(3):370-378.
99. Waldrop SL, Davis KA, Maine VC, & Picker LJ (1998) Normal human CD4(+) memory T cells display broad heterogeneity in their activation threshold for cytokine synthesis. *Journal of Immunology* 161(10):5284-5295.
100. Koretzky GA, Daniele RP, Greene WC, & Nowell PC (1983) EVIDENCE FOR AN INTERLEUKIN-INDEPENDENT PATHWAY FOR HUMAN-LYMPHOCYTE ACTIVATION. *Proceedings of the National Academy of Sciences of the United States of America-Biological Sciences* 80(11):3444-3447.
101. Chatila T, Silverman L, Miller R, & Geha R (1989) Mechanisms of T cell activation by the calcium ionophore ionomycin. *J Immunol* 143(4):1283-1289.

102. Feinerman O, Veiga J, Dorfman JR, Germain RN, & Altan-Bonnet G (2008) Variability and robustness in T cell activation from regulated heterogeneity in protein levels. *Science* 321(5892):1081-1084.
103. Podtschaske M, *et al.* (2007) Digital NFATc2 Activation per Cell Transforms Graded T Cell Receptor Activation into an All-or-None IL-2 Expression. *Plos One* 2(9).
104. McKarns SC & Schwartz RH (2008) Biphasic regulation of Il2 transcription in CD4(+) T cells: Roles for TNF-alpha receptor signaling and chromatin structure. *Journal of Immunology* 181(2):1272-1281.
105. Mariani L, *et al.* (2010) Short-term memory in gene induction reveals the regulatory principle behind stochastic IL-4 expression. *Molecular Systems Biology* 6.
106. Szabo SJ, *et al.* (2000) A novel transcription factor, T-bet, directs Th1 lineage commitment. *Cell* 100(6):655-669.
107. Ketchen DJ & Shook CL (1996) The application of cluster analysis in strategic management research: An analysis and critique. *Strategic Management Journal* 17(6):441-458.
108. Cantrell DA (2002) T-cell antigen receptor signal transduction. *Immunology* 105(4):369-374.
109. Das J, *et al.* (2009) Digital Signaling and Hysteresis Characterize Ras Activation in Lymphoid Cells. *Cell* 136(2):337-351.
110. Henrickson SE, *et al.* (2008) T cell sensing of antigen dose governs interactive behavior with dendritic cells and sets a threshold for T cell activation. *Nature Immunology* 9(3):282-291.
111. Corse E, Gottschalk RA, & Allison JP (2011) Strength of TCR-Peptide/MHC Interactions and In Vivo T Cell Responses. *Journal of Immunology* 186(9):5039-5045.
112. Kumar V, *et al.* (1995) MAJOR HISTOCOMPATIBILITY COMPLEX BINDING-AFFINITY OF AN ANTIGENIC DETERMINANT IS CRUCIAL FOR THE DIFFERENTIAL SECRETION OF INTERLEUKIN-4/5 OR INTERFERON-GAMMA BY T-CELLS. *Proceedings of the National Academy of Sciences of the United States of America* 92(21):9510-9514.
113. Chaturvedi P, Yu Q, Southwood S, Sette A, & Singh B (1996) Peptide analogs with different affinities for MHC alter the cytokine profile of T helper cells. *International Immunology* 8(5):745-755.
114. Itoh Y & Germain RN (1997) Single cell analysis reveals regulated hierarchical T cell antigen receptor signaling thresholds and intraclonal heterogeneity for individual cytokine responses of CD4(+) T cells. *Journal of Experimental Medicine* 186(5):757-766.
115. Song Q, *et al.* (2010) On-Chip Activation and Subsequent Detection of Individual Antigen-Specific T Cells. *Analytical Chemistry* 82(2):473-477.
116. Ansel KM, Djuretic I, Tanasa B, & Rao A (2006) Regulation of Th2 differentiation and Il4 locus accessibility. *Annual Review of Immunology* 24:607-656.
117. Villarino AV, *et al.* (2007) Helper T cell IL-2 production is limited by negative feedback and STAT-dependent cytokine signals. *Journal of Experimental Medicine* 204(1):65-71.

118. Duitman EH, Orinska Z, & Bulfone-Paus S (2011) Mechanisms of cytokine secretion: A portfolio of distinct pathways allows flexibility in cytokine activity. *European Journal of Cell Biology* 90(6-7):476-483.
119. Black RA, *et al.* (1997) A metalloproteinase disintegrin that releases tumour-necrosis factor-alpha from cells. *Nature* 385(6618):729-733.
120. Huse M, Lillemeier BF, Kuhns MS, Chen DS, & Davis MM (2006) T cells use two directionally distinct pathways for cytokine secretion. *Nature Immunology* 7(3):247-255.
121. Matek TR (2008) The biology of interleukin-2. *Annual Review of Immunology* 26:453-479.
122. Pardoll DM (2002) Spinning molecular immunology into successful immunotherapy. *Nature Reviews Immunology* 2(4):227-238.
123. Rochman Y, Spolski R, & Leonard WJ (2009) New insights into the regulation of T cells by gamma(c) family cytokines. *Nature Reviews Immunology* 9(7):480-490.
124. Krammer PH, Arnold R, & Lavrik IN (2007) Life and death in peripheral T cells. *Nature Reviews Immunology* 7(7):532-542.
125. Lenardo MJ (1991) INTERLEUKIN-2 PROGRAMS MOUSE ALPHA-BETA-LYMPHOCYTES-T FOR APOPTOSIS. *Nature* 353(6347):858-861.
126. Waldmann TA (2006) The biology of interleukin-2 and interleukin-15: implications for cancer therapy and vaccine design. *Nature Reviews Immunology* 6(8):595-601.
127. Steenblock ER & Fahmy TM (2008) A comprehensive platform for ex vivo T-cell expansion based on biodegradable polymeric artificial antigen-presenting cells. *Molecular Therapy* 16(4):765-772.
128. Steenblock ER, Fadel T, Labowsky M, Pober JS, & Fahmy TM (2011) An Artificial Antigen-presenting Cell with Paracrine Delivery of IL-2 Impacts the Magnitude and Direction of the T Cell Response. *Journal of Biological Chemistry* 286(40):34883-34892.